National Technical University of Athens

School of Civil Engineering

Analysis and Design of Earthquake Resistant Structures MSc.

2011-2012

Postgraduate Thesis

Proposed Methodology for Simulating Historic Masonry Structures and Interventions upon Them

graduate student:

Matei-Teodor Sumbasacu

supervising professor:

Elizabeth Vintzileou

Contents

Table of figures

ACKNOWLEDGEMENTS

I would like to thank everyone who contributed and guided me for the completion of this work and, nevertheless, for the completion of the postgraduate program.

My gratitude goes to Ms. Elizabeth Vintzileou who provided me with guidance and aid whenever requested and, most importantly, who accepted to be my postgraduate thesis supervisor, thus granting me the opportunity to do my thesis in the field I like. I will be forever thankful for her guidance both as a professor and as a role model

I am grateful, as well, to Ms. Lucia Karapitta who, during my work on the thesis, supported me and was always there to answer my questions and to help resolve any unclear things which would arise.

I would also like to thank some of the professors and teaching staff at the National Technical University of Athens, who inspired me during my stay here, being real-life examples of professionalism, namely: I. Psycharis, P. Carydis, H. Mouzakis, I. Taflampas, K. Spiliopoulos, G. Bouckovalas, I. Haloulos, D. Karamitros.

Last but not least, I will always be grateful to everyone at the National Technical University of Athens, for accepting me in the program and for delivering the highest quality of information throughout the post-graduate courses.

Matei-Teodor Sumbasacu *Athens, 2012*

ABSTRACT

This work comprises the modeling and study of a historical masonry structure which was tested on the shake table of the National Technical University of Athens. An as accurate as possible modeling is required in order to correctly assess the behavioral patterns of the building under seismic load and accurately interpret the results measured during the test.

The tested building was constructed at a ½ scale. This is the scale which, with some adjustments, still renders realistic results.

The materials used for the construction of the building are stone masonry and, for the floor, wood. Also, the techniques used for the effective construction process were the traditional techniques (i.e.: manual placing of the blocks and the mortar), so the outcome is as realistic as possible.

Throughout this work, we will deal with a lot of uncertainties and we will employ a number of finite element models in order to reach the final results which can, afterwards, be accurately interpreted.

The present modeling and the experiment which was conducted in the premises of the National Technical University of Athens are part of the NIKER European project. The NIKER (New Integrated Knowledge based approaches to the protection of cultural heritage from Earthquake-induced Risk) program aims at developing a validating innovative materials and technologies for systemic improvement of the seismic behavior of cultural heritage structures.

1 INTRODUCTION

"Nobody believes in theoretical calculations – except the one who did it.
Everybody believes in experimental results – except the one who did it."
Albert Einstein

Masonry is the construction material produced using natural or man-made stones (blocks), laid with or without mortar.

The analysis of masonry structures, in general, and historic masonry structures, in particular, has been the subject of numerous papers, publications, arguments and debates throughout the years. Although this material has been ever-present in our lives since the ancient times, there still is very little known about its behavior and, moreover, about the correct assessment of its behavior.

1.1 Masonry in history

Stone masonry is a traditional form of construction that has been practiced for centuries in regions where stone is locally available. Stone masonry has been used for the construction of some of the most important monuments and structures around the world. Buildings of this type range from cultural and historical landmarks, often built by highly skilled stonemasons, to simple dwellings built by their owners in developing countries where stone is an affordable and cost-effective building material for housing construction. Stone masonry buildings can be found in many earthquake prone regions and countries including Mediterranean Europe, North Africa, the Middle East, and Southeast Asia

1.1.1 Ancient times

The beginnings of masonry construction are represented by the structures made of *adobes*. The adobes were blocks made of clay, similar to bricks. The main difference between the more recent bricks and the adobes is that, whereas the latter are sun-dried blocks of clay, the former are burnt blocks of clay. The oldest non-fired masonry block was found in Jericho and dates back to approximately 8000 BC.

The adobe blocks were usually made from sand, clay, water and some kind of fibrous or organic material (sticks, straw, branches etc.). The adobe blocks were dried in the sun and then put in place by the builders of the time.

Adobe buildings are extremely durable and account for some of the oldest existing buildings in the world. They can usually be found in hot and dry climates (West and Northern Africa, Spain, West Asia etc.) due to their great thermal mass which ensured a cool temperature for the interior of the houses, regardless of the extreme temperatures outside.

Unfortunately, adobe is a material which is particularly susceptible to earthquake damage and its faulty performance during earthquakes has been the reason for which people started to search for a better, stronger material.

Around the year 3000 BC, in Mesopotamia, a new type of building material was discovered: fired blocks. Fired blocks are, basically, adobe blocks which were set on fire. From this point of view, it is reasonable to assume that their discovery was, probably, accidental. Most likely, it was after a fire that people of that time discovered how much better characteristics the fired blocks have.

Fig. 1 Ancient Greek stone masonry wall detail

Indeed, fired blocks have proven to be stronger and more adequate for the construction of structures in seismic areas. As proof for this statement, there are numerous structures from this material in seismic areas.

Stone masonry is another type of masonry which appeared around the Stone Age. It is characterized by buildings made up of stone blocks, fitted together in order to achieve a satisfactory load distribution. Early stone masonry constructions can be found in seismic areas such as Mediterranean Europe, Middle East, North Africa or Nepal. This gives an indication that this type of constructions exhibits an adequate seismic behavior.

In the Ancient period, a very popular monument construction material was dry-stone masonry. This type of masonry is represented by the elements made up only of blocks, without any morar joints. The masonry blocks were simply stacked one on top of another. Representative for this type of construction are the ancient monuments such as the Parthenon, the temple of Zeus, etc.

The World Housing Encyclopedia contains nine reports describing stone masonry housing construction practices in Greece(WHE Report 16), Italy (WHE Report 28), India (WHE Report 18 and 80), Nepal (WHE Report47 and 74), Palestinian Territories (WHE Report 49), Slovenia (WHE Report 58), and Algeria(WHE Report 75).
Along with the rise of the Roman Empire, stone masonry became less used throughout the Western Europe territories, giving way to timber as a construction material.

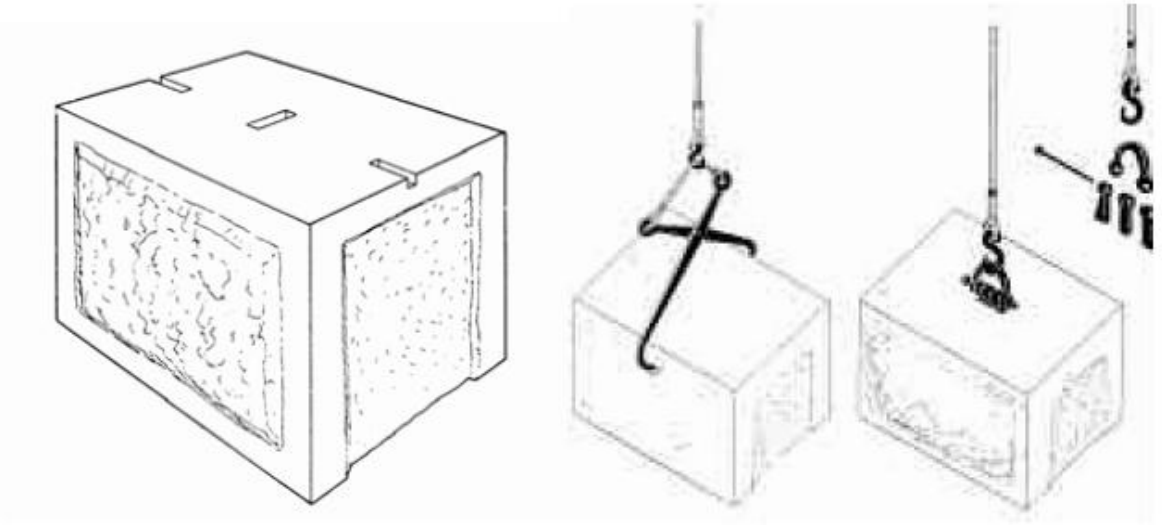

Fig. 2 Roman stone masonry blocks and lifting devices (from E. Vintzilaiou – "Lecture notes on Advanced Mechanics of Masonry")

1.1.2 Medieval Age

In the Medieval Age, the use of masonry was rehabilitated and numerous masonry structures were erected in those times.
The main reason for this "resurrection" of masonry was the construction of numerous cathedrals throughout Europe, as a necessity for expanding the influence of the Church, at the time.

Masonry construction was regarded as a noble trade and the first stonemasons' guilds were formed. Also, a 7 year apprenticeship program was the status quo for entering the profession.

The masons in the Medieval Age were highly skilled and the great masonry monuments erected at the time stand as testimony for this.

Fig. 3 Medieval (18th century) stone houses in Longanikos, Greece

Due to the fact that masonry became widespread among the materials used for the construction of monuments, and due to the highly specialized workforce available, masonry had a growth in popularity throughout the Middle Age.

People started preferring a stone masonry house to a wooden house and more and more cities were built mainly out of masonry.

The type of stone masonry used in throughout this period was, mainly, three-leaf stone masonry. This means that the wall is composed by three more or less separate layers. The exterior masonry leaf, which has, usually, the tidiest aspect, is made up of large stones and it has thinner mortar joints. The leaf facing the interior of the building is, also, rather tidy in aspect, being made up of moderate size blocks with thin enough mortar joints.

The main problem of the three-leaf masonry walls is the interior leaf of the walls. This leaf is made up of rubble stone and other materials (such as mortar) used to fill in the gap between the two exterior leaves. This interior filling, having very poor mechanical characteristics and a high void ratio, has a very negative effect on the overall strength of the masonry wall, which will be discussed further on.

1.1.3 Modern masonry

Nowadays, masonry is still one of the most popular materials used in the small residential units' construction. It's very good thermal inertia, low price and widespread availability, make it one of the most often chosen construction materials for personal homes.

Masonry is, at the present time, usually combined with other construction materials (such as RC or wood) in order to improve its characteristics and behavior. Dual systems, such as confined masonry, are very popular throughout the earthquake-prone regions in the world, whereas simple, plain masonry is widespread in non-seismic regions.

Relatively recent, the invention of cement-based mortars meant that modern masonry has dramatically improved mechanical properties.

Modern masonry is comprised by several materials, depending on the role the masonry element will play in the structure. We can have: structural elements, exterior walls, interior partitioning walls etc.

Usually, modern masonry is reinforced with horizontal steel elements (earthquake prone regions) or it presents a concrete core.

Fig. 4 Typical modern masonry

1.2 Historic masonry mechanics

Masonry is a heterogeneous, anisotropic and brittle material. This means that it is a particularly difficult material to assess.

Within all of the masonry research papers, masonry is modeled using finite element method. One of the assumptions employed in this method is that its properties are constant throughout its thickness. This is, of course, a simplistic assumption and the civil engineer must take into account that masonry is a material whose properties vary greatly throughout its volume.

Fig. 5 Various masonry types (from E. Vintzilaiou – "Lecture notes on Advanced Mechanics of Masonry")

As we can see in Fig. 5, masonry as a construction material is, by its nature, a very variable material. It is obvious, without any analysis, that its mechanical properties cannot be the same throughout its volume.

The mechanical properties of masonry depend on the blocks' characteristics, the mortar's strength, the type of masonry employed, the construction technique, weathering of the materials and many other parameters. Therefore, the actual strength of a historic masonry wall is very hard to assess.

1.2.1 Assessing the compressive strength of masonry walls

If we take into account that the mortar's strength is around 1 or 2 MPa and the masonry blocks' strength is, usually, over 15-20 MPa, we would expect that, in compression, the mortar will crack and the masonry will fall because of the failure of the mortar. However, this is not the case, as we will see below.

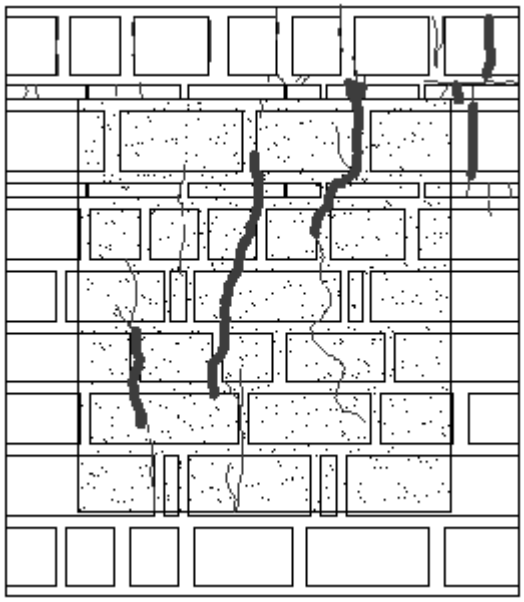

Fig. 6 Compressive cracks in tested masonry wallet (from E. Vintzilaiou – "Lecture notes on Advanced Mechanics of Masonry")

Experimental results showed that compressive cracks propagate through the blocks in the masonry wall. This means that the blocks are the first to fail, not the mortar.

Additional investigation has shown that this compressive failure, which occurs in the blocks, is a problem of Poisson ratio and tri-axial stress conditions. The masonry blocks, with a lower Poisson's ratio and a higher compressive strength, are subjected to compression in the vertical axis and to tension in the other two axes. This happens because the mortar has a higher Poisson's ratio and tends to laterally deform, but it is kept in place by the masonry blocks. Thus, the mortar, even if it has much lower compressive strength, is subjected to the very favorable tri-axial compression conditions, being provided a kind of confinement by the masonry blocks.

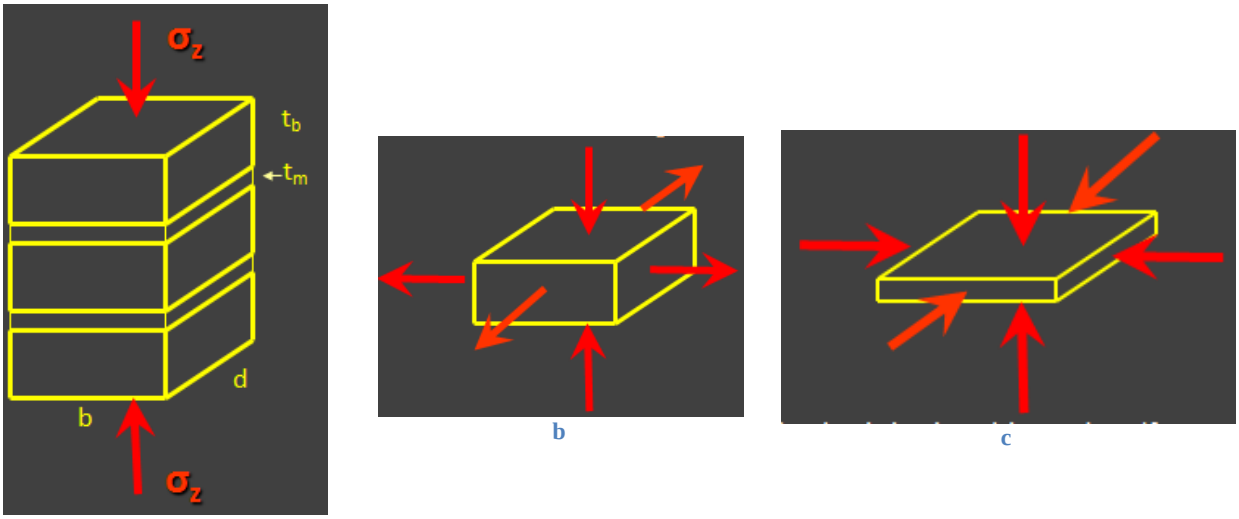

Fig. 7 State of stresses within compressed masonry wallet (a), masonry unit (b) and mortar (c) (from E. Vintzilaiou – "Lecture notes on Advanced Mechanics of Masonry")

In conclusion, for a single leaf masonry wallet, its compressive strength does not depend on the actual strength of the mortar. The mortar has, however, a very important impact on the overall compressive strength due to other properties. The mortar joint's thickness is especially important, the thicker the joint the lower the overall compressive strength.

In order to accurately assess the compressive strength of masonry, the designer needs several mechanical data of the masonry. These include the Young's modulus of elasticity or the Poisson's ratio. It is very difficult to acquire this data even in the case of modern masonry, let aside the historic masonry. Due to this reason, even for modern masonry, empirical formulae are to be used.

In the case of historic masonry, the compressive strength is computed as well using empirical formulae. One formula, suggested by prof. Tassios (Tassios, Chronopoulos: "Aseismic dimensioning of interventions on low strength masonry buildings", Middle East and Mediterranean Regional Conference on low strength masonry in seismic areas, Middle East University, Ankara, 1986) is shown below:

$$f_{wc} = \left(\frac{2}{3}\cdot\sqrt{f_{bc}} + k_1\cdot f_{mc} - k_2\right) \div \left[1 + 3.5\left(\frac{V_m}{V_w} - 0.3\right)\right] \qquad 1.1$$

Where:

V_m, V_w: the volume of the mortar and the volume of masonry (their ratio is at least equal to 0.3)

f_{bc}: compressive strength of blocks (not exceeding 100 MPa)

f_{mc}: compressive strength of mortar

k_1 = 0.6, for rubble stone masonry or 0.2 for brick or regular stone masonry

k_2= 0 MPa for brick or regular stone masonry, 0.5 MPa for semi-regular masonry or 2.5 MPa for rubble stone masonry.

However, this formula above is used in order to find out the compressive strength of a single masonry leaf. Most of the time, historic masonry structures are made of three-leaf masonry, whose compressive strength is even harder to find.

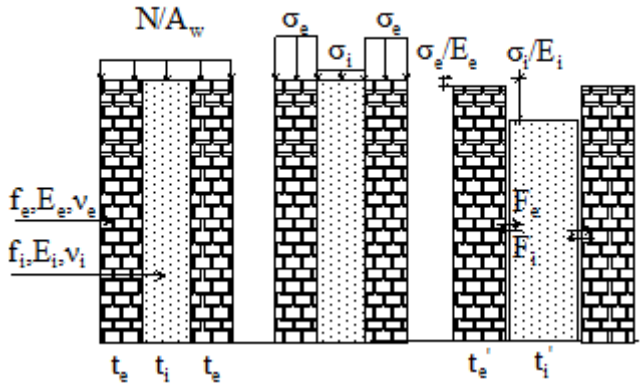

Fig. 8 Typical three leaf masonry behavior in compression (from E. Vintzilaiou – "Lecture notes on Advanced Mechanics of Masonry")

As it can be observed from Fig. 8, the three leaf masonry has some particularities when it comes to its behavior in compression. First of all, most of the load is taken by the exterior leaves, the interior filling, being more deformable, takes a lot less of the total load. Secondly, due to its lateral deformation, the interior leaf presses on the exterior leaves' surfaces and creates out-of-plane stresses on them. This is a very unfavorable condition for the exterior leaves and, in case the bond is broken between the interior filling and the exterior leaves, they fail due to out of plane bending.

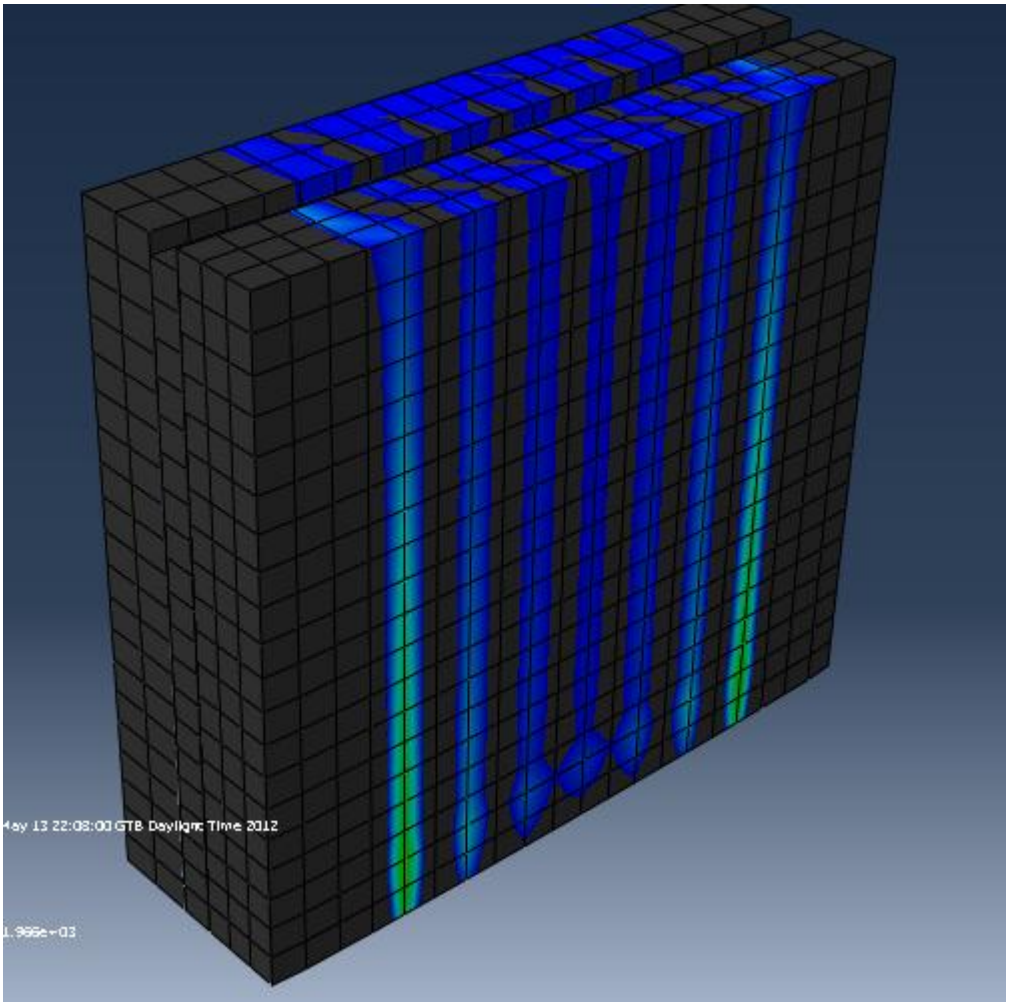

Fig. 9 Out of plane stresses in three leaf masonry subjected to vertical compression

Fig. 9, above, depicts the stresses which the interior material exerts onto the outer leaves due to the difference in Poisson's ratio and Young modulus between the two of them. It is to be noted that in the figure above the compressive stresses were ignored, so the colored areas represent tensile stresses due to out of plane actions.

In order to estimate the strength of the three leaf masonry, empirical formulae will be used once more.

In 2004, Valuzzi proposes an empirical formula for computing the compressive strength of three-leaf masonry:

$$f_{wc\_0} = \frac{V_e}{V_w} \cdot \theta_e \cdot f_{ce} + \frac{V_i}{V_w} \cdot \theta_i \cdot f_{ci} \qquad 1.2$$

In 1.2, the symbols mean the following:

f_{wc_0} : the compressive strength of three leaf masonry

V_e, V_i, V_w : the volume of the exterior leaves, interior filling and whole masonry, respectively

θ_e, θ_i : empirical coefficients taking into account interactions between exterior leaves and infill, $\theta_e < 1$ and $\theta_i > 1$.

f_{ce}, f_{ci} : compressive strength of exterior leaves and infill, respectively.

Another formula for computing the compressive strength of three-leaf masonry has been proposed by prof. Tassios:

$$f_{wc} = \left(2\lambda_e \cdot \delta \cdot f_{wc\_e} + \lambda_i \cdot f_{wc\_i}\right) \div (1 + 2\delta) \qquad 1.3$$

The value of the symbols in 1.3 is explained below:

f_{wc} : compressive strength of three-leaf masonry (and of the exterior and interior leaves, respectively)

$\lambda_e = 1 - 0.06\zeta_e \cdot t_e \cdot h_w^{\frac{-4}{3}}$, is a correction factor, where t_e is the thickness of the exterior leaves (in mm) and h_w is the height of the masonry (in mm),

$$\zeta_e = \frac{E_{we}}{f_{wc\_e}}$$

δ: ratio between the thickness of the exterior leaf and that of the infill.

Using the above mentioned formulae, we can assess the compressive strength of three-leaf masonry and, afterwards, its resistance to different kinds of stresses can be estimated.

1.2.2 Assessment of other mechanical characteristics

In the sections before, the assessment of the compressive strength of three-leaf masonry walls has been presented. While this is the starting point for the estimation of most of the mechanical properties of masonry, it has to be borne in mind that, for a realistic modeling, other mechanical characteristics have to be estimated as well.

1.2.2.1 Estimating the modulus of elasticity (E)

Experimental tests performed on wallets of masonry showed that, while a connection between the compressive strength and the elasticity modulus of masonry can be observed, there is a significant scatter of data when it comes to the actual numerical values.

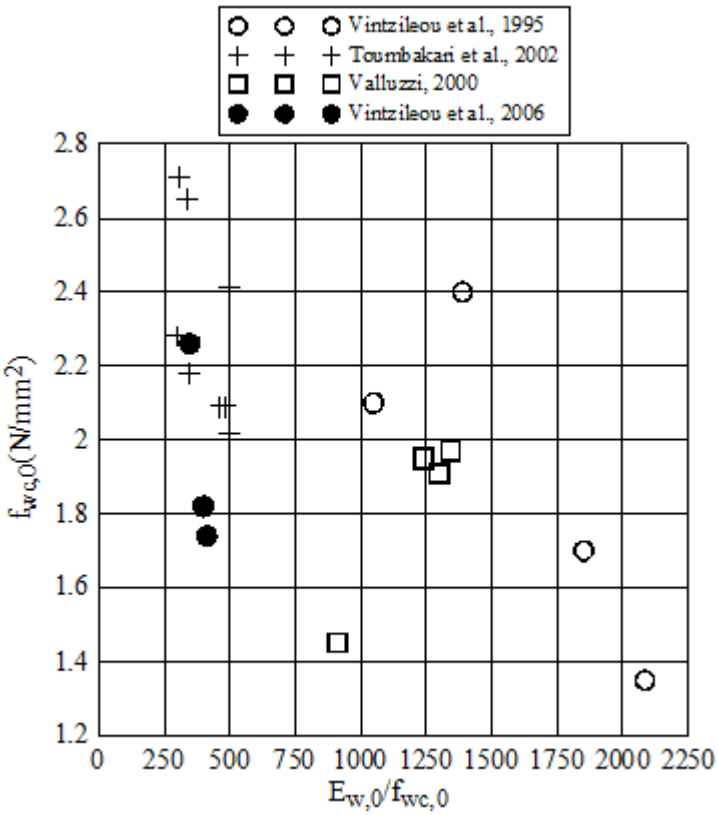

Fig. 10 The scatter of elasticity modulus with respect to compressive strength (from E. Vintzilaiou – "Lecture notes on Advanced Mechanics of Masonry")

As it can be seen in Fig. 10, the masonry elasticity modulus's values can range anywhere from 300 up to 2100 times its compressive strength. This is a very large interval and, for better results, a parametric study is often undergone when the elasticity modulus's exact value is desired, especially when the deformations are of significance.

1.2.2.2 Shear strength of masonry

In-plane shear is one of the two critical action-effects that affect masonry structures subjected to earthquakes. During the shear deformation of the masonry, the inclined strut which is formed is subjected simultaneously to compression and to transverse tension. This state of stresses is very unfavorable, as it significantly decreases its compressive strength. Failure normally occurs due to the opening of the inclined cracks.

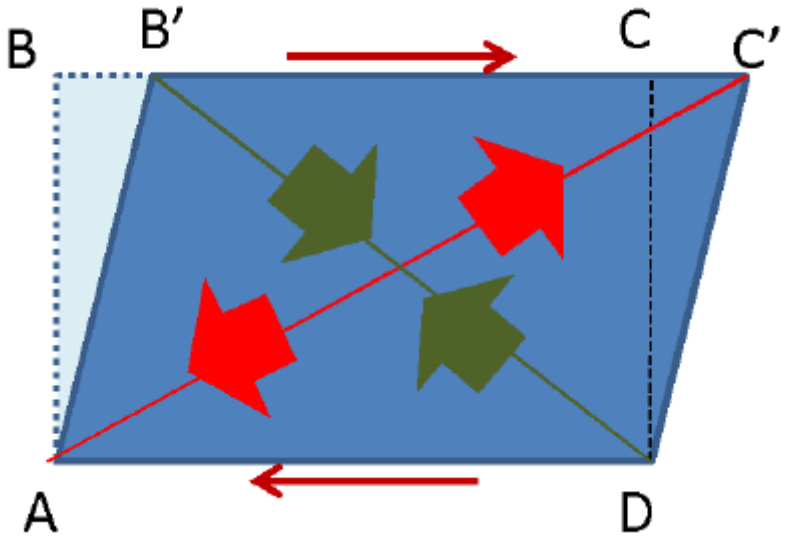

Fig. 11 Typical block deformed due to shear action

Fig. 12 Shear failure of masonry (from E. Vintzilaiou – "Lecture notes on Advanced Mechanics of Masonry")

As we can see in Fig. 12, the shear cracks do not necessarily have to be bi-directional (i.e. in the both diagonal directions). This depends on the characteristics of the motions, because in order for

the second shear crack to form, the first one must close and, thus, a higher displacement is necessary.

In general, the mechanisms resisting shear within a masonry structure are the cohesion and the friction between blocks or blocks and mortar.

$$f_v = c + \mu\sigma \quad (1.4)$$

Where:

f_v : shear strength of masonry

c : cohesion (shear resistance under zero normal stress) ~ 0.10-0.20 MPa

μ : friction coefficient (conservative values around 0.40-0.50)

σ : normal stress on the analyzed masonry.

It has to be taken into account that, due to the very limited ductility presented by the masonry, a cyclic shear loading of the masonry will result in a disintegration of itself.

1.2.2.3 Tensile strength of masonry

The tensile strength of masonry is very small and for this reason it is not relied upon to sustain loads. This assumption comes not only from the very small tensile strength of masonry but also because the appearance of tensile cracks does not necessarily mean that the masonry has failed.

Tensile stresses occur more often due to the masonry element being subjected to out-of-plane bending.

1.2.2.4 Masonry subjected to out-of-plane bending

Due to the fact that, in a masonry element, eccentricities are inherent and unavoidable, almost every load-bearing masonry element will be subjected, to a certain extent, to out-of-plane bending.

Also, out of plane bending occurs when the infill is compressed and, due to higher Poisson ratio, “pushes” on the exterior leaves.

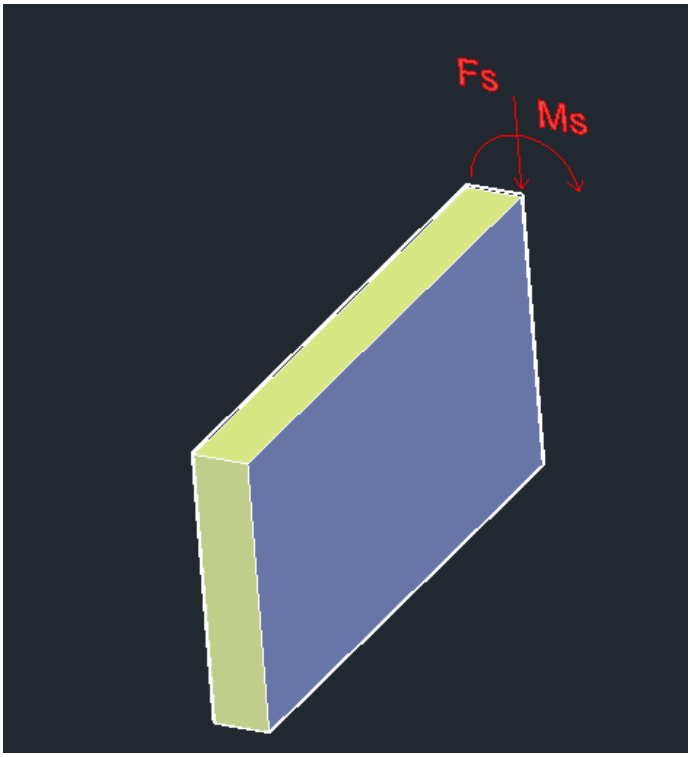

Fig. 13 Out of plane bending typical situation

For the situation described above, the resisting moment of every section (throughout the height of the masonry element) can be computed with the following formula:

$$M_R = \frac{\sigma \cdot l \cdot t^2}{2} \cdot \left(1 - \frac{\sigma}{f_c}\right) \geq M_S \qquad 1.5$$

In 1.5 above, the symbols have the following meanings:

M_R : the resisting moment of the wall section

σ : normal stress on the cross-section we compute the moment for

l : length of the masonry element (height of cross-section)

t : thickness of masonry element (width of cross-section)

f_c : compressive strength of the masonry element.

1.2.3 Interventions on masonry structures

1.2.3.1 Basic aspects

The interventions for masonry structures have been a subject for numerous works and papers throughout the years. Because of the very special cases encountered in this domain, separate opinions continue to exist to this day in what regards the acceptable interventions to be applied to historic masonry structures.

The aim of these interventions is not to prevent any type of crack or other minor damage. Due to the fragility of this type of buildings, preventing every possible failure is, practically, impossible. The interventions should, therefore, ensure an approximate structural integrity to the building in question. These measures should, firstly, safeguard against the collapse of the building in case of an extreme event (such as an earthquake) and, in many cases, the interventions are specially designed so that they protect certain valuable elements in the historic building (frescos, mosaics etc.).

A multiple static indeterminate system is desired, so that the total collapse of the building is prevented (in case one or more elements fail).

Depending on their specific characteristics and of their objective, the interventions for masonry structures can be categorized in several groups:

1. Local interventions to load bearing elements

   These interventions are applied when, in principle, the bearing system is adequate, but some elements are not resistant enough. The intervention consists in enhancing the stiffness, the bearing capacity or the deformation capacity, or the interconnection of a limited number of elements, without major alteration to the bearing system.

   If such an intervention is sufficient, it is desirable and preferable from the economic point of view.

2. Alleviation of irregularities

   It is applicable when the analysis proves that some elements cannot satisfy the deformation requirements: when the irregular distribution of mass, stiffness and strength leads to excessive requirements in some regions of the building. In these cases, the alleviation of irregularities constitutes the best solution.

   However, such a solution may not be applicable in structures of high architectural value, due to the obvious reason that, perhaps, the very irregularities consist the real value of those structures.

3. Global enhancement of stiffness

   This type of intervention is applied when it is proven that the deformations imposed in a large number of elements are larger than those they can resist.

   In such a case, a general enhancement of stiffness may lead to significant reduction of the imposed deformations (to values lower than those the elements are able to sustain)

   Two main techniques are representative for this type of interventions:

   a) The technique of reinforced concrete jackets.
      Although this intervention is technically correct, it is usually not advisable (or permitted) in the case of historic buildings. The same holds true for the similar technique of increasing the element section.

   b) The enhancement of the diaphragm action of floors and roof.
      This technique consists of improving the 'box' behavior of the building by improving the stiffness of the floors and roof. Through this procedure, all the elements should deform more or less equally and, thus, a better distribution of action effects is acquired, from the point of view that all the elements contribute to resisting the actions imposed.

4. Global enhancement of bearing capacity

   This intervention procedure is to be applied when either significant damage has occurred to a large number of elements or large inelastic deformations are expected to occur. In these cases, the procedures employed for the enhancement of global bearing capacity are as follows:

   a) Strengthening of existing elements

   b) Adding new bearing elements (or transforming of selected non bearing elements to bearing elements)

   c) Combination of (a) and (b).

   It has to be noted that the inevitable enhancement of stiffness has to be taken into account when employing these techniques.

5. Reduction of masses

   In principle, this technique is employed for structures that are located in areas with seismic potential.

   Among the possible procedures employed for mass reduction, we can distinguish:

a) Modification of the system of the roof (i.e. substitution of a heavy roof by a light steel or timber roof – preferably with adequate diaphragm action)

b) Lightweight pavements

c) Change of use (reduction of live loads)

6. New independent bearing system (against seismic actions)

   When it has been proven that the existing bearing system cannot sustain the design seismic actions and when the importance of the building does not allow the application of 'heavy' interventions to existing elements, it is preferable to employ a new, independent, bearing system.

   The new bearing system can be constructed wither in the interior or in the exterior of the building, depending on the specifications of the structure in question. The main issue with this kind of intervention is its reversibility.

   If the new bearing system takes part in sustaining the vertical loads and is connected to the old system, a check of compatibility of deformations must be performed.

7. Seismic isolation or transport of entire building to another location

   These solutions are considered extreme and are very difficult to apply to the fragile historic masonry structures.

From the above-mentioned interventions, two of them were employed on the tested structure: grouting of the walls (enhancement of load bearing capacity of the walls) and the enhancement of the diaphragm action of the floor and roof.

1.2.3.2 Enhancement of the diaphragm action of the floor and roof

The main object of the laboratory experiment studied was to assess (or, rather, to prove) the efficiency of the enhancement of the diaphragm action technique.

The main advantages of the enhancement of diaphragm action of floors and roof are:

- It is a 100% acceptable intervention, as it does not alter the original bearing system
- Its efficiency, as it ensures (more or less) equal displacements to all vertical elements. Thus, localized large displacements and resulting local damages are avoided

- It modifies the support conditions of vertical elements (from cantilever to fixed-fixed), thus, out-of-plane bending moments in critical areas are reduced
- It reduces the necessity of interventions on other elements
- It is very feasible, as the materials employed can be either modern or similar to the original ones
- To an extent, this technique can be considered reversible
- It does not lead to a significant increase of the masses
- As it significantly increases the global stiffness of the structure, it may result the shift of the structure to the left portion of the response spectrum, thus reducing the conventional seismic actions

However benefic this technique may be, certain prerequisites are needed in order to ensure an adequate behavior and outcome of the intervention.

First of all, the diaphragm must be adequately connected to the vertical elements. This feat ensures that the diaphragm is playing its part and transmits the loads equally to the load bearing element. The lack of a good connection can mean that the efficiency of the intervention is compromised.

The second important prerequisite is that the masonry supporting the diaphragm should be adequately repaired or strengthened. If the vertical masonry elements do not have sufficient strength so that they can withstand the loads coming from the diaphragm, this technique backfires and has a negative effect, due to the difference in stiffness. In case of a seismic event, the diaphragm (much stiffer) will crash with the vertical elements (less stiff) and will, possibly, destroy the vertical elements, as it is presented in Fig. 14 below.

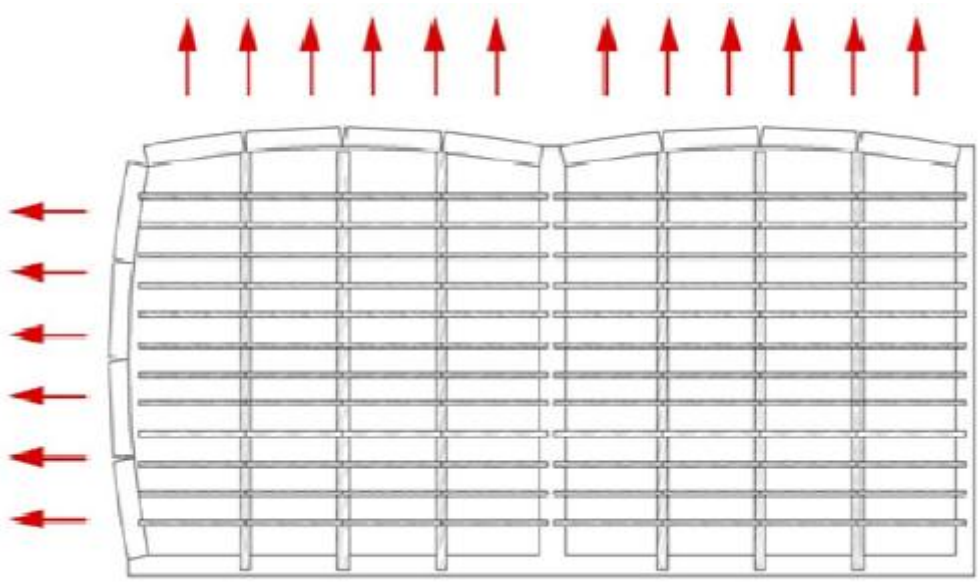

Fig. 14 Typical failure due to inadequate strength of the vertical elements supporting the diaphragm (from E. Vintzilaiou – "Lecture notes on Advanced Mechanics of Masonry")

This type of failure is a very plausible scenario and several real-life events have proven that great attention should be paid to the adequate strengthening of the vertical elements supporting the diaphragm. In the studied case, the walls of the strengthened building have been grouted.

Fig. 15 Typical failure due to inadequate stiffness of the wall (a) (from E. Vintzilaiou – "Lecture notes on Advanced Mechanics of Masonry")

Fig. 16 Typical failure due to inadequate stiffness of the wall (b) (from E. Vintzilaiou – "Lecture notes on Advanced Mechanics of Masonry")

Fig. 17 Typical failure due to inadequate stiffness of the wall (c) (from E. Vintzilaiou – "Lecture notes on Advanced Mechanics of Masonry")

Fig. 18 Typical failure due to inadequate stiffness of the wall (d) (from E. Vintzilaiou – "Lecture notes on Advanced Mechanics of Masonry")

The techniques used for applying this procedure must ensure the efficiency of the intervention and, also, safeguard against the aforementioned risks and failures.

The enhancement of diaphragm action of the timber floors can be acquired by using several strategies. The most commonly adopted techniques are as follows:

- Overlaying of another layer of flooring, oriented at another angle (usually 45˚), from the original layer (Fig. 19).
- Improvement of diaphragm action by employing diagonal steel ties (Fig. 20).
- Pouring of a concrete slab over the existing flooring, connected to this by stud connectors (not recommended for historic structures, especially of architectural value) (Fig. 21).
- Using Fiber Reinforced Polymers (FRP) in order to improve the diaphragm action (Fig. 22).

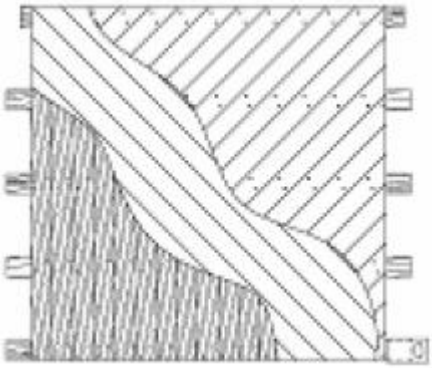

Fig. 19 Overlaying of another, skewed flooring layer (from E. Vintzilaiou – "Lecture notes on Advanced Mechanics of Masonry")

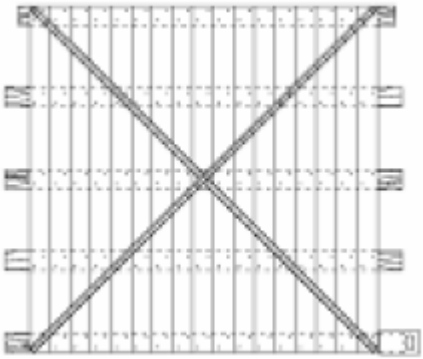

Fig. 20 Employing diagonal steel ties (from E. Vintzilaiou – "Lecture notes on Advanced Mechanics of Masonry")

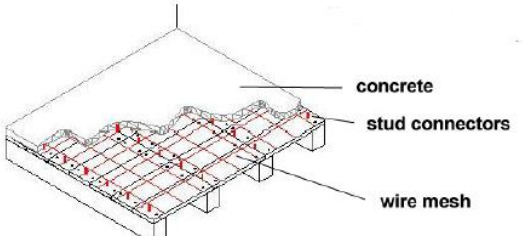

Fig. 21 Pouring of concrete slab (from E. Vintzilaiou – "Lecture notes on Advanced Mechanics of Masonry")

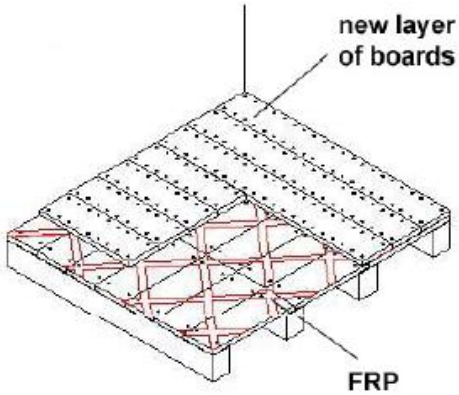

Fig. 22 Employing FRP-s for enhancing diaphragm action (from E. Vintzilaiou – "Lecture notes on Advanced Mechanics of Masonry")

Apart from the techniques employed for improving the diaphragm action per se, another set of measures must be taken in order to improve the connection between the newly-created diaphragm and the vertical elements.

The connection between the floors and the walls can be improved using a multitude of techniques, such as:

- Connecting the floors to the walls using steel bars (Fig. 23)
- Improving the connection by using steel bolts (Fig. 25, Fig. 26)
- Improvement of the connection by the use of nailed wooden elements (Fig. 24)

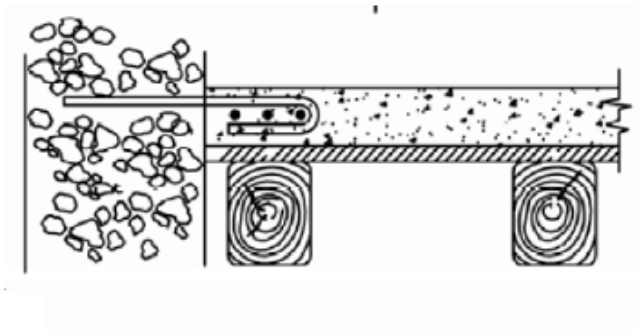

Fig. 23 Steel bars used for connection improvement (from E. Vintzilaiou – "Lecture notes on Advanced Mechanics of Masonry")

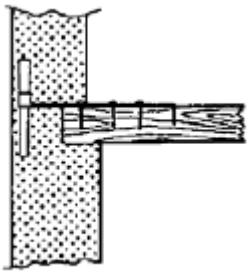

Fig. 24 Wooden elements used for connection improvement (from E. Vintzilaiou – "Lecture notes on Advanced Mechanics of Masonry")

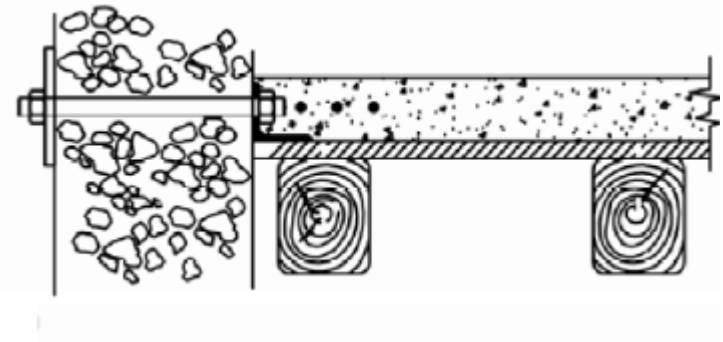

Fig. 25 Steel bolts used for connection improvement (a) (from E. Vintzilaiou – "Lecture notes on Advanced Mechanics of Masonry")

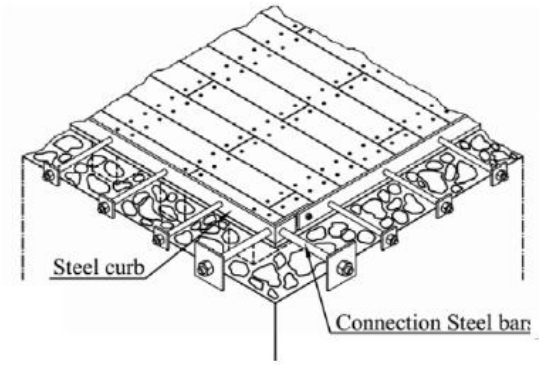

Fig. 26 Steel bolts used for connection improvement (b) (from E. Vintzilaiou – "Lecture notes on Advanced Mechanics of Masonry")

Within the studied structure, the improvement of the diaphragm action was acquired employing another layer of flooring, placed over the original layer at an angle on 45˚ and fixed to the timber beams (joists) using long bolts.

The connections were improved using steel elements, similar to the ones in Fig. 25.

1.2.3.3 Grouting

As three-leaf masonry is a construction type very common in buildings belonging to the cultural heritage, grouting is a very popular intervention technique when talking about these buildings.

- *Advantages, prerequisites and techniques*

Grouting is one of the most efficient intervention techniques for the improvement of the behavior of three-leaf masonry. It consists in injecting a mortar mixture (grout) into the inner leaf (weak part) of the masonry. The idea is that the grout will fill the voids in the inner leaf and, as well, it will be absorbed by the mortar found there, increasing its bearing capacity as well. The voids in the inner leaf are created due to the decay of the material or other various actions.

The drawback of the grouting of masonry elements is that it is an irreversible technique.

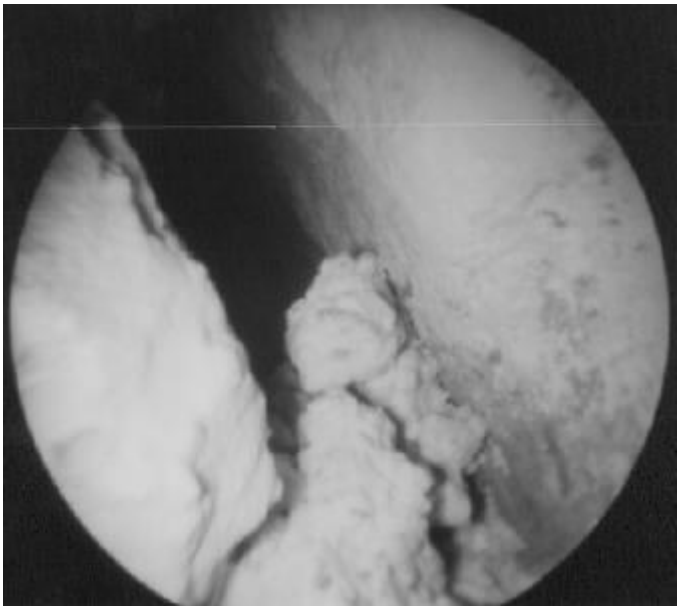

Fig. 27 Paroscope image of void in interior leaf (from E. Vintzilaiou – "Lecture notes on Advanced Mechanics of Masonry")

The application of grouts can be only undergone if some basic requirements are fulfilled:

- The grout should be compatible with the in situ materials (from the physical-chemical point of view)

- The grout should also be mechanically efficient (in terms of enhancing the basic material properties of masonry)

The first application of hydraulic grouts in order to strengthen three-leaf masonry elements dates back to the early 1980's. However, this first attempt was a failure because the grout that was used was a pure cement grout. Due to its low injectability, the experiment has failed.

The following years, attempts have been made using cement based grouts with improved injectability. These grouts contained cement in a proportion of around 50-75% and some other components like lime, pozzolan or silica fume. Their compressive strength reached around 30 MPa, whereas their tensile strength was in the region of 3 MPa. This type of grouts, however, did not render very efficient results so other alternatives were researched.

Ternary grouts have a reduced cement content (in the region of 30-50%). They have proven to be more efficient and, as well, more workable. Their compressive strength can reach up to 10 MPa and their tensile strength is in the region of 3 MPa.

Hydraulic lime-based grouts are, probably, the best solution for grouting historic masonry. They contain no cement at all and have compressive strengths of at most 6 MPa and tensile strengths in the region of 4 MPa.

Fig. 28 Masonry wallet during grouting (from E. Vintzilaiou – "Lecture notes on Advanced Mechanics of Masonry")

- *Mechanical properties of grouted masonry*

The mechanical properties of grouted masonry are a subject of discussion and there is still much progress to be made in their assessment.

After several experiments and tests, an apparent connection between the mechanical properties of the employed grout and the ones of the grouted masonry has been observed.

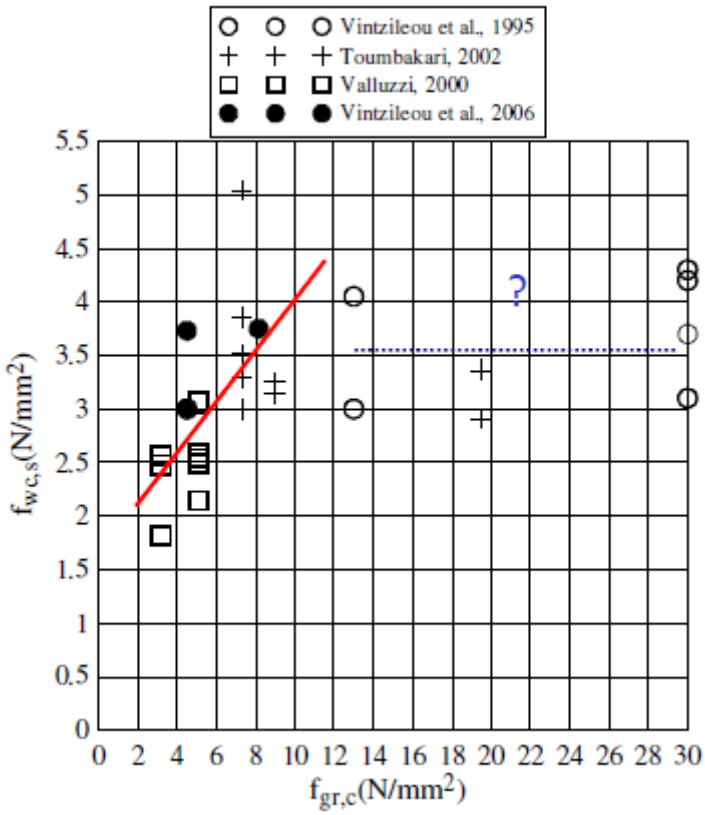

Fig. 29 Compressive strength of masonry vs. compressive strength of grout (from E. Vintzilaiou – "Lecture notes on Advanced Mechanics of Masonry")

As it can be observed in Fig. 29, an approximately linear relation can be observed between the compressive strength of the grout and the compressive strength of grouted masonry, up to a point. After that point, no matter how much the grout's compressive strength is increased, the grouted masonry seems to remain constant. This phenomenon has been largely analyzed and, after numerous debates and tests, it has been concluded that the compressive strength of the grouted masonry also depends on the grout's tensile strength. More precisely, the mechanical properties of grouted masonry are greatly increased when, for grouting, mixtures which have comparable tensile and compressive strengths.

The key parameter for everything to render the best results is the bond between the grout and in-situ materials. This bond is ensured by a good tensile strength of the grout.

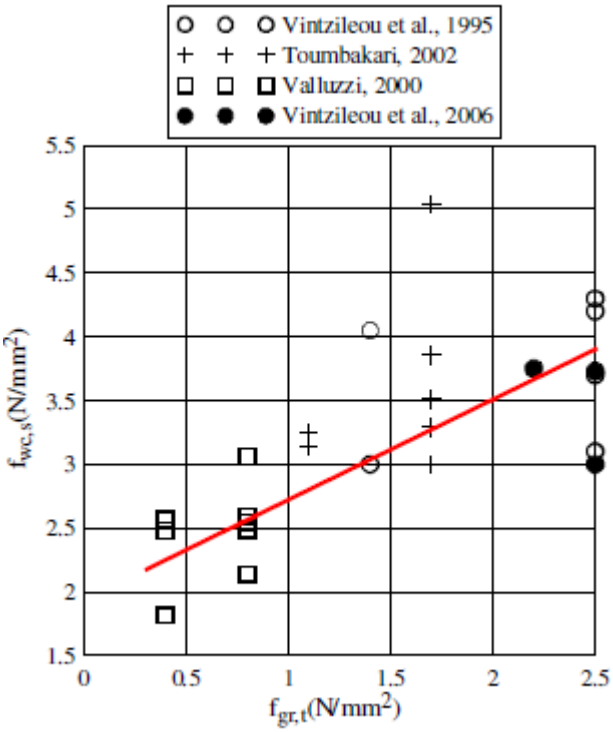

Fig. 30 Compressive strength of masonry vs. tensile strength of grout (from E. Vintzilaiou – "Lecture notes on Advanced Mechanics of Masonry")

As it can be seen in Fig. 30, the parameter which is the best assessment for the efficiency of the grout is its tensile strength. However, the parameter used (in empirical formulae) to compute the capacity (compressive strength) of masonry is the grout's compressive strength. This is because these formulae only refer to a certain class of grouts, more exactly hydraulic lime-based grouts, which have the ratio between their tensile and compressive strengths in a certain range.

- *Assessing the mechanical properties of grouted masonry*

As it has been previously stated, the assessment of the mechanical characteristics of grouted masonry is a very delicate subject and the main aspect to be kept in mind when dealing with such a situation is that the natural phenomena are impossible to replicate.

Taking this into account, some empirical formulae have been developed for assessing the compressive strength of the grouted masonry. As the name suggests, these formulae are based on experimental results and they are, to this date, the best approximations of the real phenomena that occur within these cases.

$$f_{wc\_i} = f_{wc\_0} \cdot \left(1 + 1.25 \frac{V_i}{V_w} \cdot \frac{\sqrt{f_{gr\_c}}}{f_{wc\_0}} \right) \qquad 1.6$$

The formula 1.6 is the first proposed formula for assessing the compressive strength of grouted masonry. The terms in the formula have the following significances:

f_{wc_i}	-	Compressive strength after grouting
f_{wc_0}	-	Initial compressive strength of the masonry
V_i	-	Volume of the interior leaf (infill)
V_w	-	Total volume of the wall (element)
f_{gr_c}	-	Compressive strength of grout

Although this formula has been proven to be rather accurate, tests have shown that an additional safety factor (usually of 1.35) is needed in order for the result to be "on the safe side".

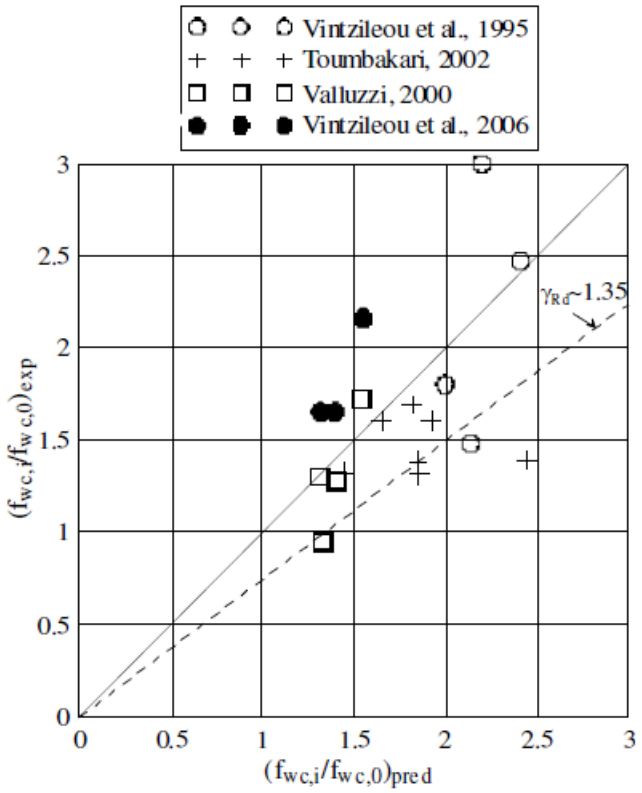

Fig. 31 Fitting of the first formula for assessing grouted masonry (from E. Vintzilaiou – "Lecture notes on Advanced Mechanics of Masonry")

The second formula for assessing the compressive strength of grouted masonry was proposed by Valluzzi in 2004. It has been deducted from tests on cylinders containing infill and grout.

$$f_{wc\_i} = f_{wc\_0} \cdot \left(1 + \frac{V_i}{V_w} \cdot \frac{f_{i\_s}}{f_{wc\_0}}\right) \quad 1.7$$

In formula 1.7 above, the symbols used have the following meanings:

$f_{i\_s} = 0.31 \cdot f_{gr\_c}^{1.18}$ - Compressive strength of infill after grouting

f_{wc_i} - Compressive strength after grouting

f_{wc_0} - Initial compressive strength of the masonry

V_i - Volume of the interior leaf (infill)

V_w - Total volume of the wall (element)

f_{gr_c} - Compressive strength of grout

Experimental results have shown that:

$$f_{i\_s} = 1.6 + 0.5 f_{gr\_t} \quad 1.8$$

Where:

f_{gr_t} - Tensile strength of grout

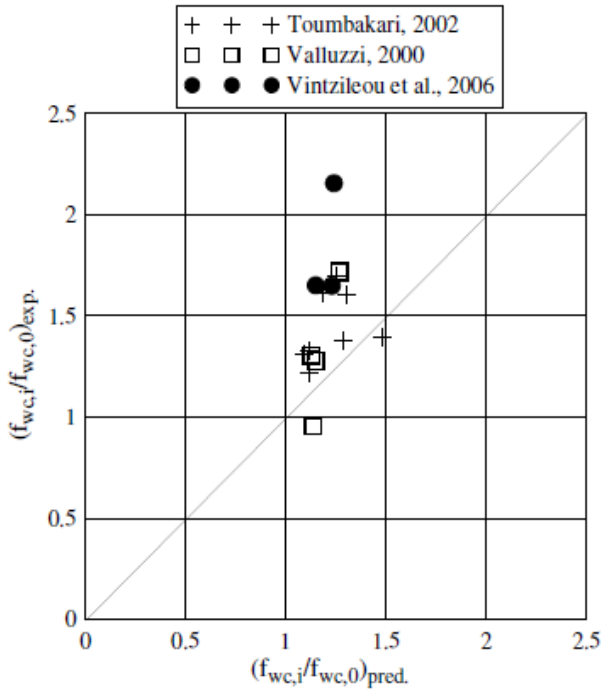

Fig. 32 Fitting of formula 1.7 to experimental data (from E. Vintzilaiou – "Lecture notes on Advanced Mechanics of Masonry")

In some cases, however, rubble stone masonry in historic structures does not have a clear intermediate zone of filling material. For these instances, a new formula has been elaborated.

$$f_{wc\_s} = f_{wc\_0} \cdot \left[1 + 0.013 \left(100 \cdot \frac{G_{gr}}{G_0} \right)^3 \right] \qquad 1.9$$

In 1.9, the symbols used have the following significances:

- f_{wc_0} - Initial compressive strength of the masonry
- f_{wc_s} - Compressive strength after grouting
- G_{gr} - Total volume of the injected grout
- G_0 - Volume of masonry

The above mentioned formula is based on experimental results obtained by Tomazevic, Sheppard (1982), Tomazevic, Apih (1993) and Betio et al. (1993).

1.3 Presentation of the NIKER project

As it has been mentioned before, the experiment analyzed in this paper is part of the NIKER European project. This project is founded by the European Union and is carried out as a cooperative project by several universities and institutions throughout Europe and Israel, Egypt, Morocco and Turkey.

The project tackles the problem of earthquake-impact on Cultural Heritage assets starting from basic consideration that efficient protection, with substantial guarantee of compatibility and low-intrusivity, can only be achieved with minimum intervention approach. This requires that potentialities of existing materials and components are as much as possible exploited in terms of strength and energy dissipation, and candidate interventions are validated and optimized on specific, real application conditions.

At the project start, earthquake-induced failure mechanisms, construction types and materials, intervention and assessment techniques were cross-correlated with the aim of developing new integrated methodologies with a systemic approach. The enhancement of traditional materials by an industrial process is also desired (e.g., nano-limes or micro-silica for injection), and new high-performance (e.g. dissipative) elements are to be developed. Novel collaborative combinations of the aforementioned materials are tested on structural components (walls, pillars, floors, vaults) and on structural connections (wall-, floor- and roof-to-wall), which converge the behavior of single strengthened elements into the global structural response.

The envisaged techniques have to be validated on model buildings and substructures. Advanced numerical studies are carried out and will allow parameterizing the results and deriving simple and optimized design procedures. Early warning techniques for intelligent interventions and advanced monitoring techniques for knowledge based assessment and progressive implementation of interventions will be also developed.

This bottom-up approach will bring new integrated materials, technologies and tools for systemic improvement of seismic behavior of CH assets. The new solutions will be condensed into guidelines for end-users. The large participation of research centers, SME, and end-user from various countries, including ICPC and MPC, ensures increased impact of the research.

2 MODELING OF THE STRUCTURE

This work will include two main models: one model in order to assess the behavior of the structure in its initial (unreinforced) state and the other model to analyze the reinforced masonry building.

The building is a three-leaf unreinforced rubble-stone masonry structure, built at a scale of ½ from the real model. Additional loads have been placed at the 1st floor and at the roof level, in order to provide accuracy and a more realistic approach.

Apart from the models mentioned above, there will be other additional models in order to enable a good and accurate analysis of the studied case.

2.1 Materials used in the modeling

The studied building is made up of two materials: three-leaf rubble stone masonry and timber class C18. In order to assess the properties for these materials, we need some data to start with.

2.1.1 Timber C18

The strength of a timber, whether new or historic, depends on its species and the effects of certain growth characteristics. In particular, knots and shakes (splits along the grain which occur as the timber dries) and the slope of its grain reduce its strength – the ideal timber has straight grain with no knots or drying shakes. Strength grading involves assessing the effect of these features.

For structural purposes new timber is supplied in 'strength classes' that determine the allowable working stresses. As the strength class depends on both the species and the grade of the piece, design engineers may specify the required strength class of the timber, leaving it to the supplier to select a species and grade to meet that specification. In all there are 16 strength classes set by the European standard BS EN 519, ranging from C14, the lowest softwood strength class through to D70 the strongest hardwood strength class.

Of course, where old and historic timbers are to be retained, the conservator is not in a position to select timber of the appropriate strength class: the existing timbers must be assessed to determine their strength, particularly where alterations are likely to impose new loadings, or where the timbers have been affected by deterioration. Although the strength class and grading system is not ideal for assessing existing historic timbers, it forms the basis of standard practice today and needs to be adapted to suit.

The timber used for the construction of the floors and the window lintels is a softwood timber, class C18.

The properties used for describing the material employed to simulate timber in our model can be seen below. Please note that we have employed an orthotropic material which has been defined by using engineering constants.

Table 1 Properties of material used to simulate timber C18

ρ (kg/m^3)	E1 (Pa)	E2 (Pa)	E3 (Pa)
	9.00E+09	5.90E+08	5.90E+08
	v1	v2	v3
400	3.40E-01	3.80E-01	4.00E-01
	G1 (Pa)	G2 (Pa)	G3 (Pa)
	5.60E+08	5.60E+08	5.60E+08

Although timber is an orthotropic material having different behavior in each direction (longitudinal 1, radial 2 and tangential 3), we will assess it as being an orthotropic material having one type of a behavior in the longitudinal direction and another type of behavior in both the radial and the tangential direction. We can do this simplification as the difference between the radial and tangential behavior is of no interest.

2.1.2 Three-leaf rubble stone masonry

For the modeling of the masonry elements, an elastic isotropic material will be employed. This is, as it has been stated before, a simplistic approach but, nevertheless, it renders accurate enough results. It has to be borne in mind that masonry is not isotropic and it can only bear very small strains.

The assessment of the mechanical properties of three-leaf masonry has been a widely debated subject, being the object of study of many papers.

Because the studied case is a laboratory test, certain properties of the components of the masonry are available, such as: the compressive strength of the blocks used, Young's modulus of the masonry, etc. Having these data available, along with the technique used in the construction process, an estimation of the mechanical properties of the masonry as a material can be undergone.

Unfortunately, even in controlled laboratory conditions, some necessary characteristics' values are very difficult to be extracted.

Table 2 Known data about the masonry in its initial state

Characteristic	Value	Description
fc_stone	100 Mpa	compressive strength of stone blocks
Ei	0.8 GPa	Young's modulus of masonry (pre-grouting)

As it can be observed in Table 2, the known values are rather limited. Fortunately, the Young's modulus of elasticity for masonry (as a composite material) is provided. This is the Young's modulus which will be assigned, in our analysis, for the elastic material used to simulate masonry.

Due to the limitations in the known data, the compressive strength of masonry is very difficult to be (exactly) assessed. As no data about the width of the leaves or the compressive strength of the mortar has been provided, the only thing that remains to be done is assessing the compressive strength of masonry by approximating it with the mean value coming from the relation between the modulus of elasticity and the compressive strength. It can be, therefore, stated that the probable masonry compressive strength lies in the region of 1 MPa, for the ungrouted masonry.

2.2 Assumptions made in the modeling phase

"Make everything as simple as you can, but not simpler"

Albert Einstein

As civil engineers, it is our responsibility to be aware that nature is inimitable.

2.2.1 General assumptions

The assumptions which are made during an analysis of a cultural heritage structure are, in fact, the turning point of the whole analysis. Their nature can seriously affect the outcome of the analysis, so the civil engineer should be very careful when assuming certain things within such a project.

As it has been stated before, nature cannot be, unfortunately, imitated. This fact reflects in the work of this project and the analysis is done bearing in mind that we are modeling an 'ideal' situation, not the real one.

One of the assumptions made in this project is, of course, the homogeneity of the material. This may be the most powerful simplification in this model as it is a well-known fact that it is very difficult to find a more non-homogenous material than masonry (especially historic masonry). In this project, however, the assumption of the same material properties in any point of the material will be employed. The characteristics which will be used to define the two types of masonry in this work have been previously computed. The masonry will be modeled as an elastic, isotropic material. Of course, masonry is neither perfectly elastic and by no means is it isotropic. When interpreting the results which will be obtained, it has to be borne in mind that the 'real' masonry will never behave like the material employed. The model used here will have estimative results and it will be a mere indication for the civil engineer to assess the behavior of the real structure.

It has to be borne in mind that the connections between masonry elements (i.e.: walls) have been considered perfect (no slip, perfect contact). This is a simplistic assumption and the analysis must be carried out with greater attention. The improvement of the connections between elements is, by itself, a way of improving the behavior of this kind of structures.

Another assumption which will be taken into account is the perfect boundary conditions assumption. This means that we have considered the building as being encased at its bases. Of course, there is no such thing as a perfect foundation; moreover, the shallow foundations used in historical structures are far from that depiction.

Also, when talking about the wooden floor, it has to be mentioned that the interactions between the wooden boards which comprise the flooring will be neglected (no friction between the boards, the boards only interact with the joists). This is, of course, a realistic and logical assumption.

2.2.2 Assessing the connection between the wooden floors and the masonry structure

Fig. 33 Detail of the connection between floor and walls

As it can be seen in Fig. 33, the beams (joists) supporting the floor boards are themselves supported by the walls at each end. This connection cannot be assessed as being rigid, because one of the intervention measures taken within this experiment is the rigidization of this connection. We will therefore have to assign, in the initial situation, a different type of connection from the rigid one. One option could be assigning a connector section in order to simulate a nailed connection.

In order to assess this connection, a detailed model will be built, in order to describe the real situation as accurately as possible. After this model is built and assessed, a new model will be sought for, one which replicates as good as possible the results from the previous model.

We will use the eigenfrequency of the floor and the respective displacements arising from different loading cases (the displacements and response in the plan of the diaphragm are of particular interest).

2.2.2.1 Initial floor model

The floor has been modeled with its real dimensions and the wooden elements supporting the floor joists have been modeled. These elements will be considered as having the vertical displacement and the rotation along their longitudinal axis restricted and they will be linked to the floor joists by connectors replicating nails.

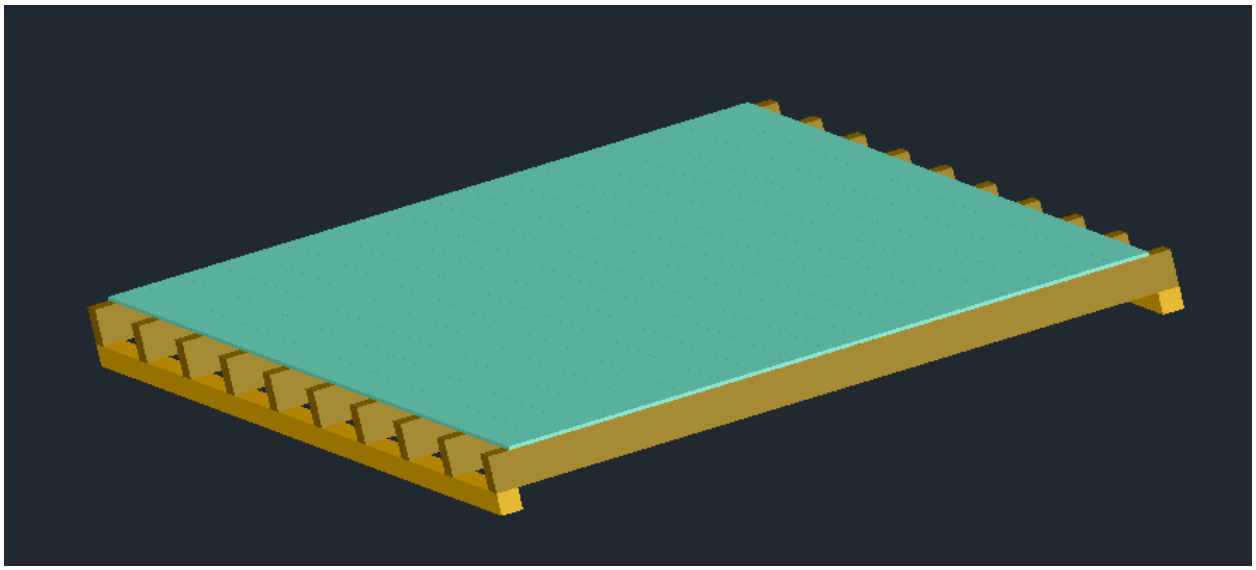

Fig. 34 3D floor realistic model

The connectors employed are basically made up of two non-linear springs each. These springs are one line spring (replicating the pull-out resistance of the nails) and one rotational with very low stiffness.

The characteristics of the connector elements used to model the nails tying the joists to the supports can be seen in the tables below:

Table 3 Pull-out resistance of modeled nails

Pull-out resistance	
F (N)	U (m)
550	0.0002
630	0.0005
660	0.002
690	0.004
700	0.005
680	0.008
650	0.01

Table 4 Rotational behavior of modeled nails

Rotational Behavior	
M (Nm)	UR (rad)
2.8	0.05
4	0.07
4.8	0.1
6	0.17
6.7	0.25
6.9	0.3
6.7	0.4

In Table 3 and Table 4 above, the characteristics of the connector elements employed to simulate the nails are depicted. These data are taken from the tests undergone by Thang Nguyen Dao and John W. van de Lindt and described in their work, "New Nonlinear Sheathing Fastener Model for Use in Finite-Element Wind Load Applications".

The meshing of this model also presented some problems, due to the very thin solid elements employed to simulate the flooring and the numerous interactions in the model.

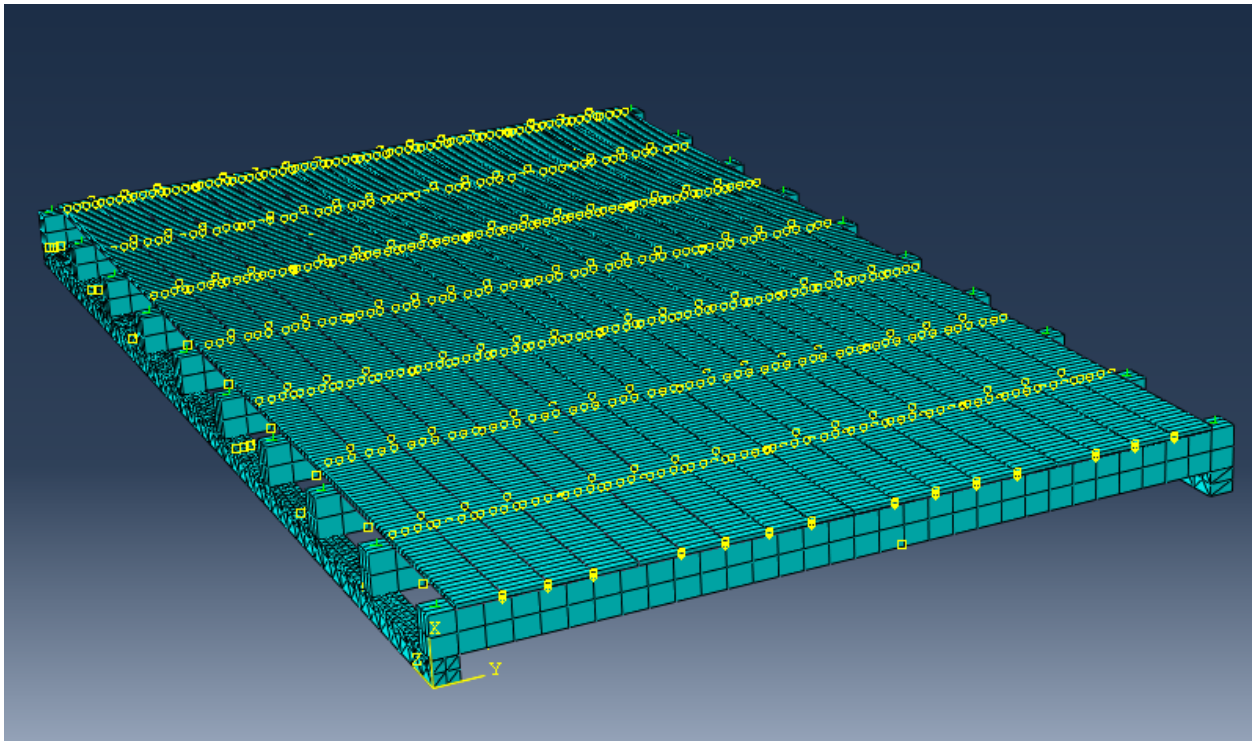

Fig. 35 Meshed floor model ready for analysis

The procedure that will be employed implies the determination of the lateral (YZ plane, in Fig. 35) modes of vibration and assessing the floor's stiffness from this data. In order to get this planar stiffness of the floor, the supporting beams will be considered encastres at one end (in

addition to the aforementioned support conditions). The self-weight of the floor will be taken into account in the modal analysis by including a step in the analysis where the gravitational acceleration is applied. This step will present a NLGEOM flag, which means that the effects of this step will still be active in the consequent steps.

After running the analysis, the following results are obtained:

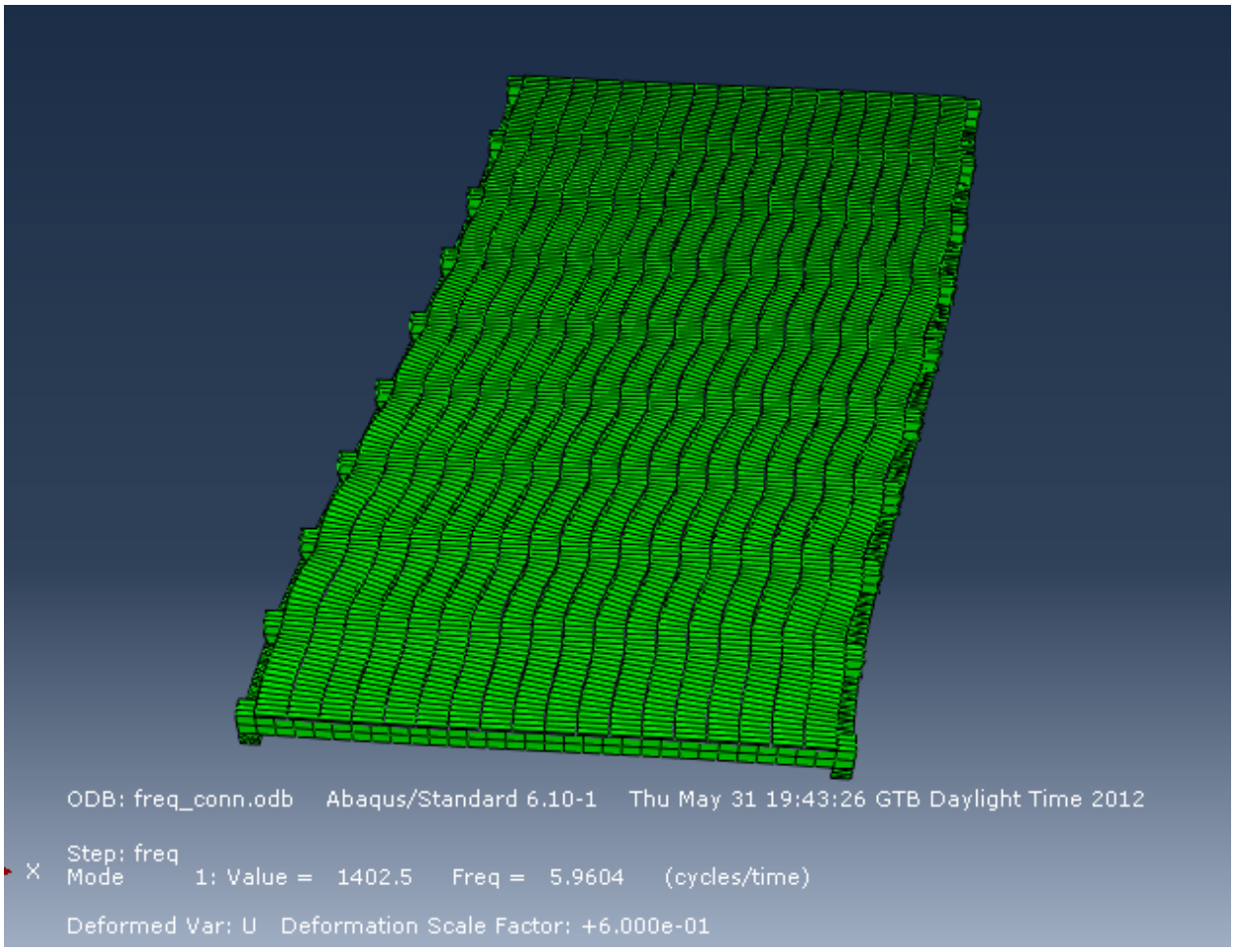

Fig. 36 Planar (first mode) vibration of the floor model

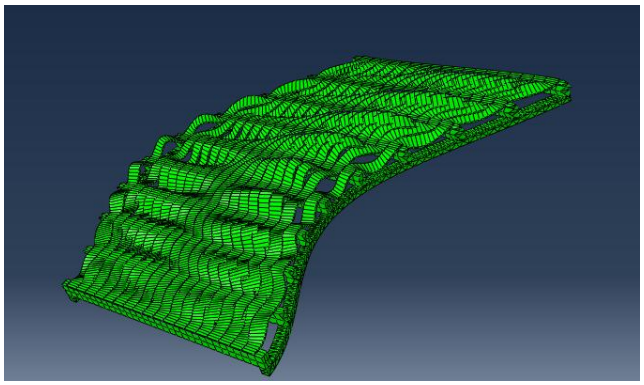

Fig. 37 Second mode of vibration of floor model

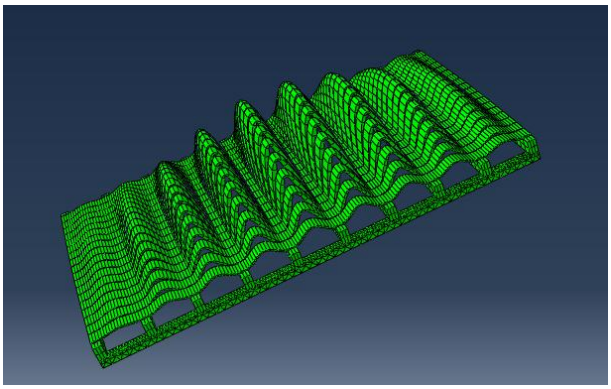

Fig. 38 Third mode of vibration of floor model

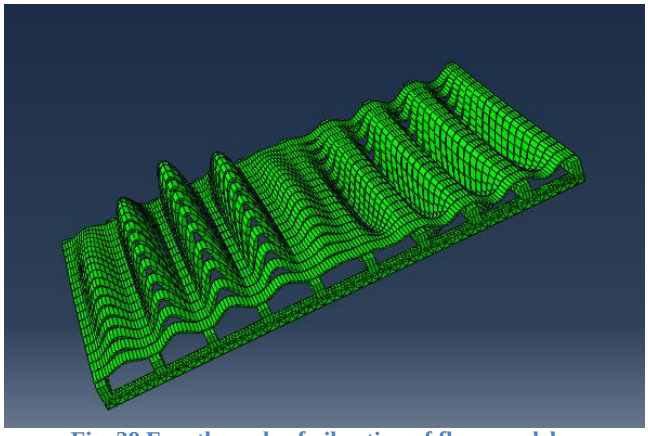

Fig. 39 Fourth mode of vibration of floor model

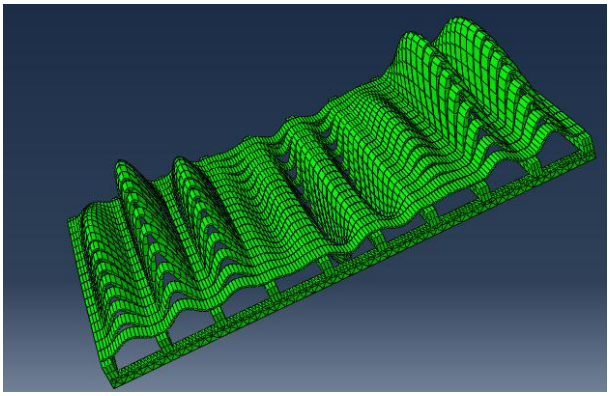

Fig. 40 Fifth mode of vibration of floor model

In the figures above, the first five modes of vibration of the floor model are depicted. The mode that is of the most interest is the first one, because this is the literally lateral vibration mode (Fig. 36).

Table 5 Analysis results for floor model

Mode no.	Frequency (cycles/s)	Period (s)	Participacion in X direction
1	5.96042	0.167773	1.37826
2	20.8959	0.047856	-6.13E-01
3	25.081	0.039871	-3.31E-03
4	25.1068	0.03983	-3.13E-03
5	25.1933	0.039693	5.33E-03
6	25.3028	0.039521	5.73E-04
7	25.4133	0.039349	1.05E-03
8	25.5073	0.039204	-7.44E-04
9	25.5769	0.039098	1.52E-04
10	25.6241	0.039026	-4.69E-04
11	25.6413	0.039	-1.74E-04
12	25.9128	0.038591	-2.17E-04
13	25.9375	0.038554	1.17E-04
14	25.966	0.038512	9.98E-04
15	26.002	0.038459	-3.65E-04
16	26.0472	0.038392	1.30E-03
17	26.1012	0.038312	1.52E-05
18	26.1055	0.038306	-3.12E-03
19	26.1186	0.038287	-6.28E-05
20	26.1578	0.03823	-5.93E-05

As it can be seen in Table 5, the first 20 modes of vibration of the floor model have been analyzed. In the fourth column, the effective participation in the X (planar) direction of the model is depicted for each node. Logically, the interesting mode will be the one that mobilizes the most mass in this direction (has the highest participation in the X direction).

As it could have been expected, the first mode of vibration is the one that indicates the lateral (planar) stiffness of the studied model. The floor exhibits an eigen-period of about 0.17 seconds in this mode and has by far the biggest participating factor.

The next phase of this step is the modeling of a shell element which exhibits an approximately similar behavior to the model above. This shell element will be the one which will be employed in the full model (because using the studied case would result in meshing problems and, in the same time, would be very costly from the point of view of the computational resources and time needed for the analysis.

The aforementioned shell element will have to exhibit the same behavior as the studied floor model for the planar vibration (first mode). This, simply put, means that their eigen-frequencies, for the modes with the highest participating factor in the X direction, will have to be comparable.

A slight difference in their eigen-periods will be tolerated and, moreover, desired. This is to account for the fact that the shell element employed in the full model will be rigidly connected to the rest of the model. A slightly larger period of vibration (smaller frequency) will be needed for the shell element.

Although, initially, the material employed for the modeling of the shell has been considered as isotropic, the analysis results have shown that a better option would be that of employing an orthotropic, lamina material. This type of material definition is more malleable and offers the possibility of a better tuning of the shell's behavior.

The density of the shell's material will be considered by dividing the actual mass of the floor to the volume of the shell to be employed (taking into account its cross-sectional thickness).

$\rho_{wood} := 400\frac{kg}{m^3}$ - Timber C18 mass density

$V_{planks} := 1.8m \cdot 3.12m \cdot 1cm = 0.056m^3$ - Volume of the planks (flooring) in the real floor

$V_{joists} := 10 \cdot 1.8m \cdot 6cm \cdot 10cm = 0.108m^3$ - Volume of the joists (supporting beams) in the real floor

$W_{real\_floor} := \rho_{wood} \cdot (V_{planks} + V_{joists}) = 65.664kg$ - Weight of the real floor

$V_{shell} := 5cm \cdot 3.13m \cdot 1.8m = 0.282m^3$ - Volume of the shell to be employed

$\rho_{shell} := \frac{W_{real\_floor}}{V_{shell}} = 233.099\frac{kg}{m^3}$ - Final mass density of the shell element

After several analyses, the shell element's properties were established, and these are:

Table 6 Shell element's properties

Mass density (kg/m^3)	233.099
Young's modulus E1 (N/m^2)	2000000000
Young's modulus E2 (N/m^2)	10000000
Poisson's ratio	0.35
Shear modulus G12 (N/m^2)	1.00E+09
Shear modulus G13 (N/m^2)	1.00E+09
Shear modulus G23 (N/m^2)	1.00E+09
Shell section thickness (m)	5.00E-02

As it has previously been stated, the shell element will be made out of lamina material, exhibiting plane stress orthotropic behavior. The shell element will be rigidly connected to the masonry walls where the joists are connected to the support beams. When talking about the other

two walls, the shell element will only interact with them by ensuring a "hard" contact in case of touching. This means that the shell element will, simply put, have the ability to "push" these other walls.

The shell thickness assigned to this shell element has been set to 5 cm. This is an average thickness, for simulating both the flooring's and the joists' thicknesses.

The modes of vibration of the shell element, along with their periods can be seen below, in Table 7.

Table 7 Shell element's modes of vibration

Mode No.	Eigenrequency (cycles/time)	Eigenperiod (s)	Participation X direction
1	5.80611	0.1722	1.39002
2	16.5446	0.0604	-1.54E-12
3	28.0707	0.0356	-8.79E-01
4	46.3945	0.0216	-2.95E-14
5	49.6544	0.0201	2.59E-13
6	49.929	0.0200	-2.87E-14
7	59.1711	0.0169	2.79E-14
8	62.3243	0.0160	5.58E-01
9	71.7555	0.0139	-1.01E-13
10	82.8259	0.0121	-1.59E-13
11	86.0829	0.0116	1.38E-14
12	98.1403	0.0102	-4.03E-01
13	101.353	0.0099	1.15E-13
14	116.101	0.0086	-5.70E-13
15	117.195	0.0085	-1.46E-12
16	127.688	0.0078	-2.02E-05
17	132.528	0.0075	4.93E-05
18	133.441	0.0075	-5.49E-11
19	134.416	0.0074	-3.00E-01
20	146.015	0.0068	-2.28E-05

As it can be seen, the 1st mode of vibration of the shell element is a good approximation of the mode of vibration of the analyzed floor model. Its eigenperiod is higher with approximately 0.01 seconds than the eigenperiod for the floor model but this is a good margin when taking into account that the shell element will be rigidly connected to the structure and not by nail connectors, as it was the case for the modeled floor.

Another indication that the shell element will behave as expected is that the other modes of vibration have much lower periods than the first one. This is a very good aspect, as the purpose

of the simulation was to obtain an element which is rather rigid, except for the first mode of vibration (planar, X direction) where the element should be comparable with the real floor. If the modes of vibration and periods are compared with the real model, it can be stated that the employed shell is a very good approximation of the real model.

2.2.3 Assessing the connection between the floor boards and the joists

The real connection between the joists and the floor boards is, of course, a nailed connection, using two nails.

However, because no special behavioral feats have been observed in these connections during the tests, it is a good enough assumption to assign a rigid connection between these elements, without significant deterioration of results.

2.3 Modeling the structure in its initial state

After having studied the particularities that arise in the modeling phase, the materials employed and the assumptions made, the modeling of the structure can take place.

2.3.1 Geometry of the structure

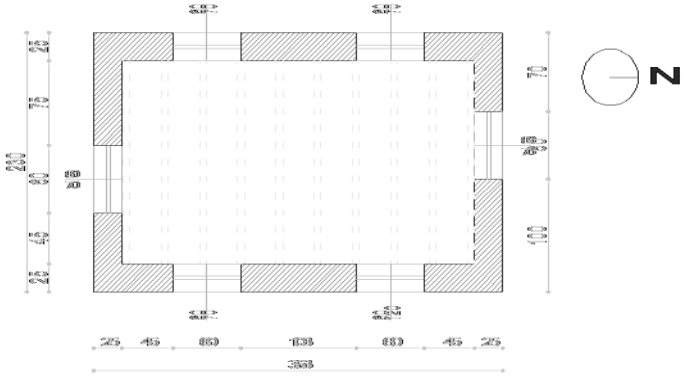

Fig. 41 Ground floor plan

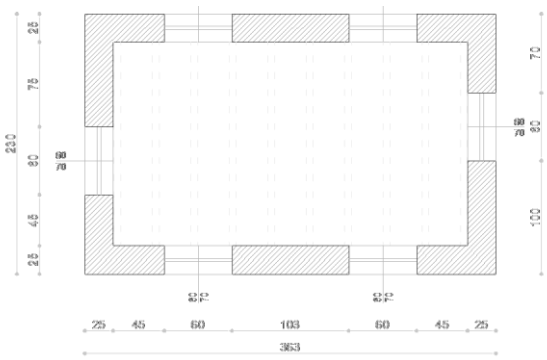

Fig. 42 First floor plan

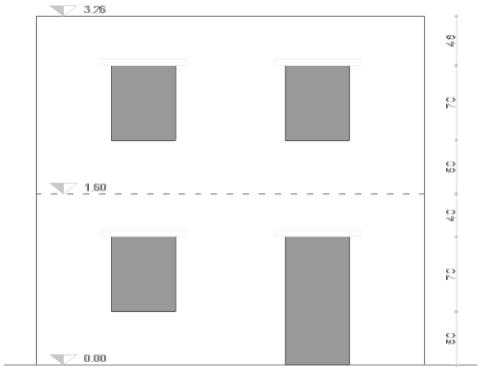

Fig. 43 East elevation

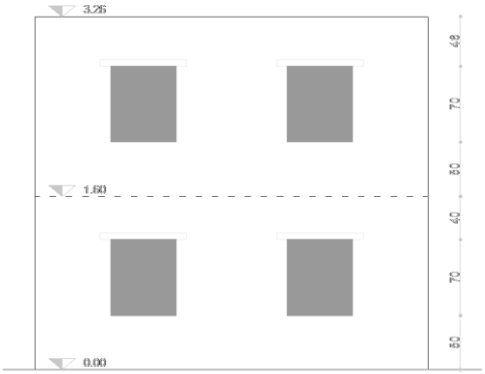

Fig. 44 West elevation

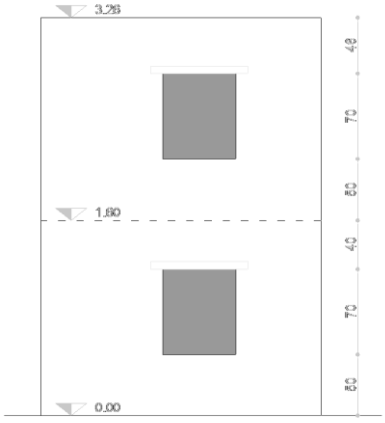

Fig. 45 North elevation

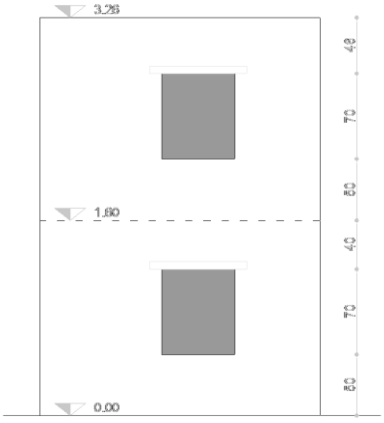

Fig. 46 South elevation

In Fig. 41 to Fig. 46, the geometry of the structure is presented. As it can be observed, the building to be dealt with is a simple, regular structure. Nevertheless, it is a representative type of building and it is similar in nature to many historical structures.

The 3D model employed for simulating the structure to be studied can be seen below, in Fig. 47.

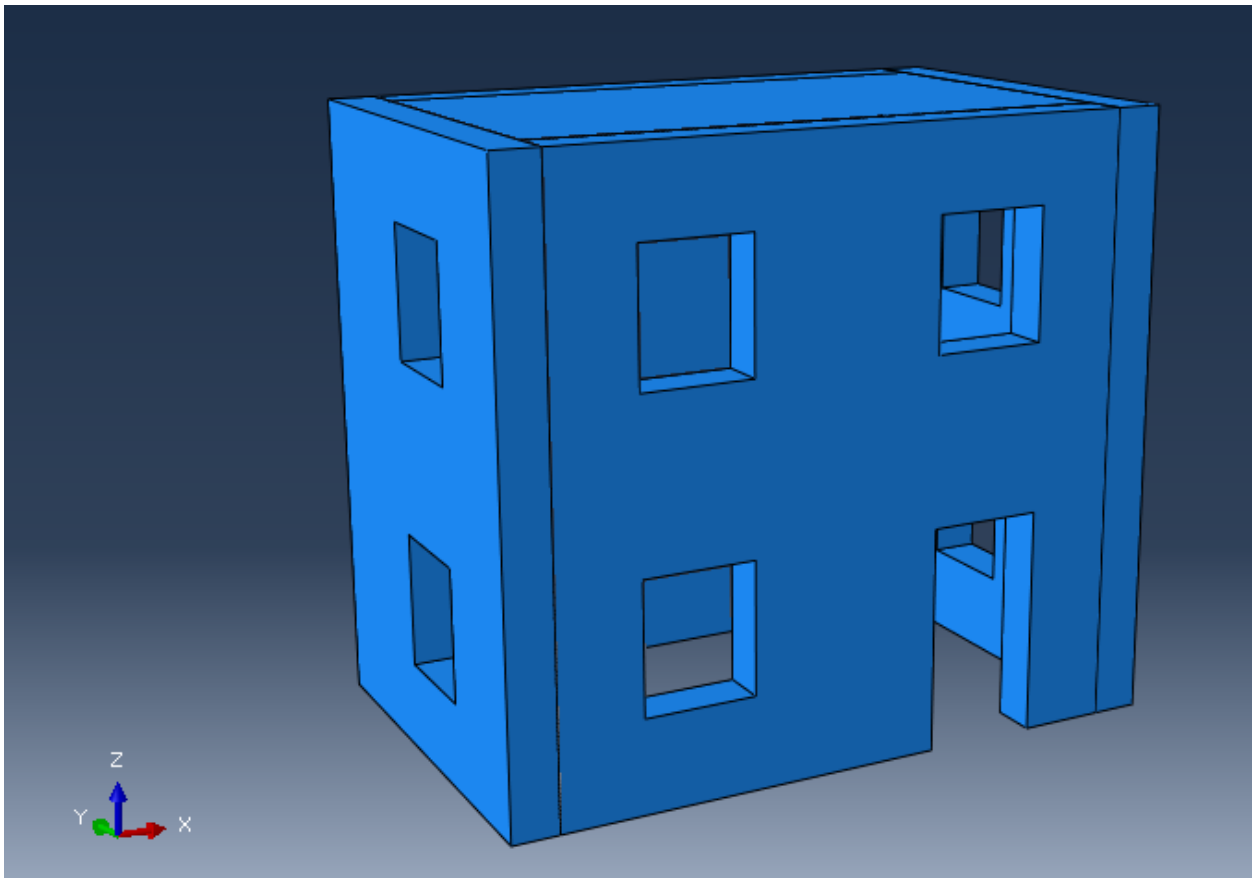

Fig. 47 3D model of the studied structure

2.3.2 Meshing the finite element model

As it has been previously stated the model will contain two types of elements: solid 3D hexahedral elements (for modeling the walls) and 2D shell elements (for modeling the floors).

The model will be meshed using a structured technique, which has proven to be very effective when dealing with masonry structures. This is because the model replicates very good the actual layout of the masonry blocks (or the masonry leaves) and a good assessment of the behavioural characteristics can be made employing this type of meshing technique.

Regarding the element size, a good indicator of its maximum, when dealing with masonry structures, would be half the thickness of the walls. This indication is very useful and should be an important criterion when establishing the dimensions of the elements used in the meshing.

Masonry structures are very special by definition and their walls have a considerable thickness. This means that the behavior throughout the thickness of the walls is not constant. Indeed, experience has shown many cases when only a part of the wall (a leaf) has failed or has been cracked. In conclusion, it is good to have at least two elements along the walls' thickness in order to correctly assess the behavior of the structure and the stresses and strains to which masonry is subjected.

Therefore, as the structure in question has a wall thickness of 25 cm, hexahedral cubic elements (6 node bricks) with the dimensions 12.5cm X 12.5cm X 12.5cm have been selected for meshing of the walls.

The shells have been meshed with 2D square shell elements of the same dimensions (12.5cm X 12.5cm) in order to provide accuracy to the model at the nodes of intersection. A structured meshing technique has been selected for the floors, also.

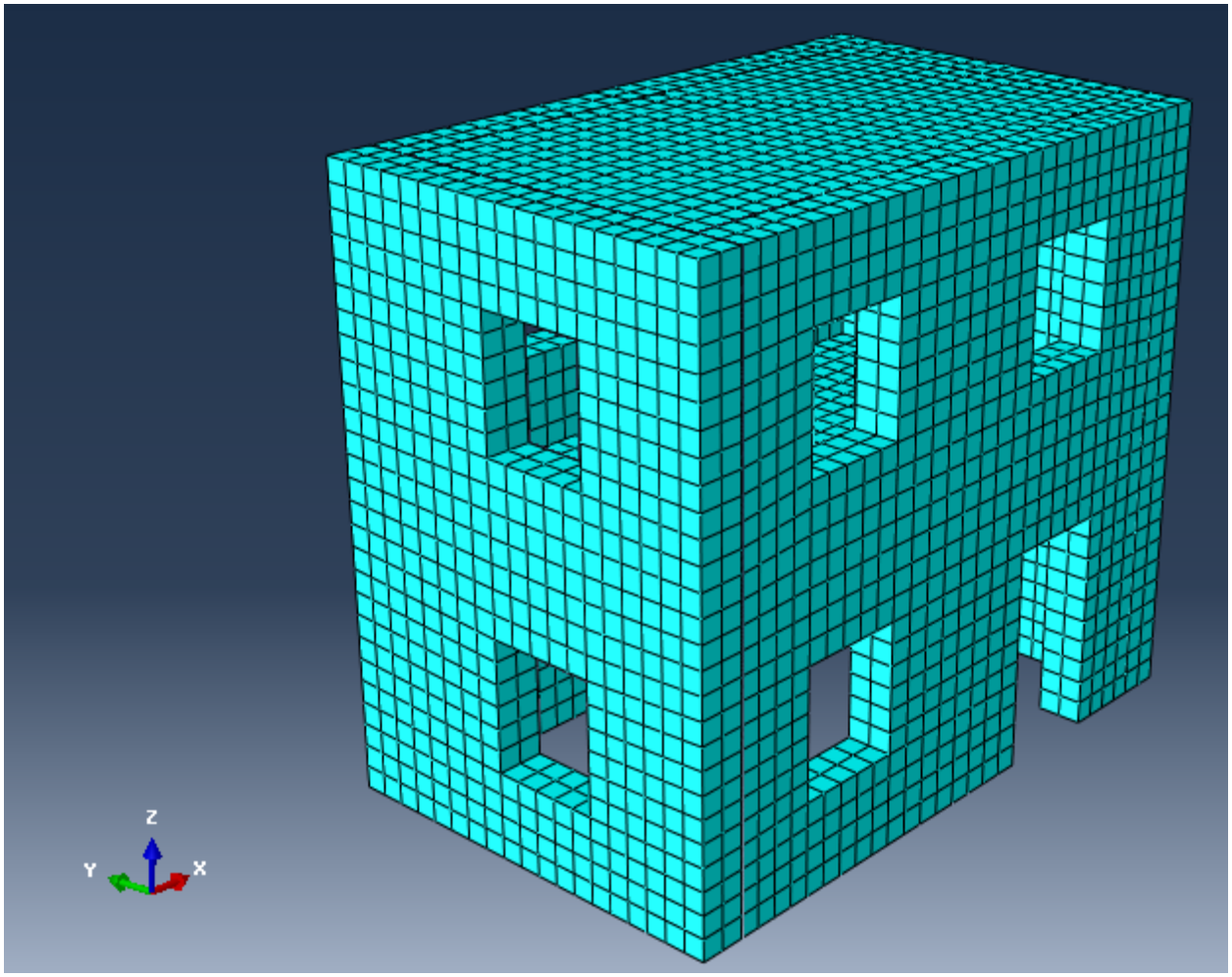

Fig. 48 Meshed building model

2.3.3 Loads, boundary conditions and interactions

In any model, the way the loads, boundary conditions and interactions are defined has a major impact on the outcome of the analysis. The definition of the above-mentioned elements has to be done with great care and respecting, as well as possible, natural phenomenon to be modeled.

2.3.3.1 Loads

The loads to be applied to the structure define the natural phenomenon that is desired to be simulated.

It is worth noting that the earthquake load will be applied, in our model, as acceleration at the base of the structure. This is a very good assessment and a much more accurate simulation than the simplistic approach of simulating the load as a force applied to the structure.

The earthquake load that the structure will be subjected to is the Kalamata earthquake. In the laboratory tests, scaled records of the Kalamata earthquake were used, respectively: 15%, 30%, 45%, 60%, 75%, and 90%. The initial, ungrouted, building displayed an approximately elastic behavior up to the 60% scaling of the Kalamata earthquake. This is why, in the analysis conducted for the initial model, only the tests up to the 60% scaled earthquake will be studied.

In order to apply these loads, the acceleration time-histories were provided for the X direction (longitudinal wall direction) and, as well, for the Y direction, as the test was a biaxial test.

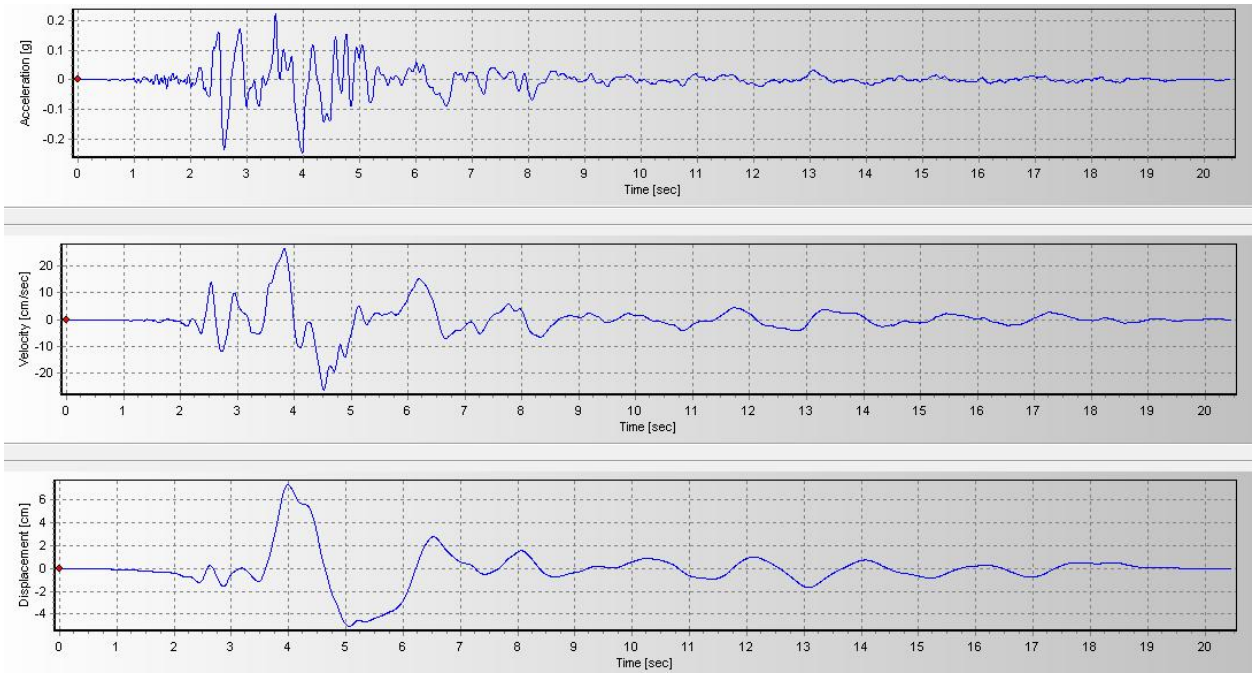

Fig. 49 Kalamata EQ time histories - X direction

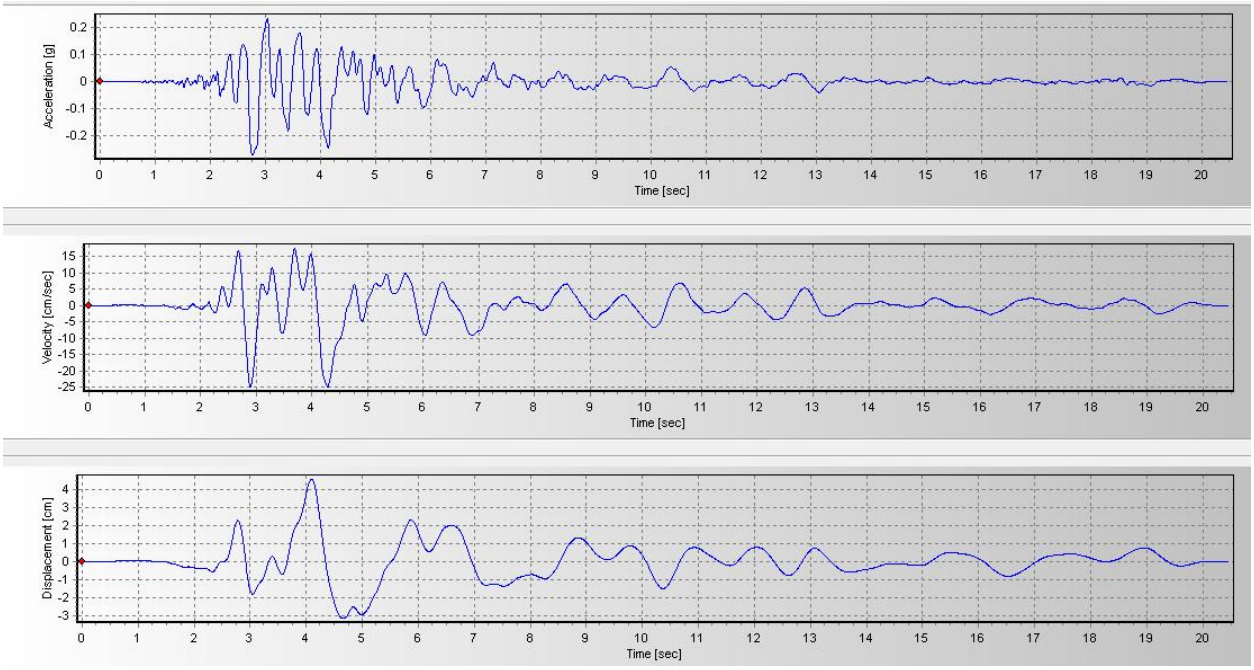

Fig. 50 Kalamata earthquake time histories - Y direction

In the figures above, the unscaled time histories of the Kalamata earthquake for each direction have been plotted.

In addition to the above mentioned load and, of course, the gravitational load, another set of loads has to be defined. The building was loaded (using some weights, in the laboratory) in order for the experiment to be considered valid. These loads are necessary for making the equivalence between the scaled test structure and a real-size structure possible.

The added weights are:

- 3 Mgr on the top floor (roof)
- 4.5 Mgr on the first floor.

The addition of the loads will not be done by employing a load, per se. This is because the weights were used, in the experiment, mainly due to their inertial effect. So, in order for those elements to be simulated, some masses have to be added at the floor levels. These masses will be added by integrating them in the shell element's (floor's) material properties. The whole mass of the real floor will be considered, along with the mass of the weights. This mass will be divided to the volume of the shell element employed and, finally, the density to be employed for each floor will be obtained.

$\rho_{wood} := 400 \frac{kg}{m^3}$ - Density of timber C18

$V_{planks} := 1.8m \cdot 3.12m \cdot 1cm = 0.056m^3$ - Total volume of flooring planks

$V_{joists} := 10 \cdot 1.8m \cdot 6cm \cdot 10cm = 0.108m^3$ - Volume of supporting beams (joists)

$W_{real\_floor} := \rho_{wood} \cdot (V_{planks} + V_{joists}) = 65.664kg$ - Selfweight of real floor

$W_{extra\_2} := 3000kg \quad W_{extra\_1} := 4500kg$ - Extra weights on each floor

$W_{floor1} := W_{real\_floor} + W_{extra\_1} = 4.566 \times 10^3 kg$

$W_{floor2} := W_{real\_floor} + W_{extra\_2} = 3.066 \times 10^3 kg$

- Weight of the loaded floor above the ground floor and above the first floor, respectively

$V_{shell} := 5cm \cdot 3.13m \cdot 1.8m = 0.282m^3$ - Volume of the shell elements employed for simulating the floors

$\rho_{floor1} := \frac{W_{floor1}}{V_{shell}} = 1.621 \times 10^4 \frac{kg}{m^3}$ - Mass density to be used for the first floor

$\rho_{floor2} := \frac{W_{floor2}}{V_{shell}} = 1.088 \times 10^4 \frac{kg}{m^3}$ - Mass density to be used for the second floor (roof)

As it can be seen above, the mass densities of the floor model shell elements to be employed are significantly larger than the initial mass density.

During the analysis, it has been observed that a mesh refinement in the shell areas is needed in order for the analysis code to support the displacements induced by these loads. Of course, large displacements were induced vertically in these elements, but this does not mean that they mimic the real vertical displacements in the respective zones.

It must be kept in mind that the shell elements employed have been selected only to accurately simulate the in-plan behavior of the real floors.

2.3.3.2 Boundary conditions

The boundary conditions in the model are relatively simple. This is due to the fact that the simulated situation is a laboratory test under controlled conditions.

The building will be considered as being translationally restrained along the perimeter of its base. This means that all its translational degrees of freedom (3) will be constraint, at this level. This is not a simplistic assumption as it simulates the real situation from the laboratory, where the building's base is fixed on the shake table.

Fig. 51 Typical placement of a structure on the shake table

2.3.3.3 Interactions

Throughout this model, we are dealing with two types of interactions:

- The interactions between walls and other walls (at the building's corners)
- The interactions between the walls and the shell elements replicating the floors

As it has previously been stated, these interactions will be considered as perfect contact, with a no slip and no separation condition. This is, as mentioned, a simplistic approach but, nevertheless, when dealing with a masonry structure it is needed to employ this type of connections. The reason for doing that is that the structure is analyzed in the elastic domain so a linear analysis is needed. If the connection between the elements would be capable to fail or slip (as in the real life) the analysis would pass to the non-linear domain.

The interaction between the shell elements and the walls of the building are considered rigid but their lack of rigidity (due to the nailed connection) has been accounted for by using a less stiff element for simulating the floors.

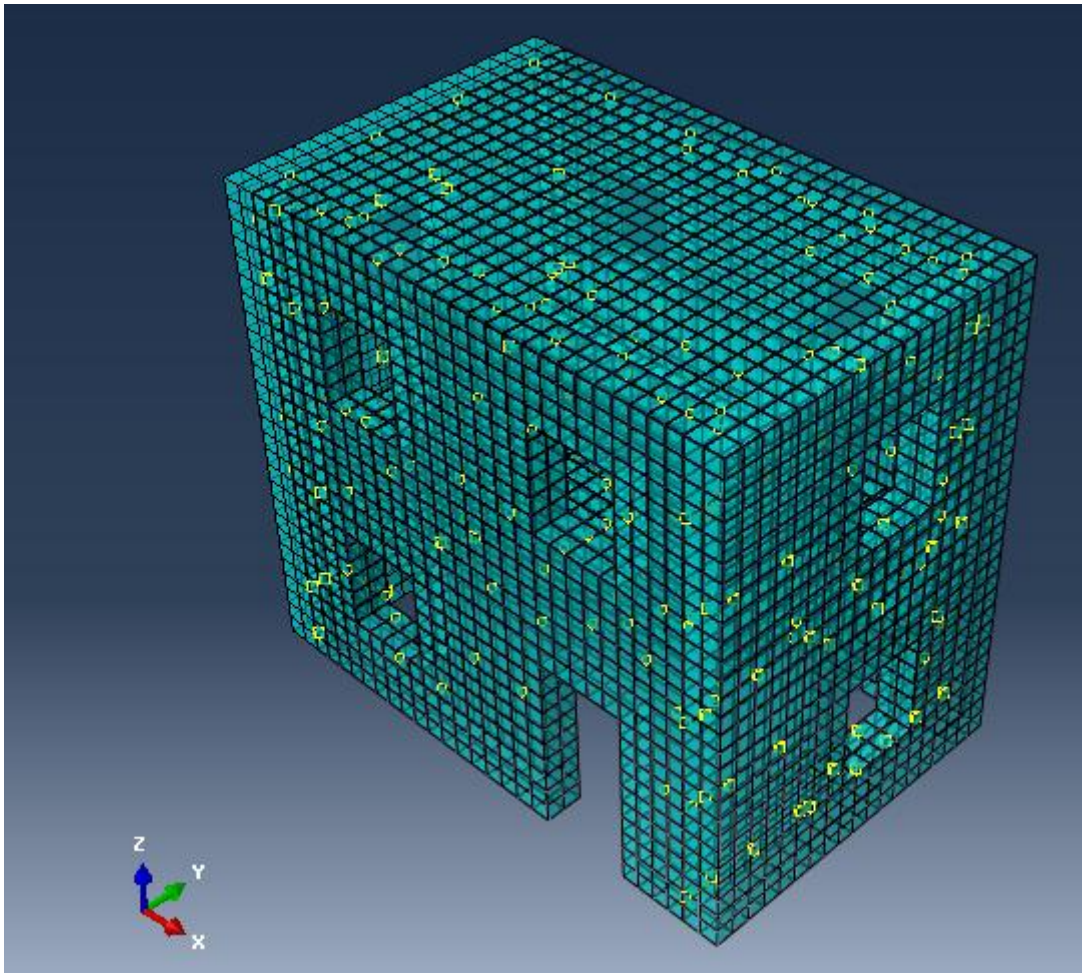

Fig. 52 Rigid ties (yellow dots) between the elements in the model

2.3.4 Analysis types

In order to assess the structure, two analysis types will be conducted:

- A linear perturbation analysis, frequency extraction step
- A linear perturbation analysis, dynamic modal analysis

The response in a linear perturbation analysis step is the linear perturbation response about the base state. The base state is the current state of the model at the end of the last general analysis step prior to the linear perturbation step. If the first step of an analysis is a perturbation step, the base state is determined from the initial conditions

The linear perturbation step will be used for finding the eigenfrequencies of the model. This is a good indicator if the model is accurately simulated. If the eigenfrequencies found in the analysis will be similar to those computed from the experiments, then the model is considered accurate.

The modal dynamic will be employed to apply the loading on the building. The loading to be applied in such an analysis can be dynamic or static. This step will be the one which will simulate the loading applied in the laboratory and special care must be provided in order to have an accurate simulation of the loads.

It has to be noted that, within the modal analysis steps, a critical damping ratio of 0.007 has been introduced. This feat has been employed in order to limit the duration of the vibrations the building has to withstand.

2.4 Modeling of the strengthened structure

2.4.1 Model of the improved floor

In order to assess the new properties of the floor to be employed, a similar model as the one used in section 2.2.2 will be employed. The new layer of boards will be applied over the existing layer at an angle of 45˚ and the behavior of the new floor will be assessed in a similar manner.

The connection between the new layer and the original floor will be considered rigid, as no behavior of significant importance was observed, during the tests, in those regions.

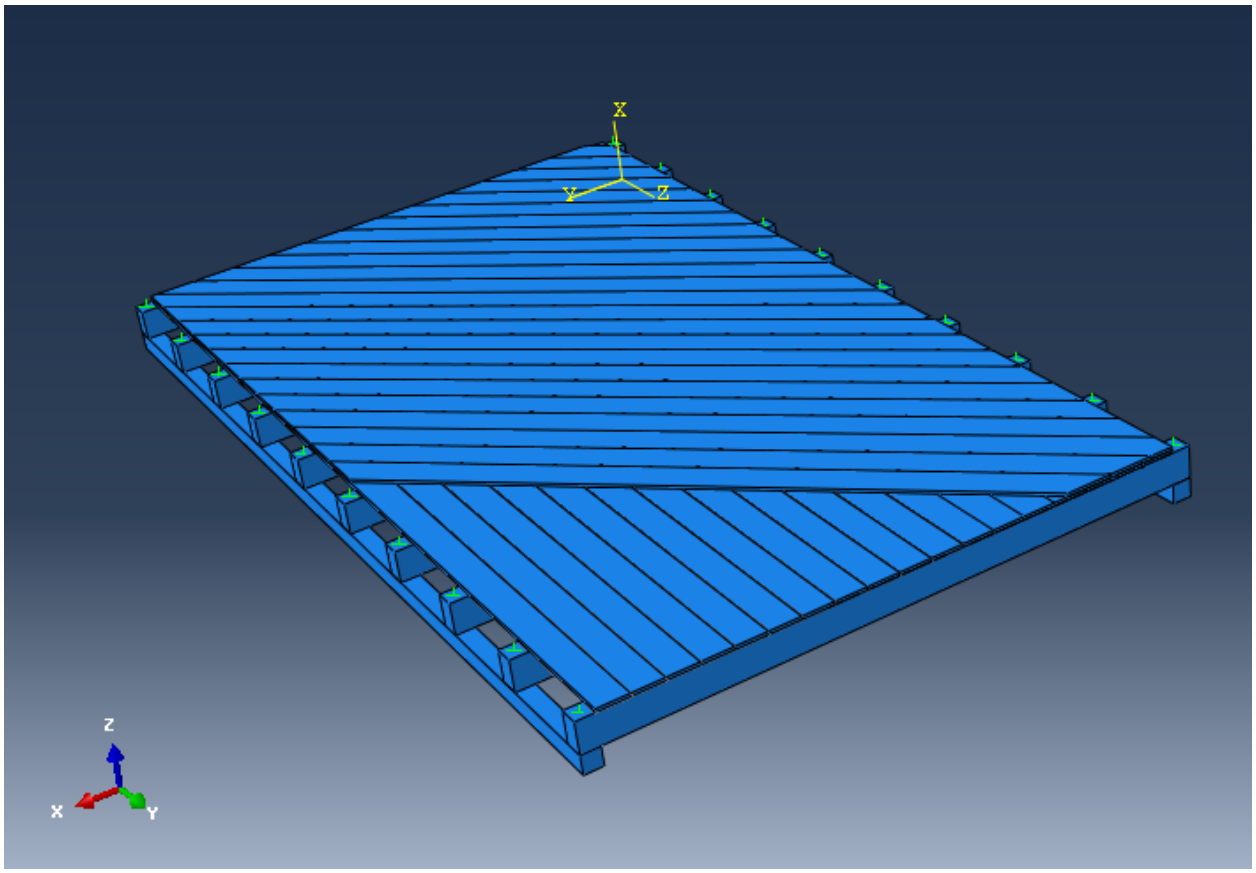

Fig. 53 3D model of the strengthened floor

In Fig. 53 above, the model employed for the estimation of the diaphragm action improvement can be seen. Some of the overlaying planks have been removed from the display group above in order to clarify the position of the new layer of boards with respect to the original layer.

Meshing of the elements has been done, as in the previous case, with relatively fine elements. This is in order to avoid the errors coming from the very small thickness of the boards and in order to have a greater accuracy in terms of interactions and, of course, results.

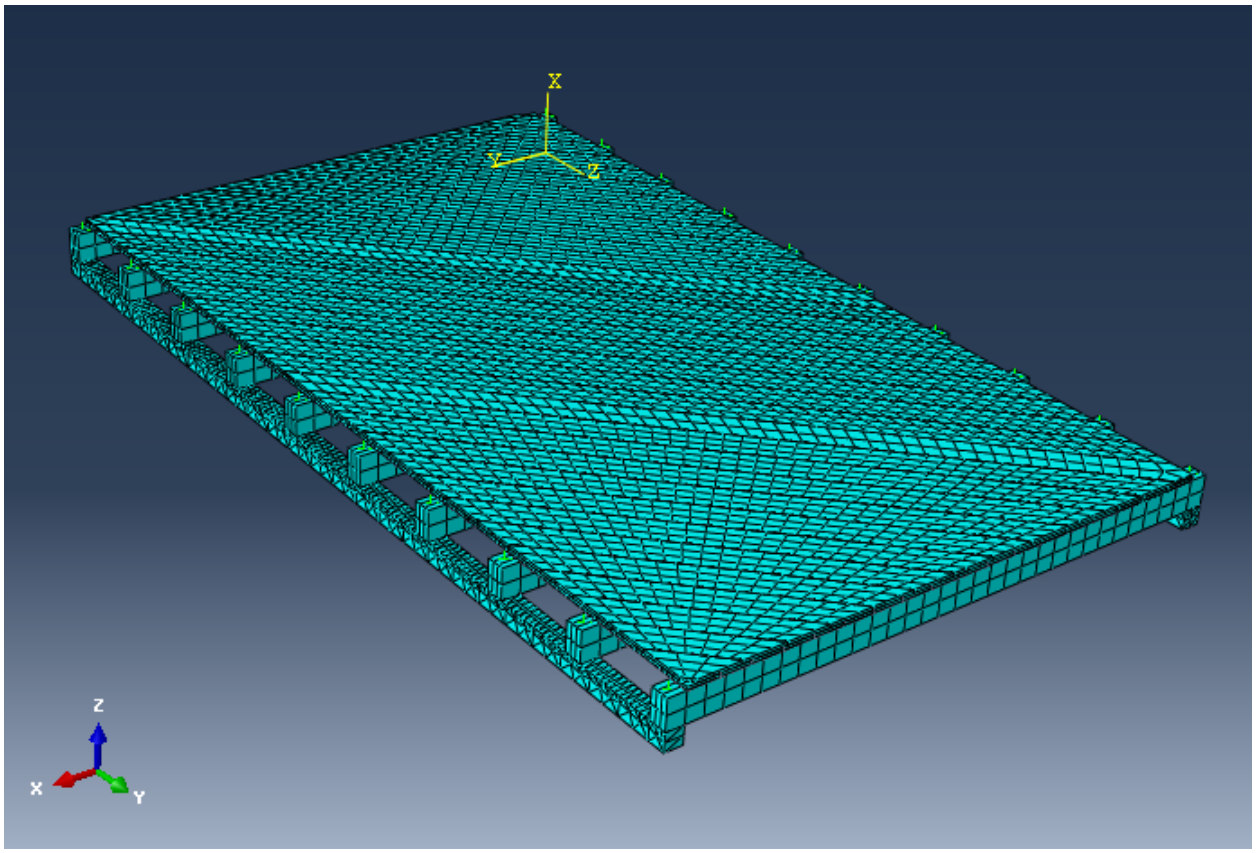

Fig. 54 Meshed floor model

In order to estimate the behavior of the strengthened floor, the same procedure as before will be employed. The floor is considered fixed at the ends of the support beams on one side. A modal analysis will be undergone and the mode of vibration in the plan OXY (direction OX) will be assessed.

After the characteristics of the mode of vibration are extracted, another model will be made in which an equivalent shell element is searched for, in order to be employed in the whole building simulation.

After the running of the analysis, apart from the eigenfrequency of the desired mode of vibration, some other conclusions can be drawn regarding the behavior of the repaired floor, in comparison to the original floor.

Table 8 Modes of vibration of the strengthened floor

Mode No.	Frequency (cycles/s)	Period (1/s)	Participation X dir.
1	31.4888	0.0318	1.24171
2	42.727	0.0234	-3.91E-01
3	45.3446	0.0221	-4.87E-01
4	49.4474	0.0202	-1.87E-02
5	57.1329	0.0175	-6.32E-03
6	66.6547	0.0150	3.51E-02
7	75.6941	0.0132	1.18E-02
8	79.9382	0.0125	-1.97E-02
9	85.7197	0.0117	4.36E-03
10	94.9892	0.0105	-5.34E-02

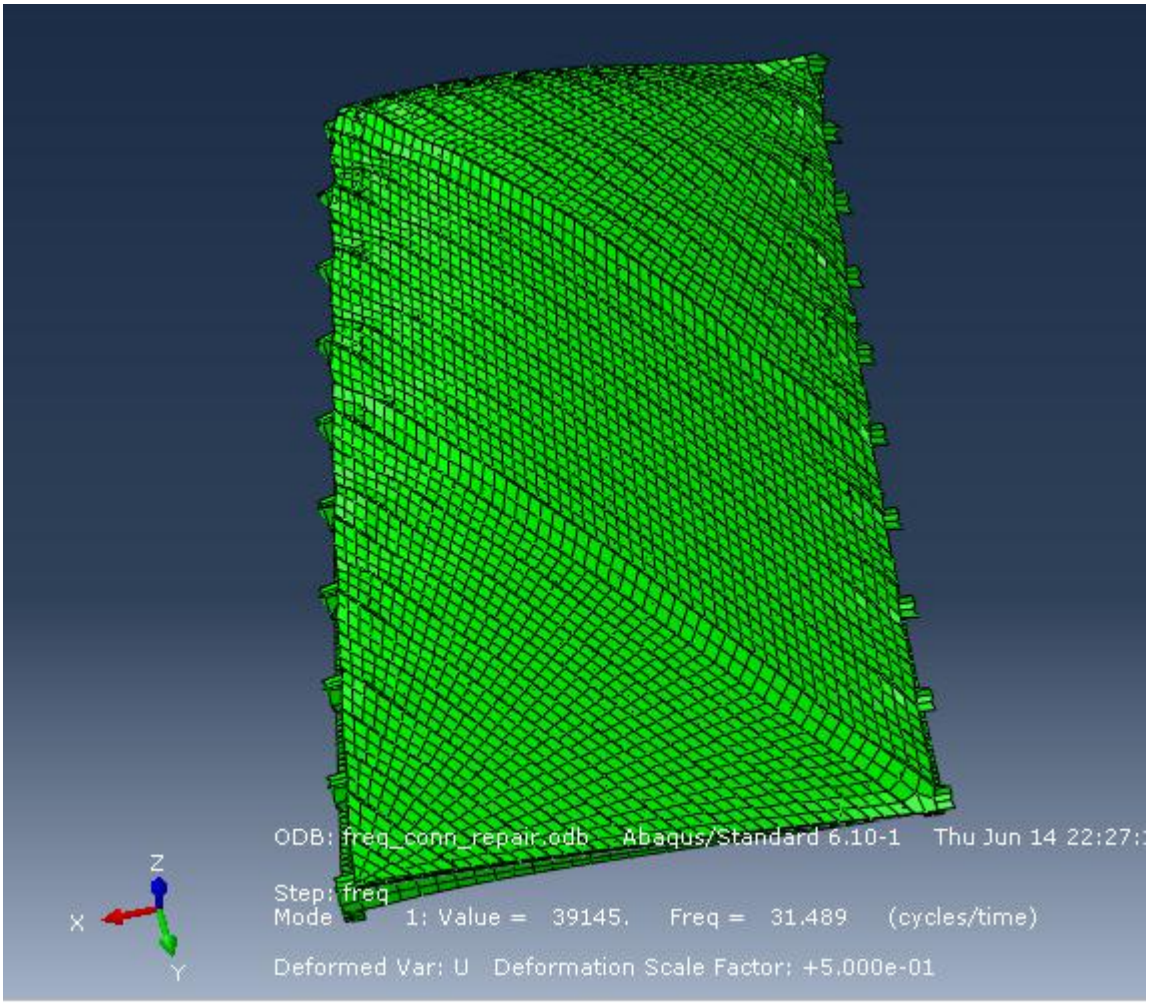

Fig. 55 The first mode of vibration of the repaired floor

As it can be seen in Fig. 55, the first mode of vibration is depicted. It is important to note the difference in the behavior of the floor after applying the repair procedure.

From Fig. 55, and by comparing it to Fig. 36 (which depicts the planar mode of vibration of the original floor), some important conclusions can be drawn. First of all, the elements that seem to deform are, this time, the joists of the floor. The flooring layer itself is much strengthened and it seems to behave like a rigid diaphragm. Notice in the figure above that the real deformations come from the deformations of the beams and the pull-out tendency in the nail connections between the beams and the support elements.

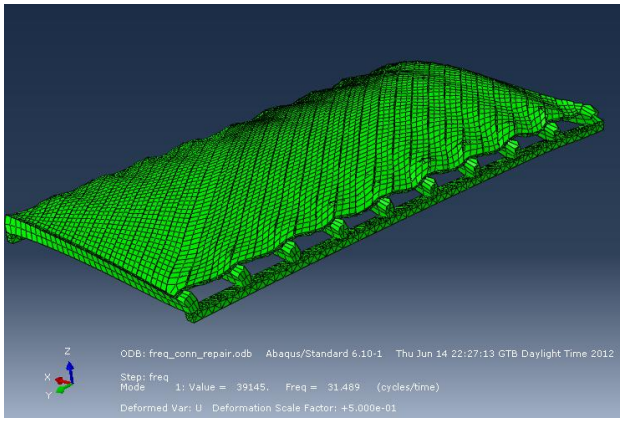

Fig. 56 First mode of vibration - side view

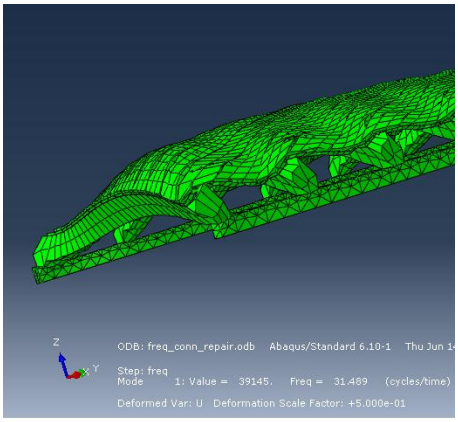

Fig. 57 Detail of the nail connections in the 1st vibration mode

Indeed, as it can be observed in Fig. 56 and Fig. 57, the elements which really suffer deformations are the joists and the nail connections. This means that, at the flooring level, the interventions made have been as effective as possible – the flooring now being the stronger element and the joists and connections the weaker ones.

As a personal opinion, the only way to further improve the stiffness of the floor (although it is not likely to be a necessity) would be to improve the connections between the flooring and the joists and, also, between the joists and the support beams. Further improvement of the floor's stiffness could be acquired by strengthening the joists.

From Table 8 above, some additional important information can be extracted. In the first place, the increase of stiffness in the OXY plane can be easily noticed. An enhancement of over 5 times of the eigenfrequency means that the additional floor layer has more than played its part.

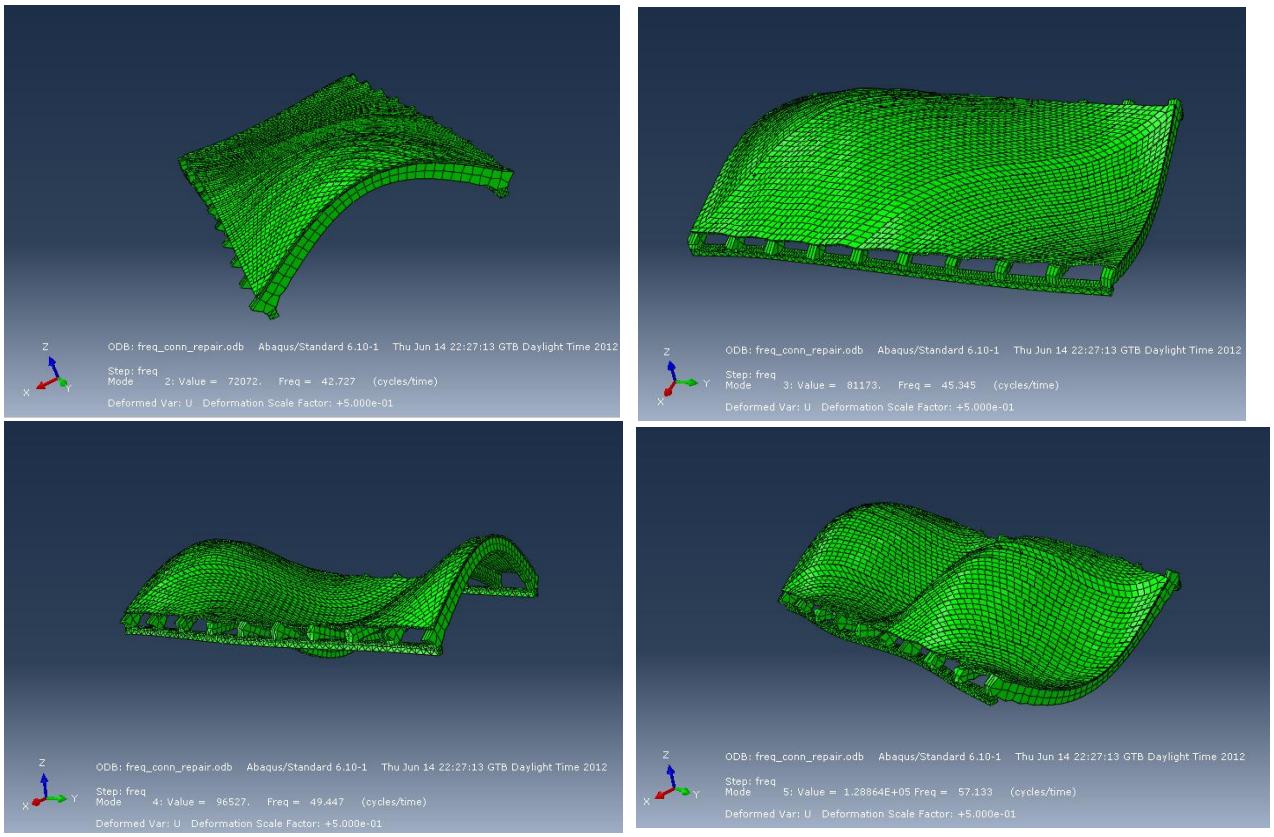

Fig. 58 Other modes of vibration of the strengthened floor

By comparing Fig. 37-Fig. 40 with Fig. 58, clear arguments for supporting the idea that the flooring layers behave like a very rigid shell (almost perfect diaphragm) can be highlighted.

The main aspect to be observed is that the flooring elements (boards) are not vibrating independently anymore. This, of course was expected, but it is still a very positive aspect arising from the analysis.

The second important detail when comparing the behaviors of the two floors is that, whereas in the original floor the modes of vibration were mainly constituted by the vibration of the flooring layer, in this strengthened model the elements which vibrate sooner are the joists and supporting beams. This means that the strengthened flooring layer has become more rigid that the joists and supporting beams and, thus, any other intervention to the flooring layer is very unlikely to have a further positive effect as the main weakness of the floor is now constituted by the joists and supporting beams.

2.4.2 Considering an equivalent shell element

After assessing the results from the analysis of the detailed floor model, the next phase is finding an equivalent shell element to be employed in the whole building model analysis.

This time, the shell element will be considered isotropic. This assumption is done due to the fact that the shell element will be connected to all the 4 walls and its behavior in both directions must be relatively the same.

Then searching for an appropriate shell element to be employed in the model, some considerations must be made and certain aspects must be paid attention to. The interactions between the overlaying flooring layer and the original flooring in the detailed model were considered as being ties. This means that, at the interactions of their adjacent surfaces, the two layers will have the same displacements and rotations. This is an exaggeration and it leads to an overly-rigid model as, in the real case, the two layers are connected by nails. From this point of view, the shell element to be considered must have a slightly higher period of vibration (lower frequency) for the desired mode.

After several tests and analysis, some satisfactory characteristics of the shell element employed have been found, which render adequate results.

The shell element to be employed will be considered as having a section thickness which is the same as the previous element (namely, 5 cm). The mass of the shell element will be computed as before and, thus, the final mass density is 233.099 kg/m^3.

Table 9 Shell element's properties

Density (kg/m^3)	233.099
Young's Modulus (Gpa)	5
Poisson's Ratio	0.35
Section thickness (m)	0.05

In Table 9 above, the properties of the shell element employed have been depicted. Using this element in the analysis, the following results are obtained:

Table 10 Vibration of the shell model

Mode No.	Frequency (cycles/s)	Period (1/s)	Participation X
1	18.6839	0.0535	5.93E-13
2	19.7984	0.0505	1.54E-12
3	24.2776	0.0412	-8.09E-13
4	27.2045	0.0368	1.43382
5	33.3512	0.0300	7.18E-13
6	48.051	0.0208	-3.78E-14
7	51.3446	0.0195	-4.02E-04
8	52.7743	0.0189	4.50E-05
9	58.4267	0.0171	-2.50E-03
10	68.2332	0.0147	3.11E-03

As it can be seen in Table 10, the real mode in the OX direction is the 4th mode of vibration of the shell model. The frequency of the 4th mode of vibration for the shell element is around 10% lower than the frequency of the similar mode of vibration from the floor model. This is an adequate result, as the employed element will have to be defined taking into account that the real strengthened floor is a little less stiff than the floor we have modeled. This happens, as it was mentioned before, due to the imperfection of the connections which, in the model, were considered perfect.

Therefore, the floor with the enhanced diaphragm action was successfully assessed. However, this is not the only intervention which was undergone in the studied structure. As it has been previously stated, the diaphragms can have an adverse effect if they are not supported by strong enough walls. As the studied structure is constructed as a historic masonry structure, the walls are not particularly strong. In conclusion, the decision to grout the walls has been made.

2.4.3 Tests conducted

As before, the analysis will be split into a linear perturbation, frequency extraction step and a modal analysis step.

The strengthened building displayed, under laboratory conditions, an approximately linear elastic behavior up to a scaling of 140% the Kalamata earthquake.

3 RESULTS AND INTERPRETATION

After running the analysis of both models, the results will be extracted and interpreted so that several conclusions about the efficiency of the interventions can be drawn.

The main objective of this paper is the accurate simulation of the intervention measures on the studied masonry structure. This means that, from the point view of analyzing the structural strength, little aspects will be studied. What is of interest is achieving the similar behavior of the building in its initial and final states. The most important aspect to be studied is the modification of the eigenfrequencies and of the modes of vibration of the structure.

The distribution of stresses is also of interest, as it is expected that an accurately simulated diaphragm will ensure and efficient, equal redistribution of stresses at the floor levels.

3.1 Control points for studying the response

In order to assess the response of the structure, several key points have to be selected in order to plot their response time histories. Four points have been selected, two at the level of each floor. Each one of these is found in the mid-span of transversal or longitudinal walls, respectively.

These points will be mainly employed when plotting the output of the model in terms of time histories. They were chosen in the midspan of each wall, at the level of the floors.

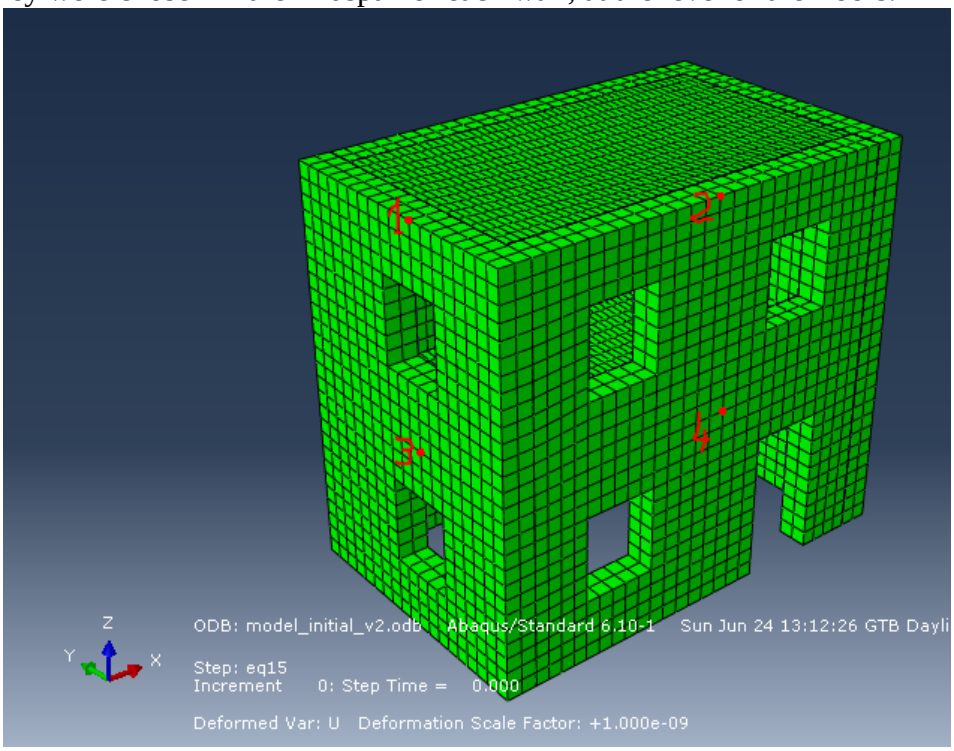

Fig. 59 Control points for studying the response of the building

3.2 Experimental results

As it has been previously stated, the validity of the model employed will be assessed by comparing the analytical results with the results obtained from the laboratory tests.

During the laboratory tests, the obtained results were expressed in terms of displacements, eigenfrequencies and accelerations. The object of the present models is to obtain results similar with those obtained in the test. This means that, if accuracy is good enough, the analysis models can be used in describing the behavior of the actual structures.

3.2.1 Eigenfrequencies

Table 11 Experimentally obtained eigenfrequencies

Studied Building	Eigenfrequency OX	Eigenfrequency OY
Initial	6.1 Hz	4.3 Hz
Strengthened	10.4 Hz	9.8 Hz

In Table 12Table 11 above, the eigenfrequencies of both models are displayed. The change in behavior is evident as there are some obvious differences between the two ways the building behaves (depending on its state).

The initial building is, as expected, less stiff than the strengthened one. This is clearly visible from the difference in the eigenfrequencies (the eigenfrequencies for the strengthened model are larger).

Another observation is that, for the strengthened building, the eigenfrequency is approximately the same for both directions. This means that the diaphragm action is efficient and the building behaves like a whole, rigid body (box-type behavior).

3.2.2 Displacements

In the following figures (from *E. Vintzileou, H. Mouzakis, C.-E. Adami, L. Karapitta: "Assessement of dynamic behavior of three leaf stone masonry building models: seismic enhancement by grouting and improvement of box behavior"*), the laboratory results of the maximum recorded displacements are plotted, for two excitation cases. The first one is the 90% Kalamata earthquake, applied on the unstrengthened building (BS). The second is the same 90% Kalamata earthquake, applied on the strengthened (AS) building. Although these particular cases have not been studied in this paper (as the behavior of the building in these tests has not been purely elastic), they provide good indices as to whether the simulation is accurate.

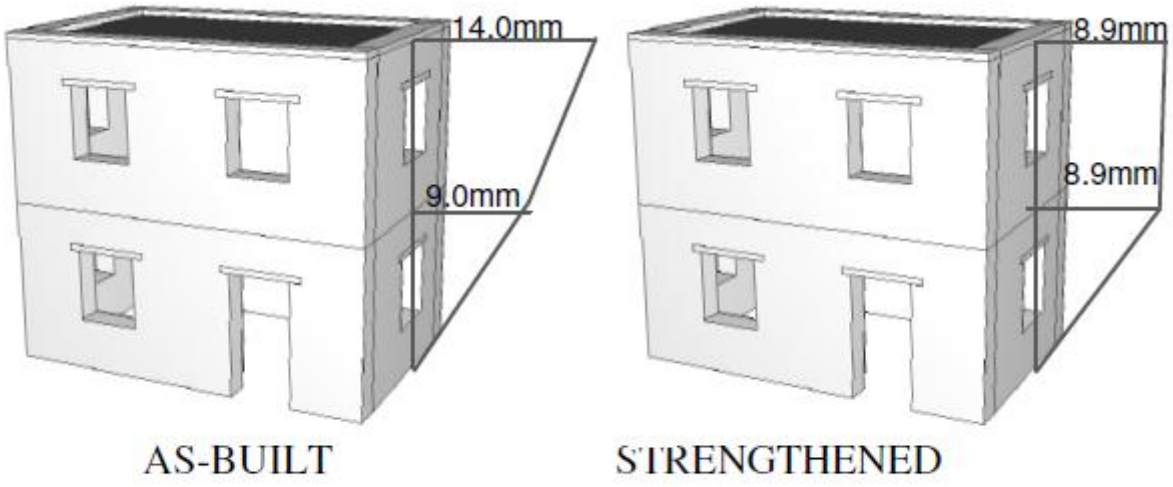

Fig. 60 OX maximum relative displacements, 90% Kalamata (courtesy of: see above)

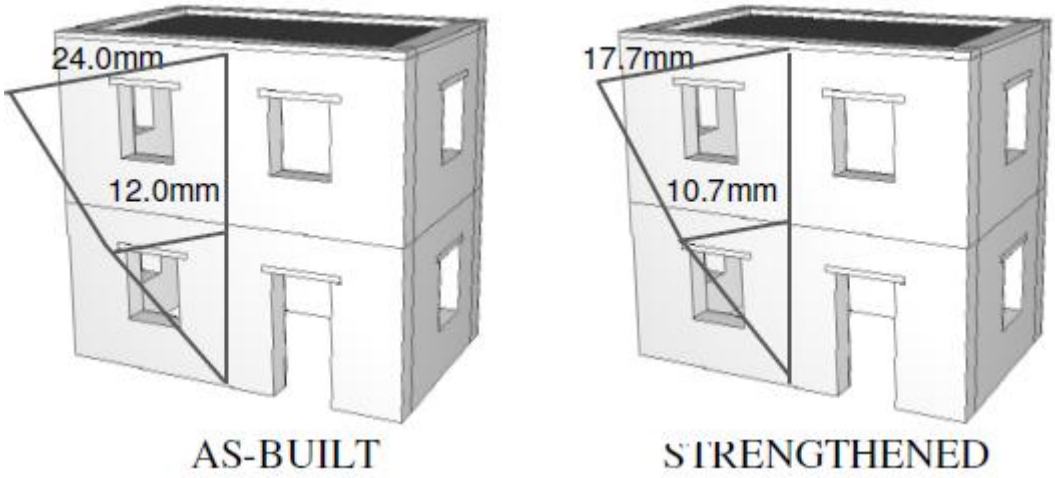

Fig. 61 OY maximum relative displacements, 90% Kalamata (courtesy of: see above)

3.2.3 Vulnerable zones

Below, a figure (from *E. Vintzileou, H. Mouzakis, C.-E. Adami, L. Karapitta: "Assessement of dynamic behavior of three leaf stone masonry building models: seismic enhancement by grouting and improvement of box behavior")* has been attached, describing the observed damages on the tested structure in its initial state, after the 90% Kalamata earthquake.

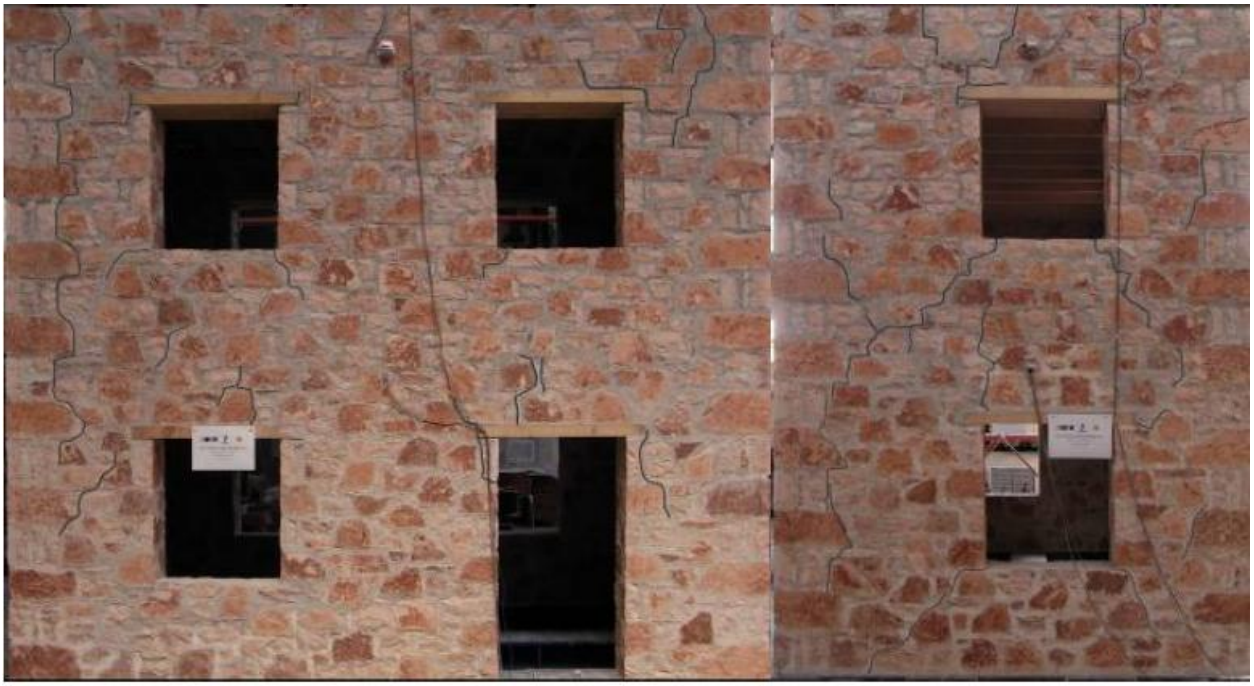

a) b)

Fig. 62 Observed damages during the tests on East Wall (a) and South Wall (b) (courtesy of: see above)

As it will be seen later on, many of the observed cracks correspond to the studied "vulnerable zones" (i.e.: the zones in which the masonry is in a triaxial tensile state). These zones, as it will be shown later on, correspond mainly to the corners of the doors and windows, the intersections of the walls and, likewise, some horizontal cracks above the windows will be likely to appear (see section 3.3.4).

3.3 Analytical results for the building in its initial situation

The building, in its initial situation has been subjected to loadings of up to 60% scaling of the Kalamata earthquake, in both X and Y directions. The building's modes of vibration will be studied and then its response to the loadings applied.

The results will be studied in terms of modal characteristics, accelerations, displacements and stresses in order to assess the behavior of the structure.

The primary focus will be assessing whether the employed model behaves in a similar manner to the real structure.

3.3.1 Eigenperiods and modes of vibration

The first step in the analysis is a linear perturbation, frequency extraction step. In this phase, the eigenperiods of the model are extracted and the mode shapes are computed. This is a very effective mean of assessing the way the building would behave in case of an earthquake.

Also, the eigenfrequencies of the structure will be used to assess the accuracy of the model, by comparing them with the experimentally obtained eigenfrequencies.

Table 12 Eigenperiods of the initial model

Mode No.	Eigenfrequency (Hz)	Eigenperiod (s)	Participation OX	Participation OY
1	2.645	0.378	-1.54E-03	4.64E-03
2	2.829	0.353	4.72E-03	1.04E-02
3	4.471	0.224	-1.25E-02	1.59419
4	4.802	0.208	-1.01E-02	-4.45E-01
5	5.212	0.192	-1.87E-02	-2.39E-01
6	5.430	0.184	1.86E-01	-6.52E-02
7	5.980	0.167	1.77433	4.44E-03
8	6.220	0.161	-1.84493	-5.35E-02
9	7.080	0.141	7.09E-03	3.30E-03
10	7.583	0.132	5.28E-03	1.28E-02
11	8.441	0.118	5.84E-02	1.02E-02
12	8.903	0.112	1.66E-02	3.78E-02
13	8.923	0.112	4.68E-02	1.94E-02
14	9.599	0.104	5.50E-03	-5.01E-02
15	9.637	0.104	-1.48E-02	3.85E-03
16	9.663	0.103	2.85E-03	2.52E-01
17	10.045	0.100	-5.27E-03	4.52E-02
18	10.440	0.096	5.44E-04	5.50E-01
19	11.038	0.091	-1.78E-03	-9.03E-03
20	12.120	0.083	2.98E-03	-7.58E-01

In Table 12, the first 20 modes of vibration are depicted in terms of period, frequency and the participation factors along the X and Y directions. By analyzing this data, it can be stated that the building has a period of vibration of about 0.224 s in the OY (east-west) direction and of about 0.167 s in the OX (north-south) direction.

By comparing the analytical values to the ones obtained from the experimental tests, we get the following results.

Table 13 Experimental/Analytical comparison of results

Result	Experimental	Analytical	Error (%)
Eigenfrequency OX (Hz)	6.1	5.98	1.97
Eigenfrequency OY (Hz)	4.3	4.471	3.98

As it can be seen, the maximum obtained error is about 4%. This is an acceptable value, taking into account the numerous assumptions and uncertainties which this model presents and which were previously discussed.

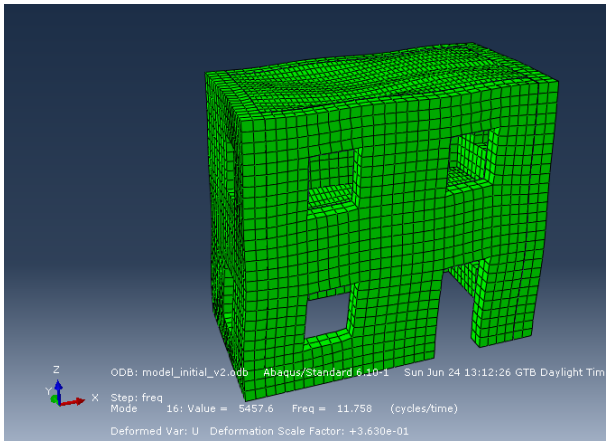

Fig. 63 OX mode of vibration (mode 16)

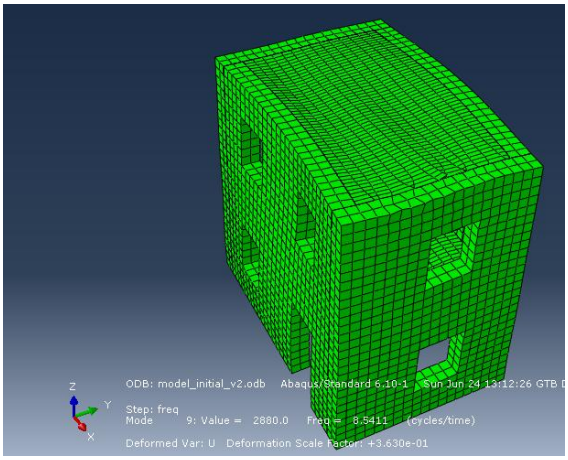

Fig. 64 OY mode of vibration (mode 9)

In the figures above, the representative modes of vibration in each direction have been depicted. The lack of diaphragm action can be noticed even here, where obviously the shells are the weakest elements in the model.

3.3.2 Displacements

When studying the displacements, only the case with the maximum loading will be studied. Due to the fact that the structure is behaving linearly elastic, the preceding load steps have no effect on the way the building behaves. As the displacements are only used to assess the accuracy of the model, the maximum displacement (at each control point) for each loading step will be found. Apart from these, the time histories of the displacements for the maximum load (60% Kalamata) will be plotted.

3.3.2.1 Maximum displacements for all loading cases

As it was previously stated, for the lower loading cases, only the maximum, out-of-plane displacements will be plotted. After the running of the analysis, the following results were obtained.

Table 14 Maximum displacements, load step 1, initial situation

Maximum displacements (m) - 15% Kalamata EQ					
	Absolute			Relative	
South Wall - out of plane - U2 (m)	Base	Node 1 (top)	Node 3 (1st floor)	Node 1 (top)	Node 3 (1st floor)
	0.011	0.0115	0.0113	0.000731	0.00042
East Wall - out of plane - U1 (m)	Base	Node 2 (top)	Node 4 (1st floor)	Node 2 (top)	Node 4 (1st floor)
	0.00682	0.00979	0.00828	0.00296	0.00146

Table 15 Maximum displacements, load step 2, initial situation

Maximum displacements (m) - 30% Kalamata EQ					
	Absolute			Relative	
South Wall - out of plane - U2 (m)	Base	Node 1 (top)	Node 3 (1st floor)	Node 1 (top)	Node 3 (1st floor)
	0.0221	0.0231	0.0226	0.00146	0.000839
East Wall - out of plane - U1 (m)	Base	Node 2 (top)	Node 4 (1st floor)	Node 2 (top)	Node 4 (1st floor)
	0.0136	0.0196	0.0166	0.00593	0.00292

Table 16 Maximum displacements, load step 3, initial situation

Maximum displacements (m) - 45% Kalamata EQ					
	Absolute			Relative	
South Wall - out of plane - U2 (m)	Base	Node 1 (top)	Node 3 (1st floor)	Node 1 (top)	Node 3 (1st floor)
	0.0331	0.0346	0.0339	0.00219	0.00126
East Wall - out of plane - U1 (m)	Base	Node 2 (top)	Node 4 (1st floor)	Node 2 (top)	Node 4 (1st floor)
	0.0205	0.0294	0.0248	0.00889	0.00439

Table 17 Maximum displacements, load step 4, initial situation

Maximum displacements (m) - 60% Kalamata EQ					
	Absolute			Relative	
South Wall - out of plane - U2 (m)	Base	Node 1 (top)	Node 3 (1st floor)	Node 1 (top)	Node 3 (1st floor)
	0.0441	0.0461	0.0452	0.00292	0.00168
East Wall - out of plane - U1 (m)	Base	Node 2 (top)	Node 4 (1st floor)	Node 2 (top)	Node 4 (1st floor)
	0.0273	0.0391	0.0331	0.0119	0.00585

As it can be seen from the tables above, the displacements (both relative and absolute) vary linearly with the load, as expected. It can be noticed, as well that the maximum out-of-plane relative displacement stands in the region of 1.2 cm. This value is an acceptable one, as, from the experimental results, a displacement in the same region has been obtained. Not only is this value acceptable but, compared to the experimentally obtained data, it can be seen that the variation of the relative displacements along the building's height respects, more or less, the same rule.

3.3.2.2 Displacement time histories in the maximum loading case (60% Kalamata EQ)

After the reports generated for the maximum displacements in all the loading cases, the maximum loading case will be further studied. The aforementioned case is the 60% Kalamata earthquake bi-axial test. This has been the last test during which the initial building behave elastically.

The studied displacements will be the total, as well as the relative ones.

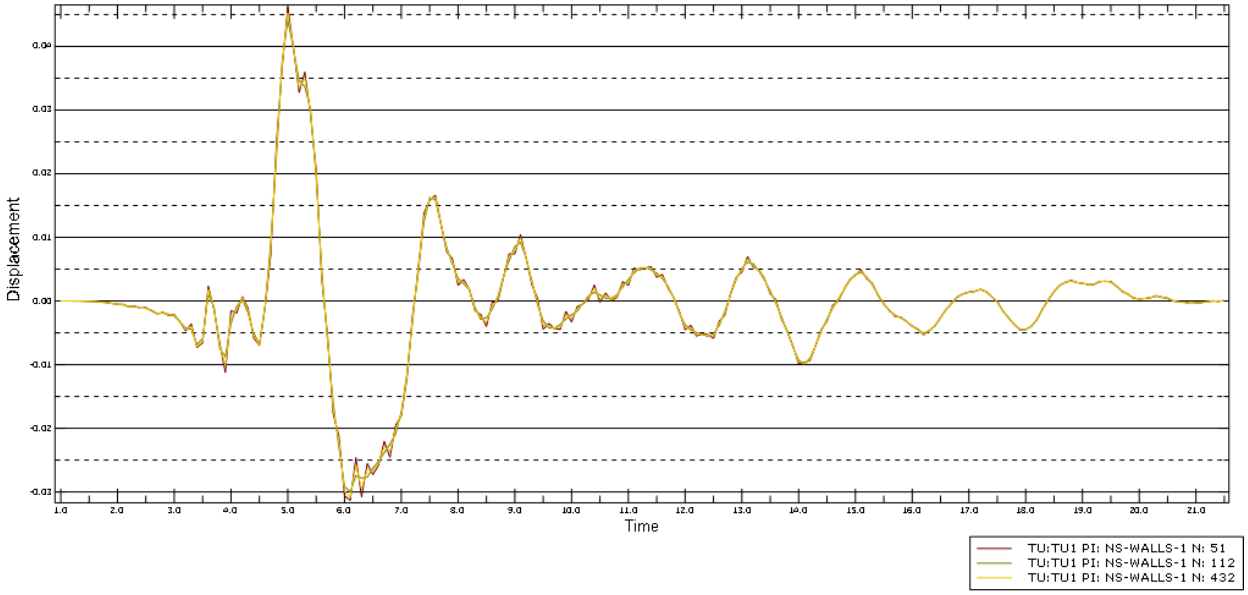

Fig. 65 Absolute displacement, OX, nodes 1, 3 and base

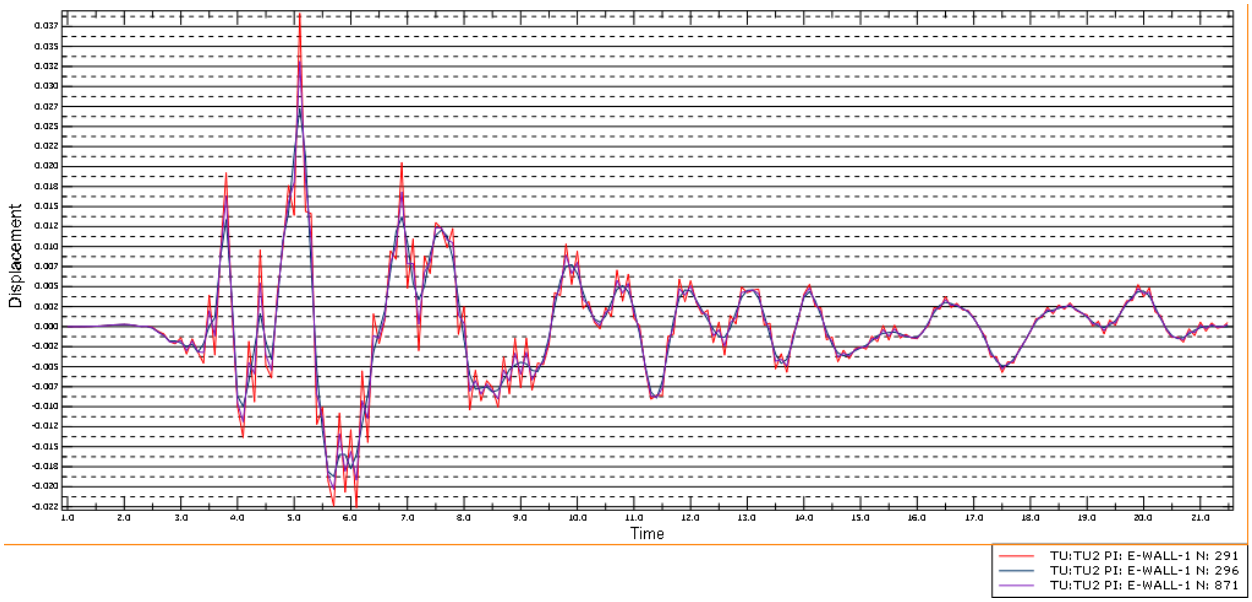

Fig. 66 Absolute displacement, OY, nodes 2, 4 and base

In Fig. 65 and Fig. 66 above, the relative displacement is clearly visible, differential vibrations appearing, as expected, at the points of discontinuity in the time history.

It can also be noticed that, especially in the OY direction, the magnitude of the relative displacements can be considered of significant importance, compared to the magnitude of the absolute displacements.

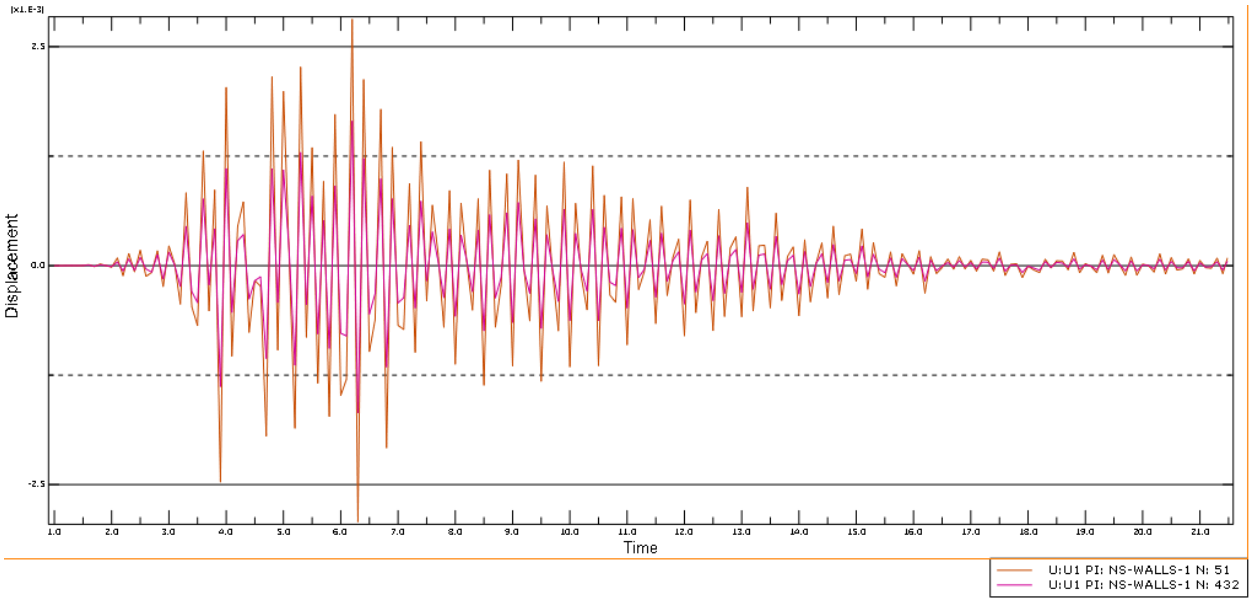

Fig. 67 Relative displacement, OX, nodes 1 and 3

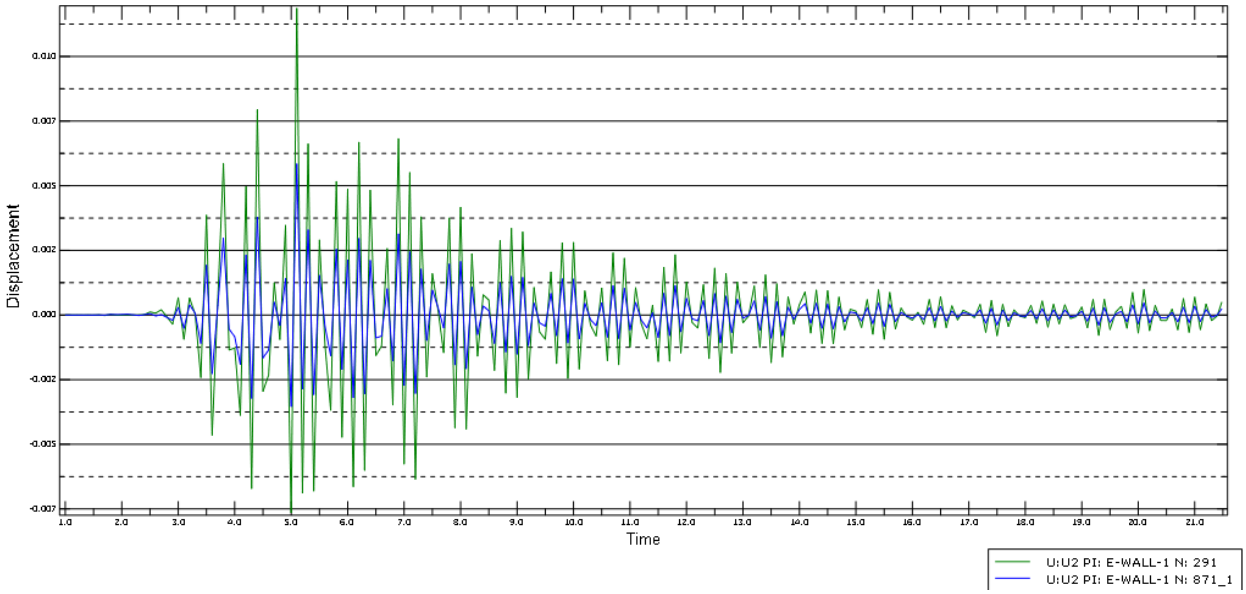

Fig. 68 Relative displacement, OY, nodes 2 and 4

Above, the relative displacements' time histories are depicted. It can be noticed that the highest disturbances appear in the interval 4 to 6 seconds of the time history. This is an important clue about the moments that should be analyzed in order to assess the most unfavorable state of stresses.

3.3.3 Accelerations

In terms of accelerations, the strategy employed will be to display the maximum values for each loading case.

Not so much attention will be paid to accelerations in this paper, as the laboratory results have been expressed in terms of displacements and eigenfrequencies, and not accelerations.

Table 18 Maximum acceleration values, 15% Kalamata EQ

Maximum accelerations (m/s^2) - 15% Kalamata EQ					
	Absolute			Relative	
South Wall - out of plane	Base	Node 1 (top)	Node 3 (1st floor)	Node 1 (top)	Node 3 (1st floor)
	0.356	1.06	0.611	1.01	0.565
East Wall - out of plane	Base	Node 2 (top)	Node 4 (1st floor)	Node 2 (top)	Node 4 (1st floor)
	0.386	2.03	1.22	1.79	0.918

Table 19 Maximum acceleration values, 30% Kalamata EQ

Maximum accelerations (m/s^2) - 30% Kalamata EQ					
	Absolute			Relative	
South Wall - out of plane	Base	Node 1 (top)	Node 3 (1st floor)	Node 1 (top)	Node 3 (1st floor)
	0.712	2.11	1.22	2.02	1.13
East Wall - out of plane	Base	Node 2 (top)	Node 4 (1st floor)	Node 2 (top)	Node 4 (1st floor)
	0.772	4.06	2.45	3.57	1.84

Table 20 Maximum acceleration values, 45% Kalamata EQ

Maximum accelerations (m/s^2) - 45% Kalamata EQ					
	Absolute			Relative	
South Wall - out of plane	Base	Node 1 (top)	Node 3 (1st floor)	Node 1 (top)	Node 3 (1st floor)
	1.07	3.17	1.83	3.03	1.69
East Wall - out of plane	Base	Node 2 (top)	Node 4 (1st floor)	Node 2 (top)	Node 4 (1st floor)
	1.16	6.09	3.67	5.36	2.75

Table 21 Maximum acceleration values, 60% Kalamata EQ

Maximum accelerations (m/s^2) - 60% Kalamata EQ					
	Absolute			Relative	
South Wall - out of plane	Base	Node 1 (top)	Node 3 (1st floor)	Node 1 (top)	Node 3 (1st floor)
	1.42	4.22	2.44	4.04	2.26
East Wall - out of plane	Base	Node 2 (top)	Node 4 (1st floor)	Node 2 (top)	Node 4 (1st floor)
	1.54	8.12	4.89	7.15	3.67

In the tables above, the maximum values of the accelerations are expressed, for different points and tests. Special attention must be paid to the very large differences between the accelerations at the base level and the accelerations at the top of the walls (which are even over 5 times larger). Of course, this result comes also from the fact that a very low damping ratio has been used in the modal analysis. The low damping ratio has been chosen because a linear elastic behavior was assumed (no cracks). This means that the building has a low energy-dissipation potential and, thus, lower damping ratios.

3.3.4 Stresses and displacements in the least favorable situation

In order to assess the load carrying capacity of the structure in its initial state, a moment in the time history has to be chosen.

Basically, a search of unfavorable conditions will be undergone in the 4-7 seconds interval of the time history of the maximum loading (60% Kalamata EQ) and then the output from this instant will be plotted. This search will take into account the moment when, in the masonry, the largest compressive stresses appear.

After some searching has been performed, the time instant at 4.1 seconds has been found as being the most unfavorable scenario.

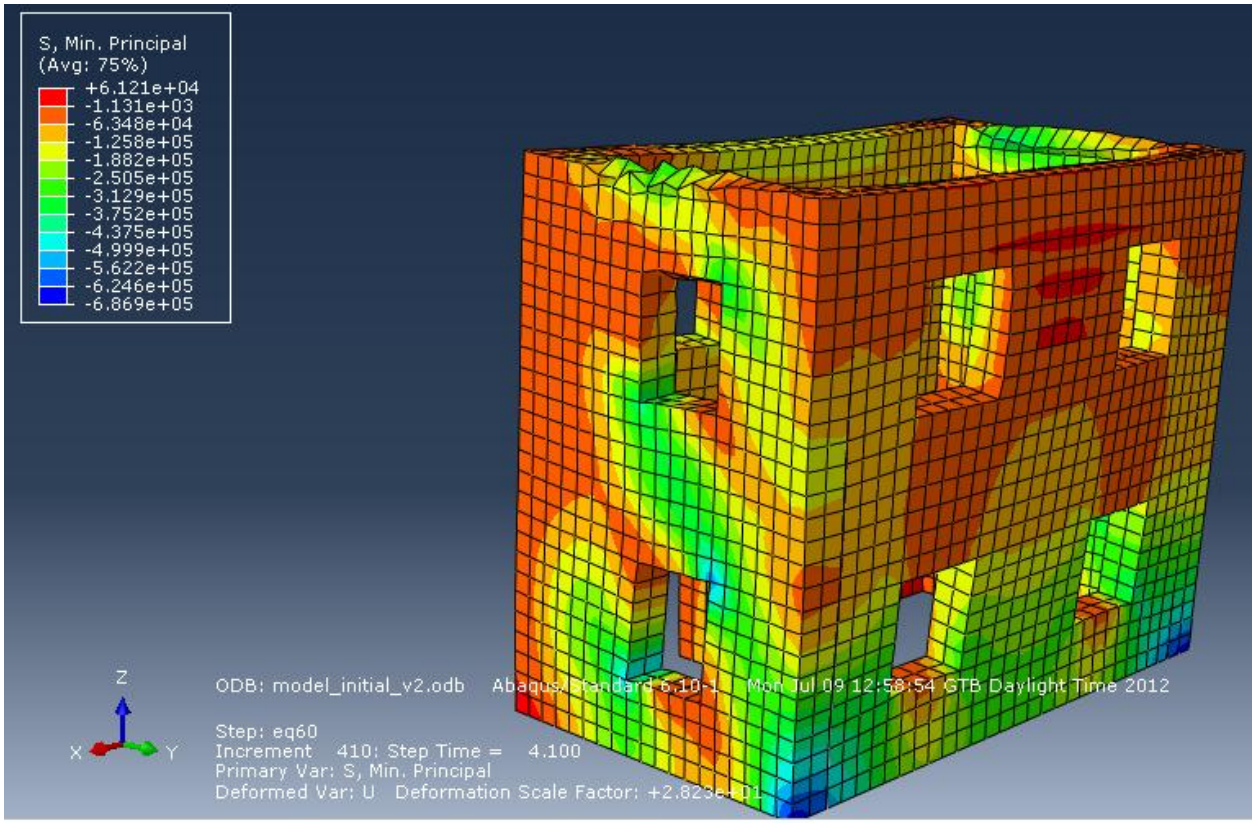

Fig. 69 Minimum stresses in the selected instant

As we can see in Fig. 69, the minimum compressive stress reached by the masonry is in the region of 0.7 MPa. This is a rather high value and it can be considered that the masonry is approaching failure (which is, probably, why the building behaved elastically only up to this point).

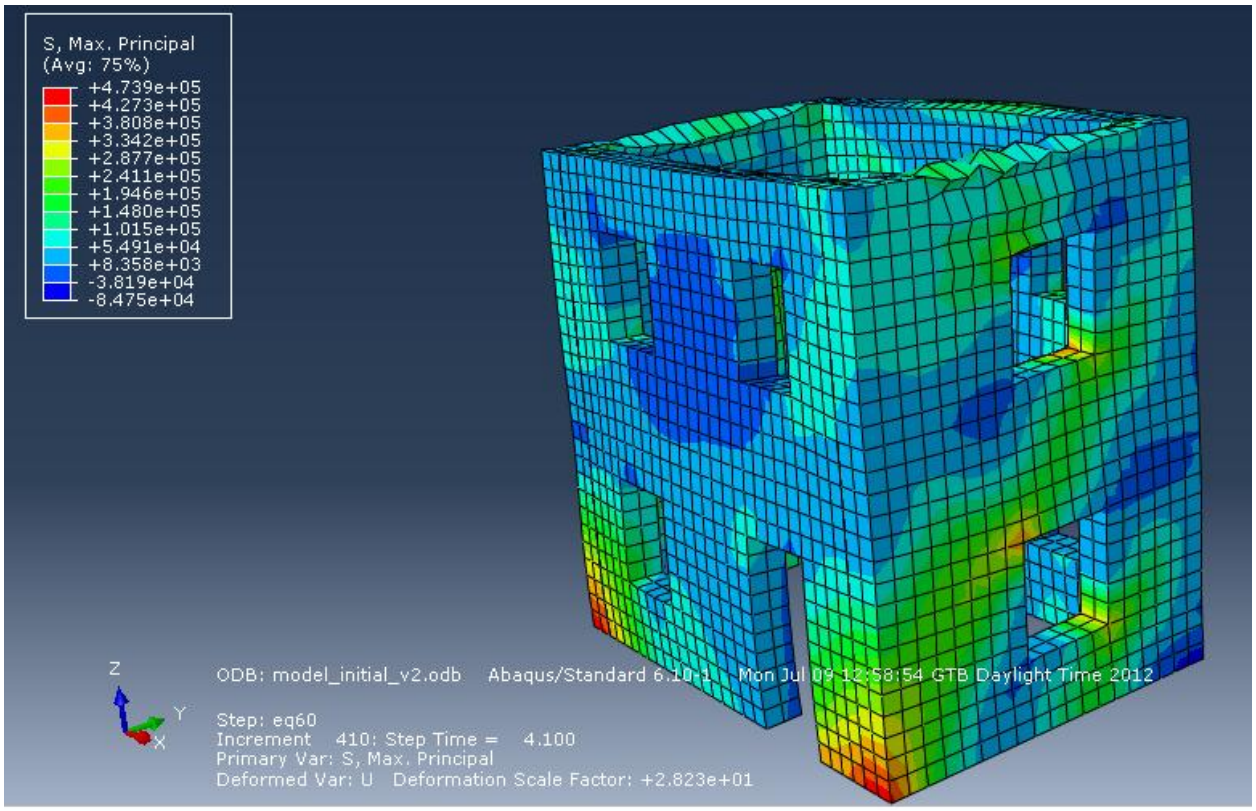

Fig. 70 Maximum principal stresses in the selected instant

In Fig. 70 above, a plot of the maximum principal stresses is depicted. The possible tensile cracks are clearly visible. The maximum tensile stress in the masonry reaches about 0.5 MPa, which is a rather high value.

As expected, we can see from the pictures above that the most vulnerable direction of the building is the east-west (OY) direction.

From the point of view of stress redistribution, it can be stated that the diaphragms do little to nothing to redistribute stresses.

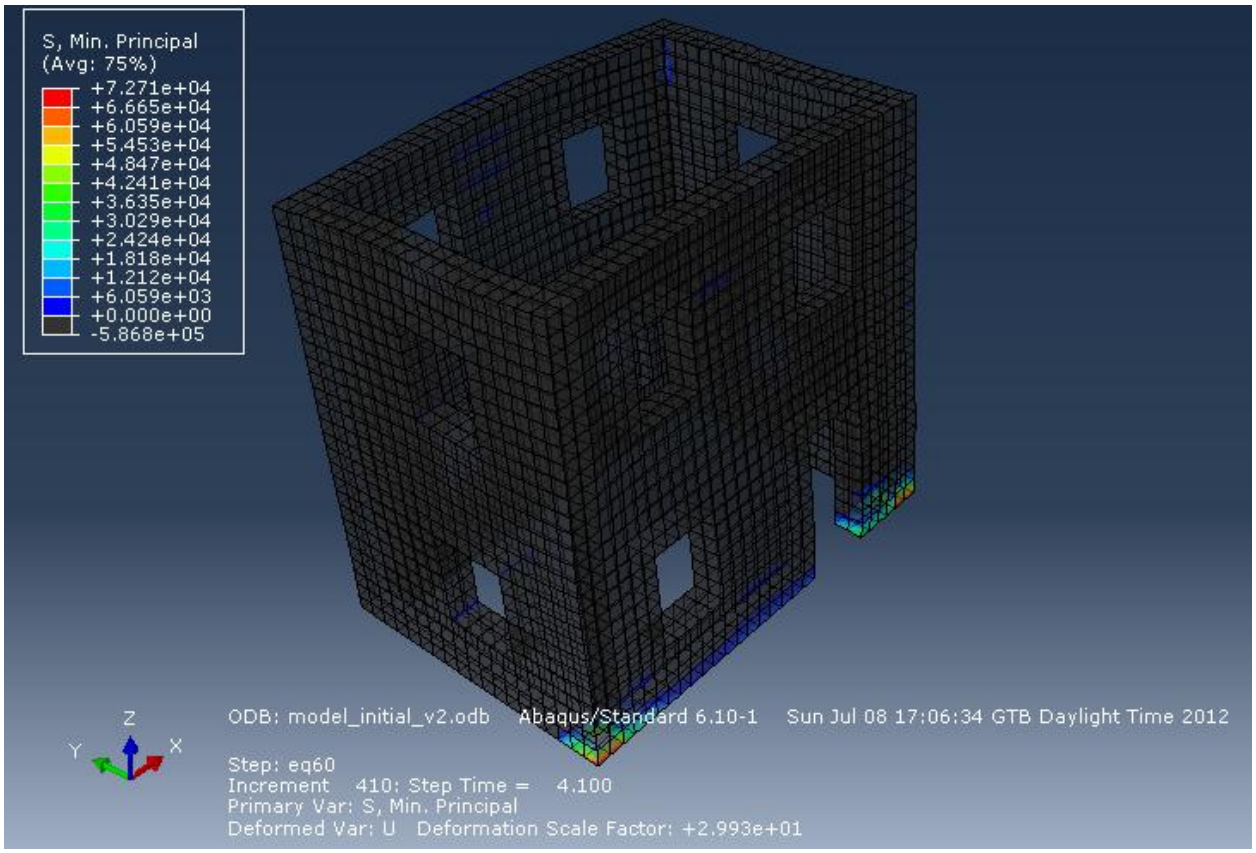

Fig. 71 Vulnerable zones

In Fig. 71, a plot of the minimum principal stresses can be seen. This plot is only colored when the minimum principal stresses are higher than zero. This means that the colored zones are regions subjected to triaxial tension and, thus, very susceptible to cracks.

These vulnerable zones can be seen at the base of the structure, window corners and walls' intersections (somehow expected) and, also, in the midspan regions of the longitudinal walls. It is apparent that some horizontal cracks could appear in those zones in the studied loading case.

As the studied time-instant is characterized by a violent motion in the OY axis, it interesting to see how the displacements in this direction are distributed.

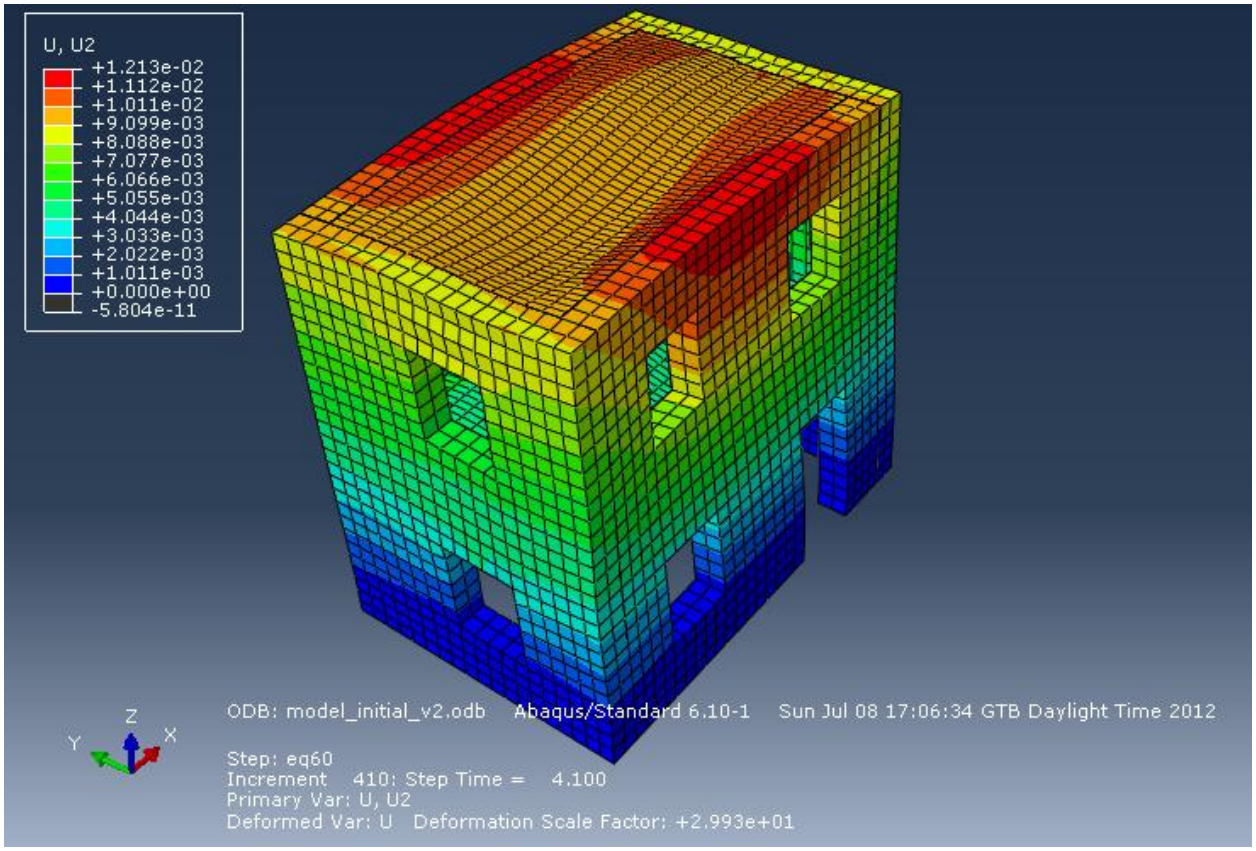

Fig. 72 OY displacements in the chosen instant

As it can be seen from the plot above, the diaphragm does little to transmit the displacements uniformly. The longitudinal walls are bending out of their plane due to the earthquake action and these displacements are not equally distributed.

3.4 Analytical results of the strengthened model

For the improved structure, a new analysis and a new model have been applied. The new model has the same geometry as the first one, the only things that differ being the interactions (shells are connected to all 4 walls) and the material properties of the elements.

As the determination of the Young's modulus for a grouted masonry is a very difficult task even when all the data is provided, the Young's modulus to be employed for the new masonry has been adjusted in order for the results to come as close as possible to the real ones and, finally, it has been concluded that the initial value of the Young's modulus was acceptable for this case.

The results for the strengthened model will be displayed, as before, in terms of eigenfrequencies, displacements, accelerations and stresses.

3.4.1 Eigenperiods and modes of vibration

The first step in the analysis performed is the extraction of the eigenfrequencies of the model. This step is very useful for assessing the accuracy of the model and, as well, for model calibration.

Table 22 Modal characteristics of strengthened model

Mode Number	Eigenfrequency (Hz)	Eigenperiod (s)	Participation OX	Participation OY
1	8.64	0.116	-1.27E-02	1.37
2	11.1	0.090	1.33	9.89E-03
3	11.8	0.085	1.92E-02	-2.44E-03
4	13.3	0.075	5.29E-02	-4.12E-03
5	16.1	0.062	5.18E-02	8.15E-03
6	18.7	0.053	3.58E-01	4.14E-02
7	19.1	0.052	-1.96E-01	-4.39E-02

As it can be seen in the table above, the frequencies are higher than they were before. Moreover, the building now behaves as a whole and the first two modes of vibration are the "real" modes, in the OX and OY directions.

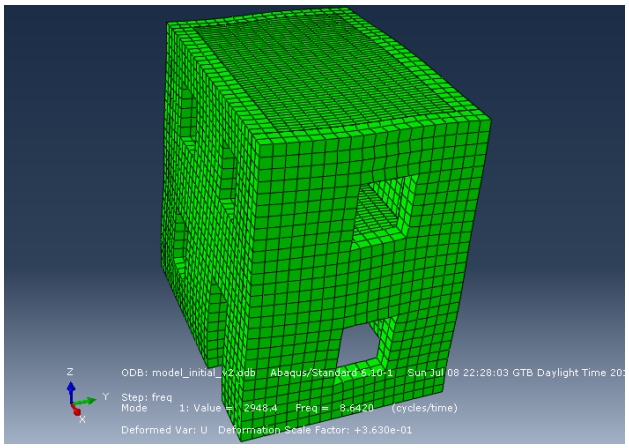

Fig. 73 1st mode of vibration

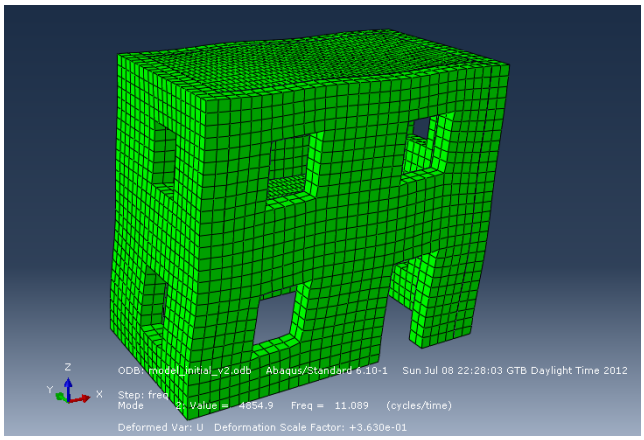

Fig. 74 2nd mode of vibration

Table 23 Accuracy of strengthened model

Result	Analytical	Experimental	Error (%)
OX eigenfrequency (Hz)	11.1	10.4	6.73
OY eigenfrequency (Hz)	8.64	9.8	11.84

As it can be seen in the table above, the errors which were present in this model are higher. This is because it is very difficult to assess the Young's modulus for grouted masonry and the

connection between the floors and the walls, which adds rigidity in both directions and has a rather high influence area. Nevertheless, the model can be considered adequate and the results which are extracted from it will be studied later on.

3.4.2 Displacements

3.4.2.1 Maximum displacements in the studied loading cases

As before, the displacements will be studied in terms of maximum displacements for the loading cases from 15% to 60% Kalamata EQ (in order to compare them with the results from the unstrengthened building) and, as well, for the maximum loading in this model, which is 140% Kalamata EQ.

Table 24 Maximum displacements, load step 1, strengthened building

Maximum displacements (m) - 15% Kalamata EQ					
	Absolute			Relative	
South Wall - out of plane - U2 (m)	Base	Node 1 (top)	Node 3 (1st floor)	Node 1 (top)	Node 3 (1st floor)
	0.011	0.0111	0.0111	0.000105	0.0000587
East Wall - out of plane - U1 (m)	Base	Node 2 (top)	Node 4 (1st floor)	Node 2 (top)	Node 4 (1st floor)
	0.00682	0.00677	0.0068	0.000246	0.000123

Table 25 Maximum displacements, load step 2, strengthened building

Maximum displacements (m) - 30% Kalamata EQ					
	Absolute			Relative	
South Wall - out of plane - U2 (m)	Base	Node 1 (top)	Node 3 (1st floor)	Node 1 (top)	Node 3 (1st floor)
	0.0221	0.0222	0.0221	0.000211	0.000117
East Wall - out of plane - U1 (m)	Base	Node 2 (top)	Node 4 (1st floor)	Node 2 (top)	Node 4 (1st floor)
	0.0136	0.0135	0.0136	0.000492	0.000245

Table 26 Maximum displacements, load step 3, strengthened building

Maximum displacements (m) - 45% Kalamata EQ					
	Absolute			Relative	
South Wall - out of plane - U2 (m)	Base	Node 1 (top)	Node 3 (1st floor)	Node 1 (top)	Node 3 (1st floor)
	0.0331	0.0333	0.0332	0.000316	0.000176
East Wall - out of plane - U1 (m)	Base	Node 2 (top)	Node 4 (1st floor)	Node 2 (top)	Node 4 (1st floor)
	0.0205	0.0203	0.0204	0.000737	0.000368

Table 27 Maximum displacements, load step 4, strengthened building

Maximum displacements (m) - 60% Kalamata EQ					
	Absolute			Relative	
South Wall - out of plane - U2 (m)	Base	Node 1 (top)	Node 3 (1st floor)	Node 1 (top)	Node 3 (1st floor)
	0.0441	0.0444	0.0443	0.000422	0.000235
East Wall - out of plane - U1 (m)	Base	Node 2 (top)	Node 4 (1st floor)	Node 2 (top)	Node 4 (1st floor)
	0.0273	0.0271	0.0272	0.000983	0.000491

Table 28 Maximum displacements, 130% Kalamata EQ , strengthened building

Maximum displacements (m) - 130% Kalamata EQ					
	Absolute			Relative	
South Wall - out of plane - U2 (m)	Base	Node 1 (top)	Node 3 (1st floor)	Node 1 (top)	Node 3 (1st floor)
	0.0956	0.0962	0.0959	0.000914	0.000508
East Wall - out of plane - U1 (m)	Base	Node 2 (top)	Node 4 (1st floor)	Node 2 (top)	Node 4 (1st floor)
	0.0591	0.0587	0.0589	0.00213	0.00106

As it can be noticed from the tables above, a clear reduction of the relative displacements is visible. The out of plane relative displacements are reduced more than 10 times from their initial values. This is a very good clue that the diaphragm action of the floors is really efficient.

The obtained displacements for this case also vary in the same way the results obtained in the lab tests did, the difference, in relative displacements, from the 1st floor to the roof being, at most, 1 mm. This means that the box behavior of the building has been achieved and the model is accurately simulated.

3.4.2.2 Displacement time history for the 60% loading scenario

In order to enable a comparison between the initial and final situation, the displacement time history will be studied for the 60% earthquake, like before.

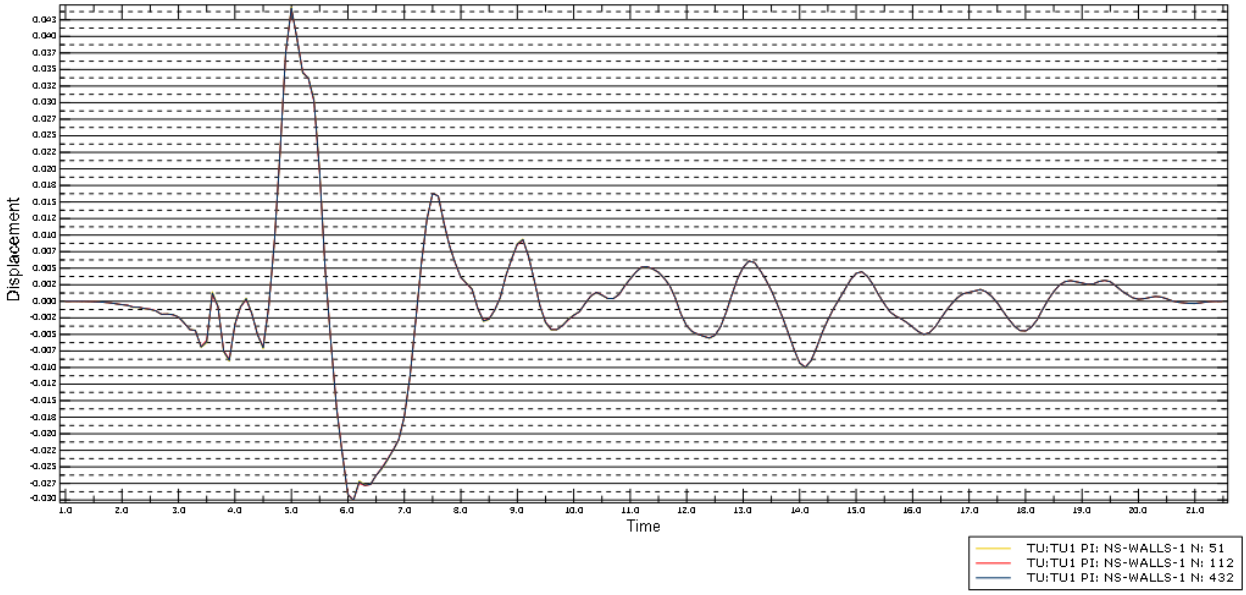

Fig. 75 Absolute displacement OX direction

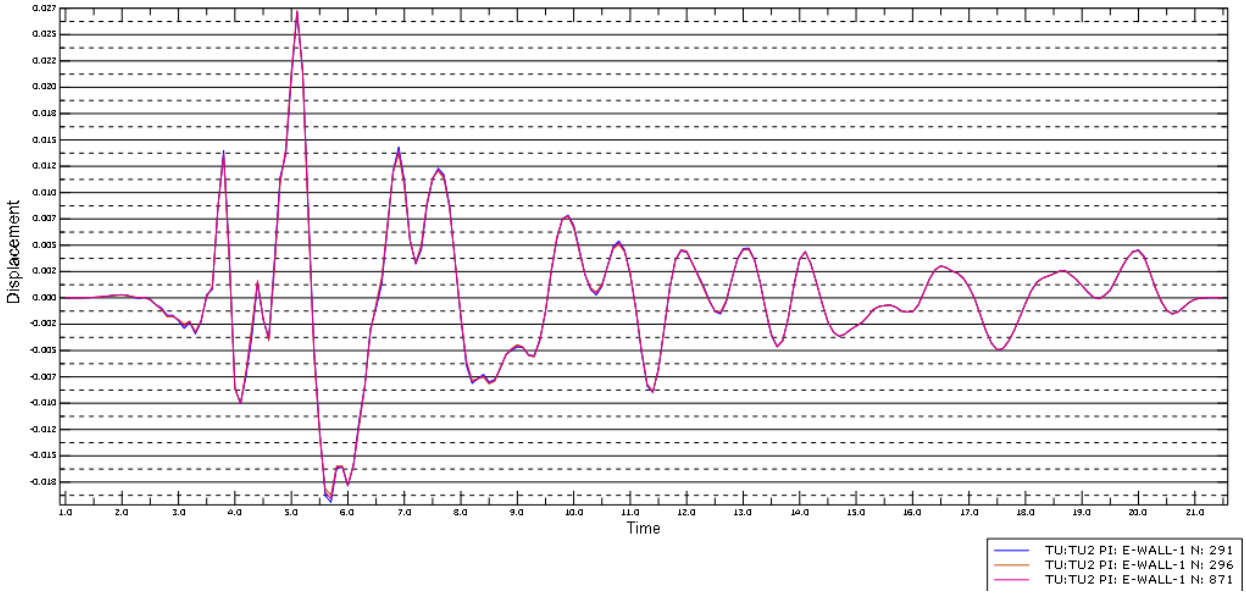

Fig. 76 Absolute displacement OY direction

As it can be seen from Fig. 75 and Fig. 76, the absolute displacements are basically the same, independent at which level of the building they are.

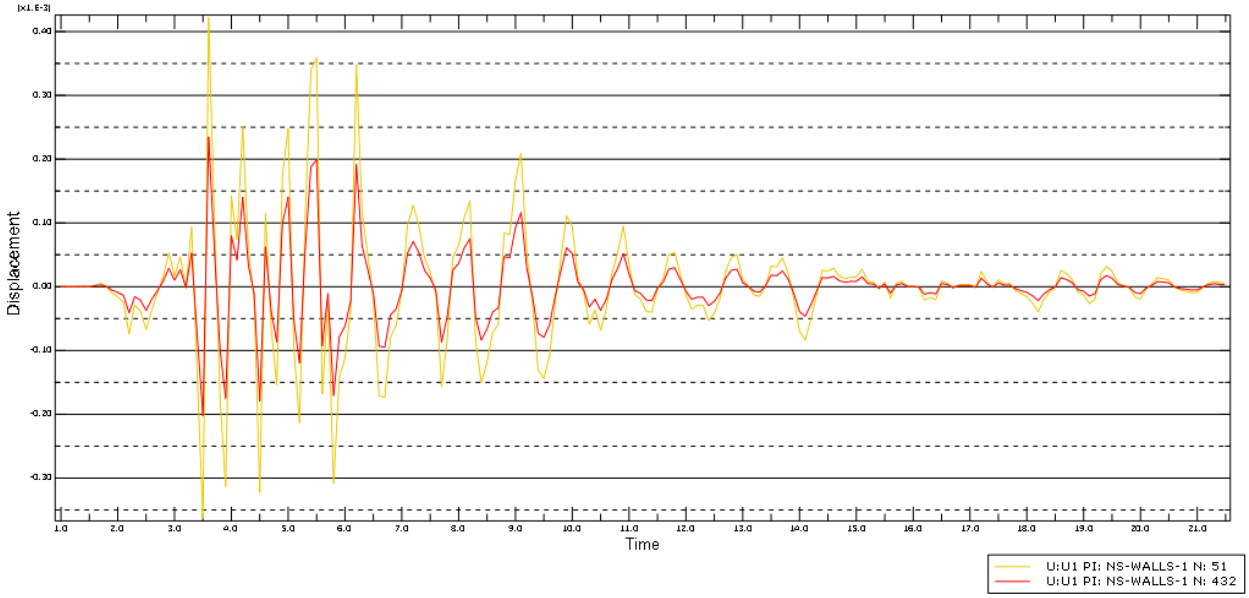

Fig. 77 Relative displacement OX of points 1 and 3

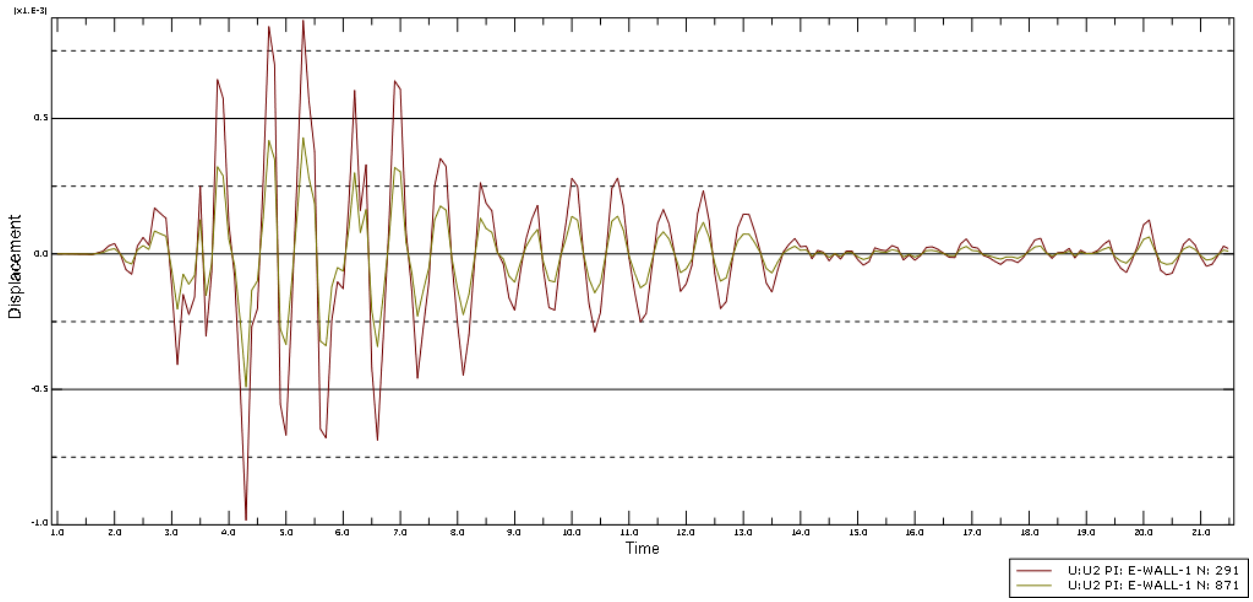

Fig. 78 Relative displacement OY of points 2 and 4

From the figures above, it can be seen that, as expected, the maximum relative displacement can be found in the same time span as before. The difference is that, for the present case, the values of the relative displacements are much lower.

3.4.3 Accelerations

The acceleration values will be assessed, as before, only in terms of their minimum and maximum values for each loading case.

Table 29 Maximum accelerations, 15% Kalamata, strengthened building

Maximum accelerations (m/s^2) - 15% Kalamata EQ					
	Absolute			Relative	
South Wall - out of plane	Base	Node 1 (top)	Node 3 (1st floor)	Node 1 (top)	Node 3 (1st floor)
	0.356	0.409	0.374	0.274	0.150
East Wall - out of plane	Base	Node 2 (top)	Node 4 (1st floor)	Node 2 (top)	Node 4 (1st floor)
	0.386	0.710	0.372	0.677	0.338

Table 30 Maximum accelerations, 30% Kalamata, strengthened building

Maximum accelerations (m/s^2) - 30% Kalamata EQ					
	Absolute			Relative	
South Wall - out of plane	Base	Node 1 (top)	Node 3 (1st floor)	Node 1 (top)	Node 3 (1st floor)
	0.712	0.817	0.749	0.549	0.301
East Wall - out of plane	Base	Node 2 (top)	Node 4 (1st floor)	Node 2 (top)	Node 4 (1st floor)
	0.772	1.420	0.744	1.353	0.677

Table 31 Maximum accelerations, 45% Kalamata, strengthened building

Maximum accelerations (m/s^2) - 45% Kalamata EQ					
	Absolute			Relative	
South Wall - out of plane	Base	Node 1 (top)	Node 3 (1st floor)	Node 1 (top)	Node 3 (1st floor)
	1.068	1.226	1.123	0.823	0.451
East Wall - out of plane	Base	Node 2 (top)	Node 4 (1st floor)	Node 2 (top)	Node 4 (1st floor)
	1.158	2.131	1.116	2.030	1.015

Table 32 Maximum accelerations, 60% Kalamata, strengthened building

Maximum accelerations (m/s^2) - 60% Kalamata EQ					
	Absolute			Relative	
South Wall - out of plane	Base	Node 1 (top)	Node 3 (1st floor)	Node 1 (top)	Node 3 (1st floor)
	1.424	1.635	1.497	1.098	0.602
East Wall - out of plane	Base	Node 2 (top)	Node 4 (1st floor)	Node 2 (top)	Node 4 (1st floor)
	1.543	2.841	1.488	2.706	1.353

Table 33 Maximum accelerations, 130% Kalamata, strengthened building

Maximum accelerations (m/s^2) - 130% Kalamata EQ					
	Absolute			Relative	
South Wall - out of plane	Base	Node 1 (top)	Node 3 (1st floor)	Node 1 (top)	Node 3 (1st floor)
	3.086	3.542	3.245	2.378	1.304
East Wall - out of plane	Base	Node 2 (top)	Node 4 (1st floor)	Node 2 (top)	Node 4 (1st floor)
	3.344	6.156	3.224	5.864	2.932

From Table 29 to Table 33 above, some basic aspects can be noticed. First of all, the value of the amplification factor (top acceleration / base acceleration) is greatly reduced, compared to the initial situation. This time, the maximum top acceleration is less than two times the base acceleration, in the worst case scenario. Rather high values of relative accelerations can still be encountered, but these relative accelerations are much lower than in the unstrengthened situation.

3.4.4 Stresses and displacements in the least favorable situation

In this section, the stresses and displacements will be studied for the least favorable moment during the seismic excitation.

In order to get a comparison about the way the interventions helped improving the behavior of the structure, an assessment of the state of stresses in the 60% Kalamata earthquake excitation case will be made.

Also, in order to assess the capacity of the structure to withstand the maximum seismic loading, the 130% Kalamata earthquake excitation case (upper limit of the test) will be studied.

Due to the fact that the structure has been modified and, thus, its response altered, another search of the least favorable situation has to be performed. From the time histories above, it is assumed that this scenario will be encountered in the same interval 4 s – 7 s, from the time history of the event.

The least favorable scenario is searched for frame-by-frame, by looking for the moment where the maximum compressive stresses in the masonry elements are present. In this case, the least favorable situation is found at 3.3 seconds during the time history, as in the previous case.

3.4.4.1 Stresses and displacements for the 60% Kalamata excitation

In the present section, the stresses and displacement which arise in the least favorable moment of the 60% Kalamata excitation will be investigated.

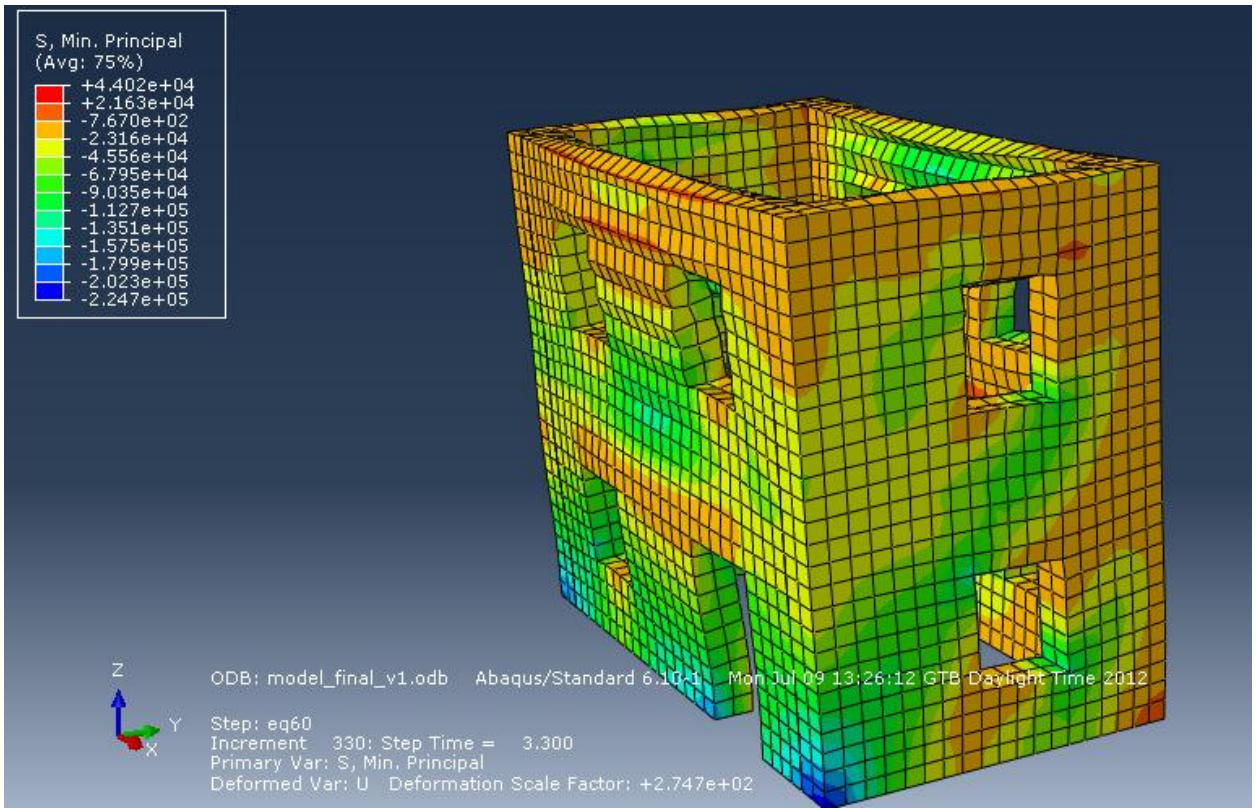

Fig. 79 Minimum stresses, 60% Kalamata, strengthened building

In Fig. 79, it can be observed that the minim principal stresses have been greatly reduced, in comparison with the worst case scenario for the same excitation but for the unstrengthened building. Whereas before, compressive stresses in the region of 0.8 MPa could be encountered, in the present case the minimum compressive stresses (appearing isolated, at the building's corners) are in the region of 0.22 MPa – three times less than in the previous case.

Fig. 80 below depicts the state of maximum principal stresses in the structure. Special attention must be given to the maximum tensile stress here, which is in the region of 0.15 MPa. This value is adequate and it is improbable that the masonry will fail in tension.

Another interesting fact to be observed is the direction and placement of the inclined cracks. Whereas before only some of the elements (walls) of the building presented inclined tensile zones, now all of the four walls contribute to withstanding the loads in the structure and display a similar crack pattern. This is another clear hint of a good behavior of the diaphragms formed by the floors.

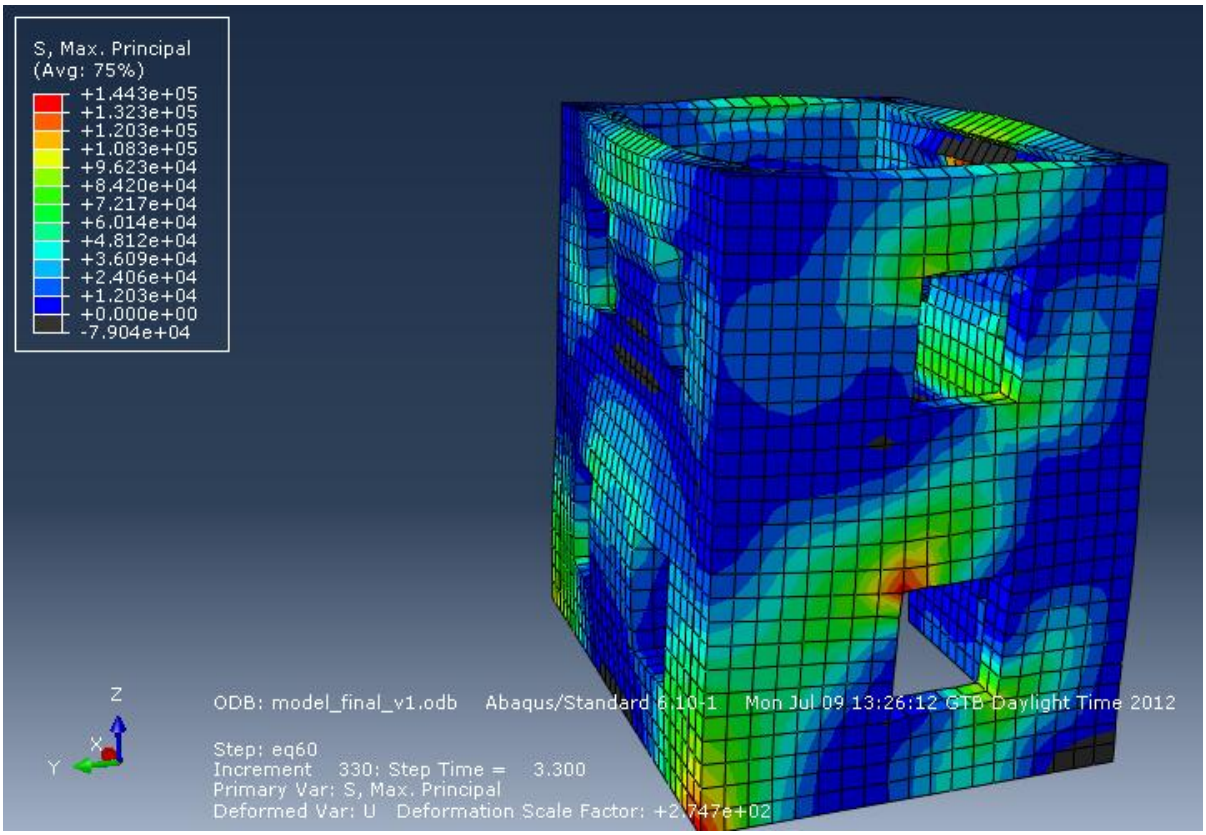

Fig. 80 Maximum principal stresses, 60% Kalamata, strengthened building

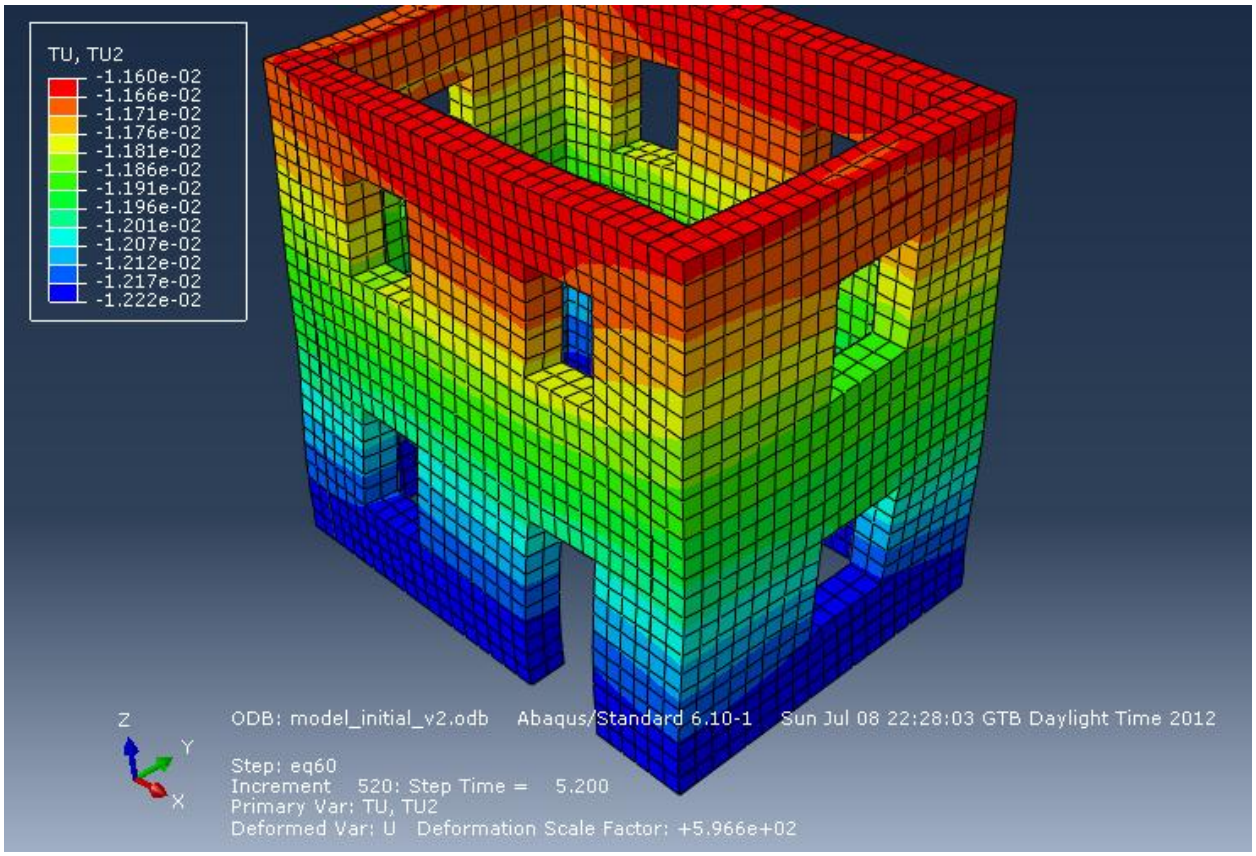

Fig. 81 Absolute displacement, OY, 60% Kalamata, strengthened building

In the figure above, the absolute displacements have been plotted, in the OY direction. It can be noticed that, in contrast with the initial situation, the two longitudinal walls no longer suffer out-of-plane deformations; the differences in deformations along the walls being of the order 0.007 cm.

The same stands for Fig. 82, where the absolute displacements in the OX direction are plotted. The short (transversal) walls hardly deform out of their plane (relative displacements of the order of 0.003 cm). It has to be noted here that a tendency of skew displacements is observed at the corners of the building. Special care must be, thus, paid to the way the connections between the walls behave.

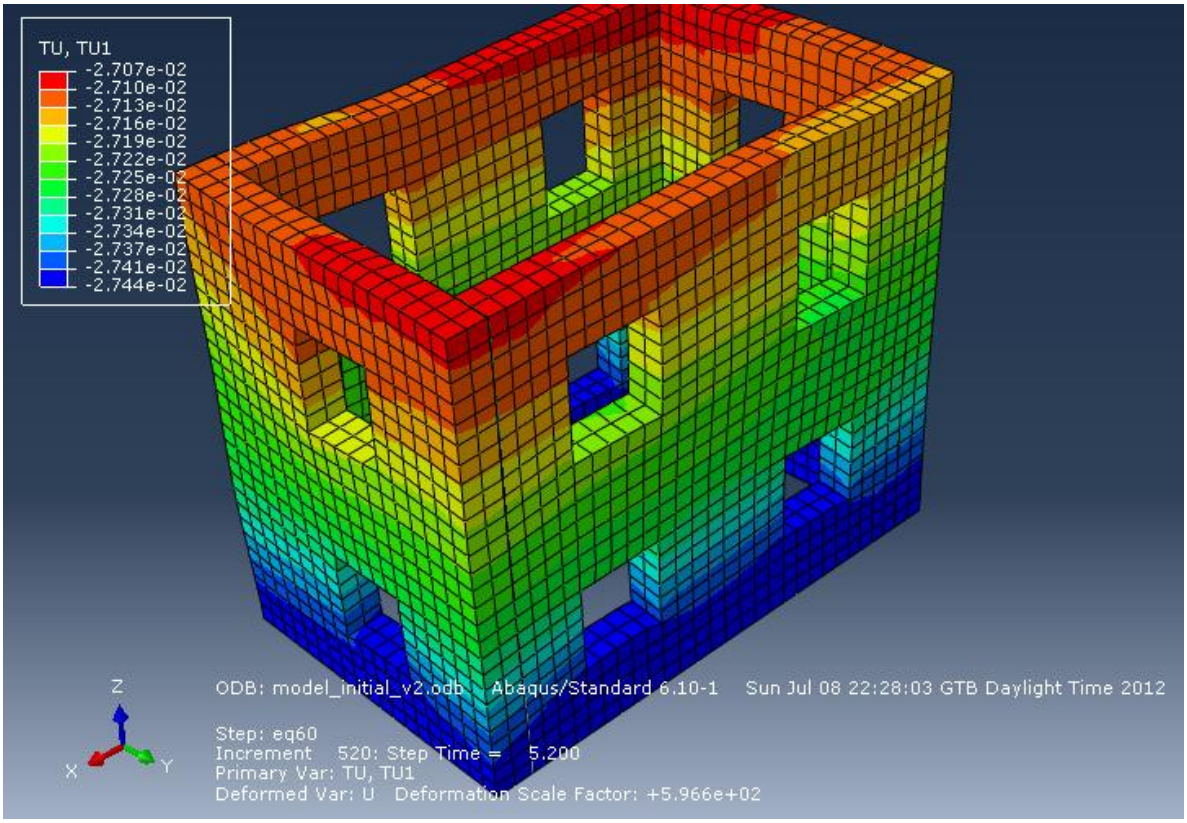

Fig. 82 Absolute displacement, OX, 60% Kalamata, strengthened building

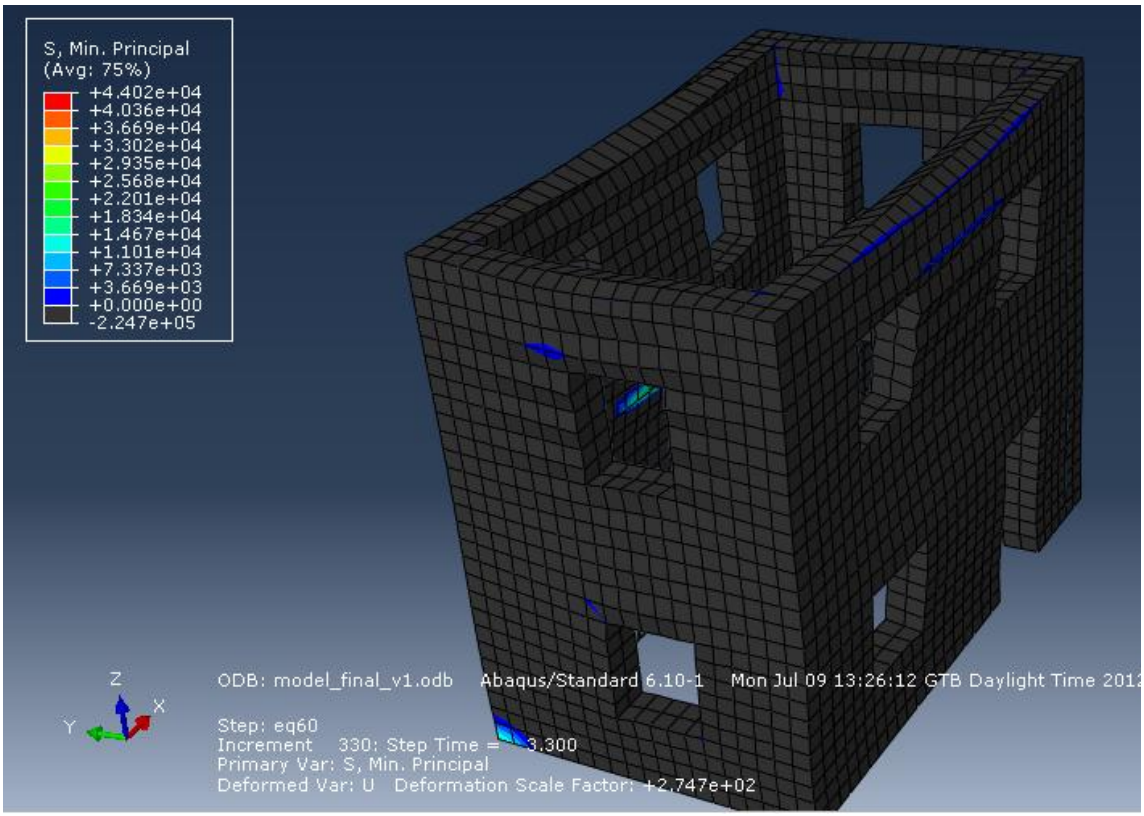

Fig. 83 Unfavorable triaxial conditions

In Fig. 83 above, the triaxial tensioned zones are displayed. Apart from the expected vulnerable zones (base of the tensioned part of the building, corners of voids) it can be noticed that the horizontal vulnerable zones at the top of the walls have disappeared. Those zones were formed by the out-of-plane bending of the walls, due to the lack of diaphragm action of the floors. Their disappearance means that the floors now behave like rigid diaphragms. Some horizontally oriented areas of triaxial tension are, however, present in the walls, at the levels of the rigid diaphragms. These areas are expected to be formed, but not due to out-of-plane bending, rather, they are formed by the action of the diaphragms in the horizontal plane. In conclusion, adequate strength of the walls must be ensured in those zones (as previously mentioned).

3.4.4.2 Stresses and displacements for the 130% Kalamata excitation

After comparing the similar situations between the initial and strengthened model, it is time to move on and assess the resistance of the new model. Its response to the 130% Kalamata earthquake excitation will be assessed and several conclusions regarding the ability of the strengthened structure to withstand the loads will be drawn.

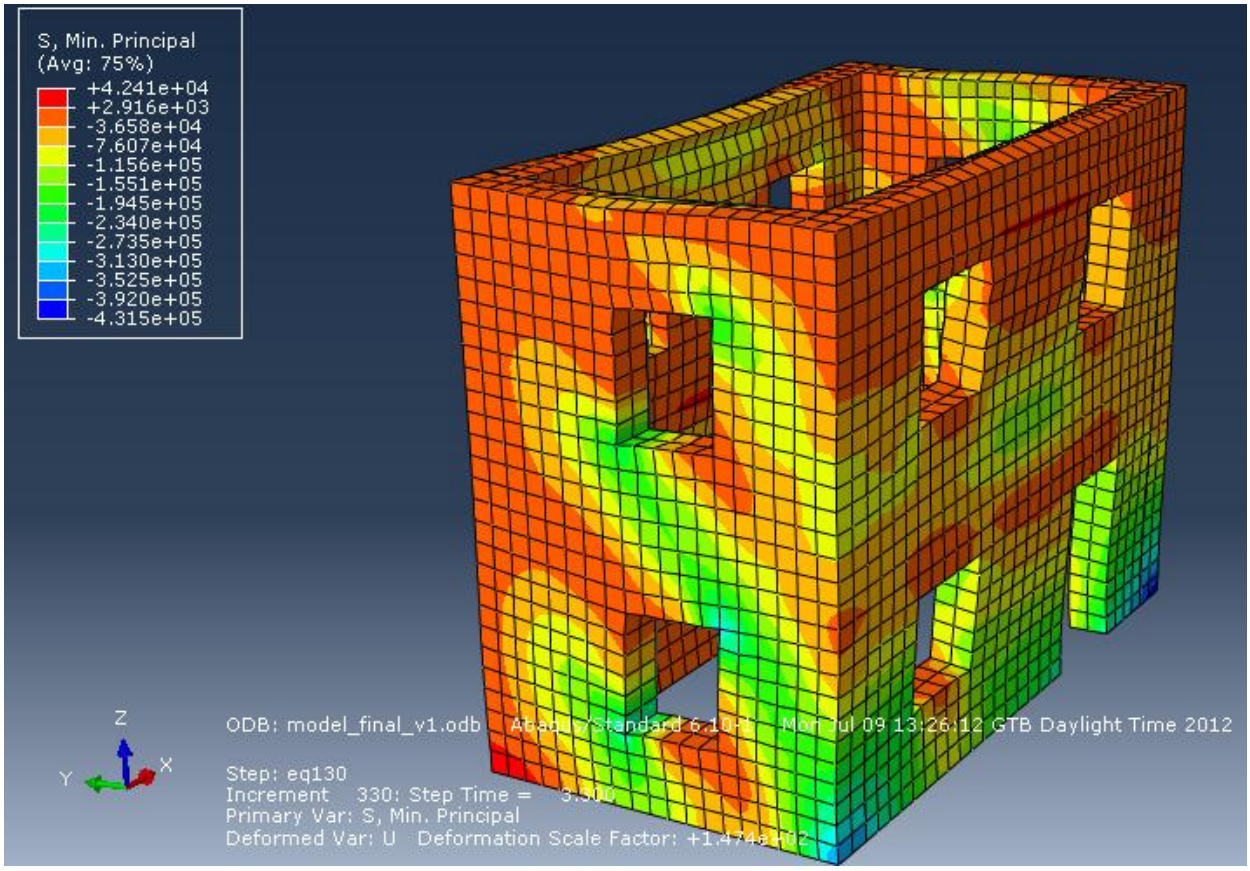

Fig. 84 Minimum principal stresses, 130% Kalamata, strengthened building

From Fig. 84, it can be easily observed that, even in this extreme case (more than twice the maximum excitation from the initial test) the extreme compressive stresses are still low. The extreme value of the compressive stress can be found, like before, in the corners of the building, at the base level. Its value, around 0.43 MPa is less than a half of the compressive strength of most masonry elements (moreover, the masonry used in this model is grouted, so its strength has been seriously increased).

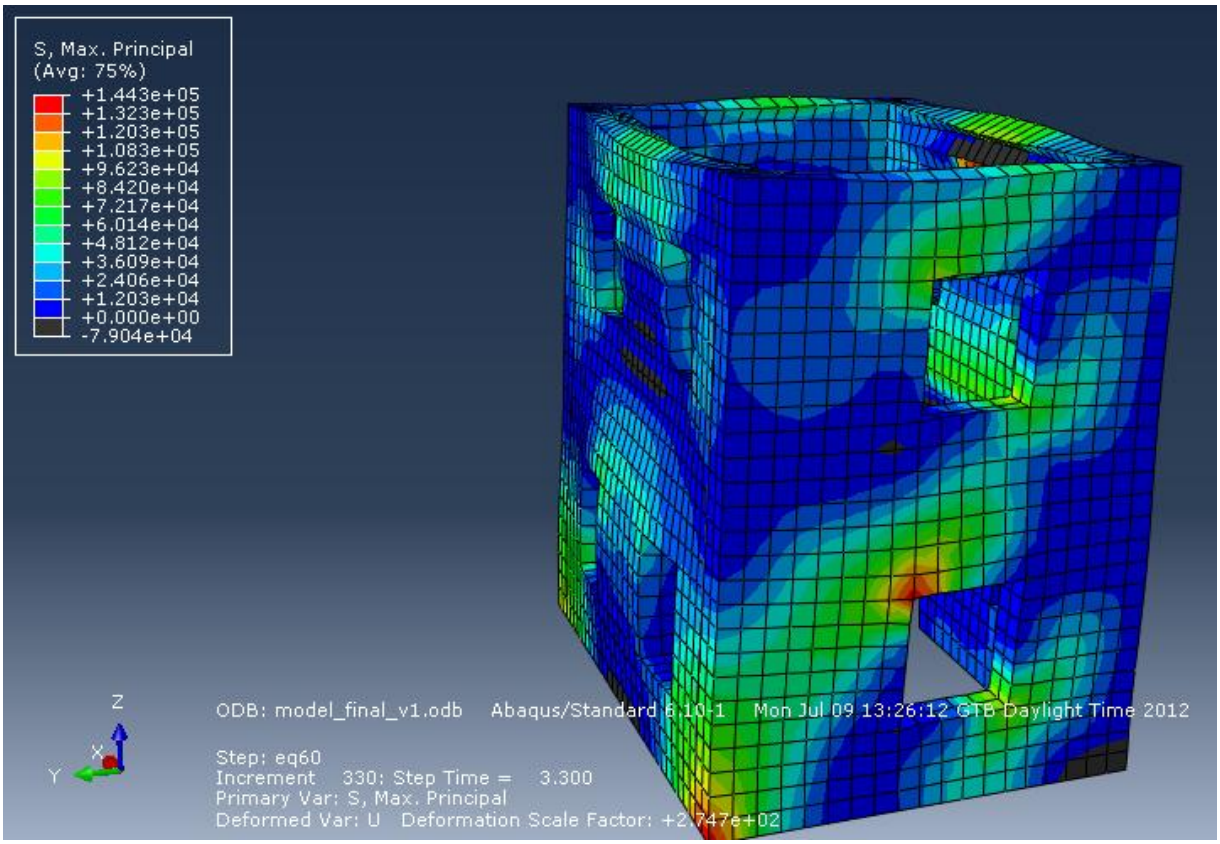

Fig. 85 Maximum principal stresses, 130% Kalamata, strengthened building

In the figure above, a plot of the maximum principal stresses has been displayed. It can be noticed that the maximum tensile stress is in the region of 0.15 MPa. This stress level should be easily withstood by the grouted masonry elements.

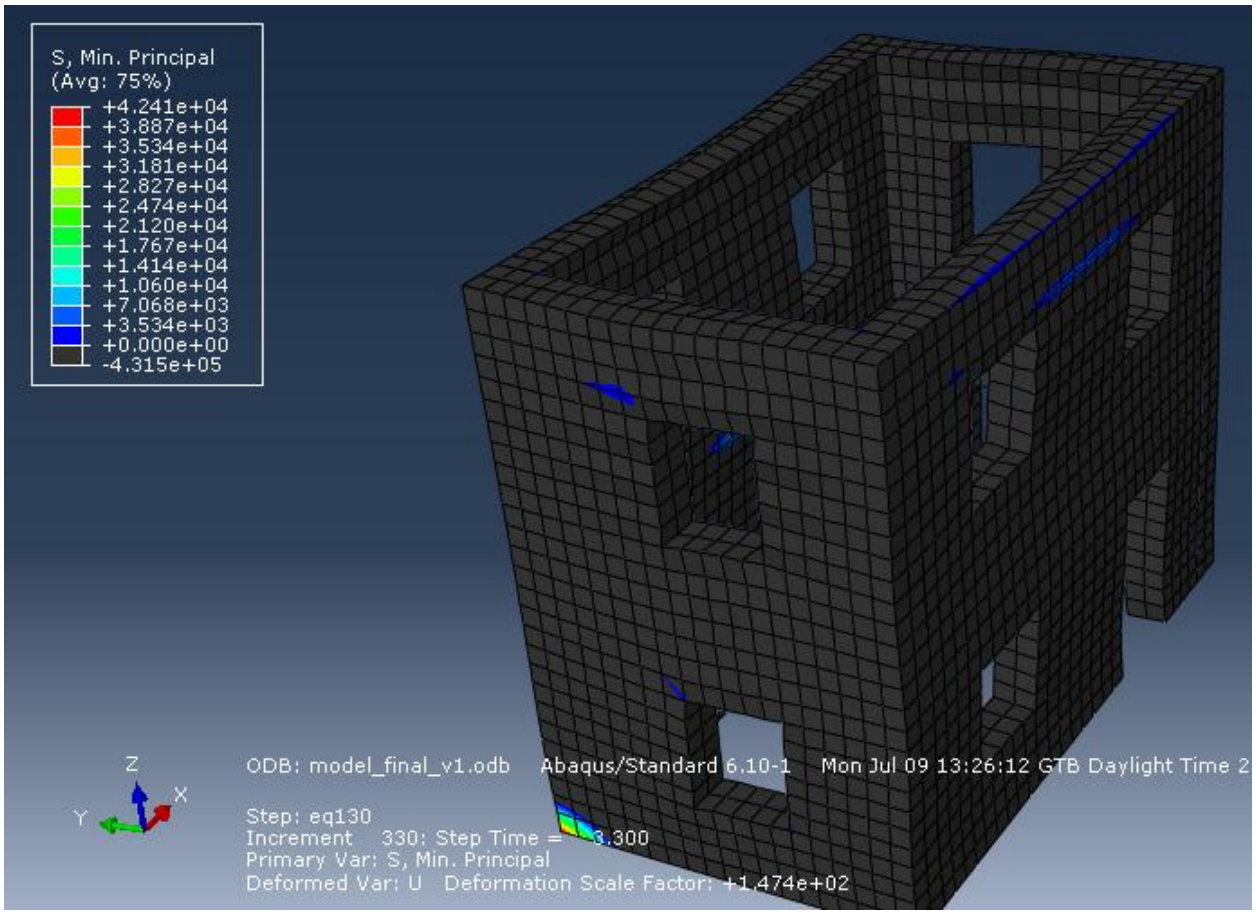

Fig. 86 Unfavorable triaxial conditions

As it can be observed above, the unfavorable triaxial zones remain, practically, the same as before, with the corners of the windows and the zones of the walls at the level of the floors being the problematic areas.

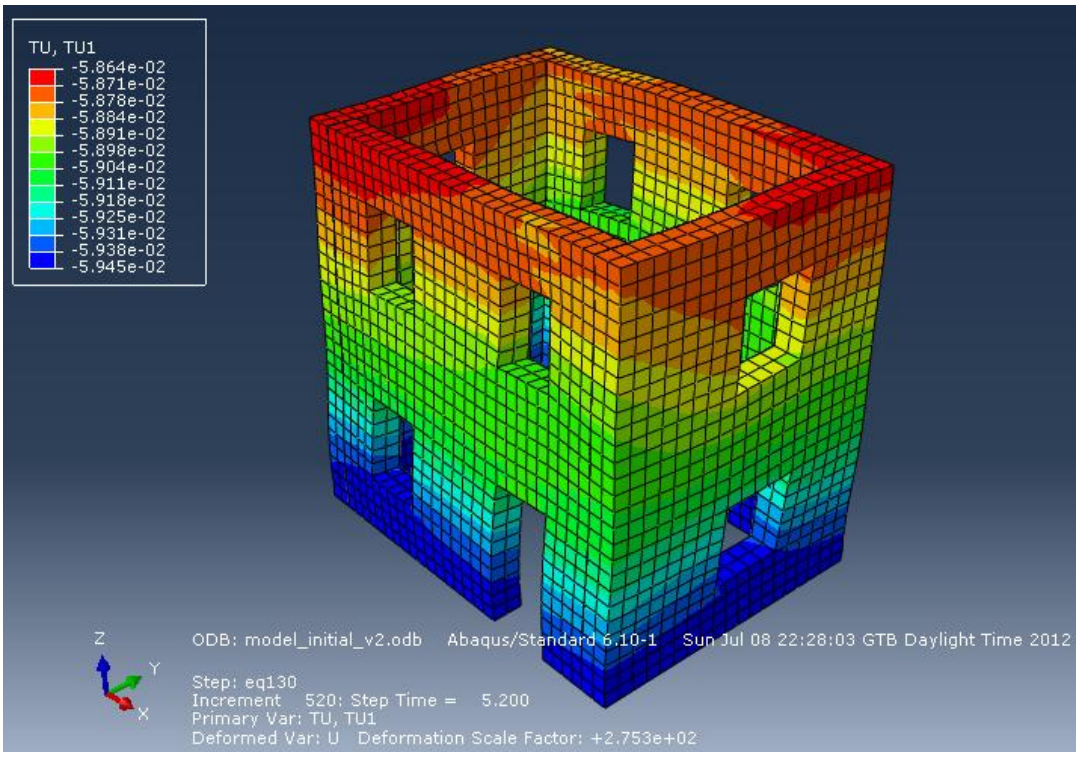

Fig. 87 OX absolute displacement

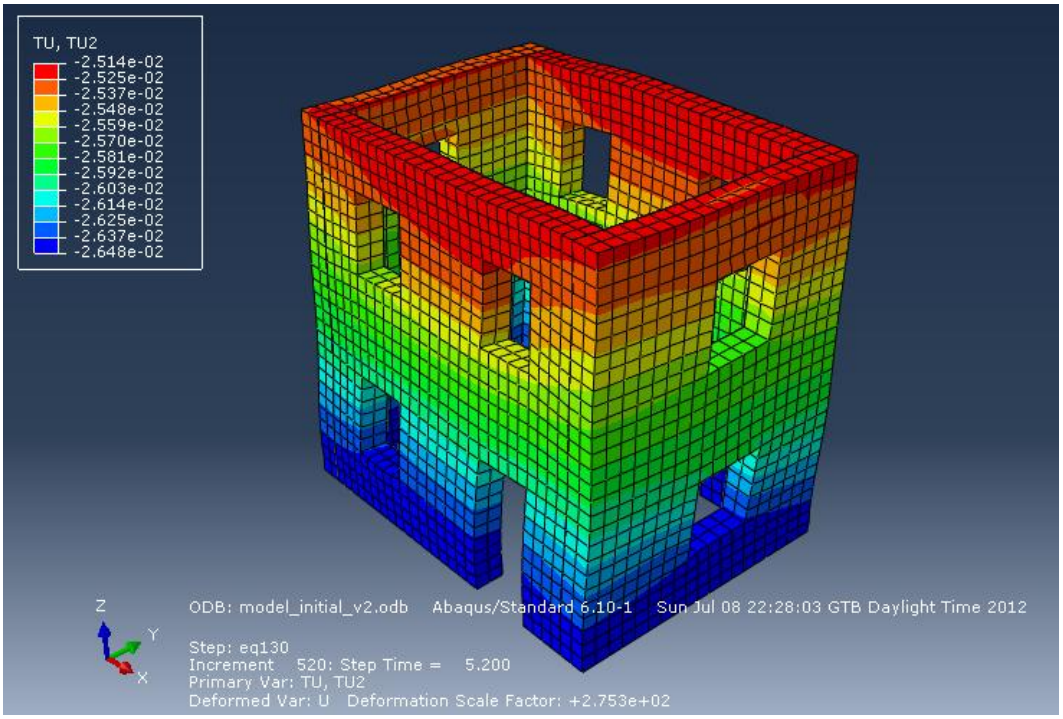

Fig. 88 OY absolute displacement

Above, the state of displacements is plotted, in this case of loading. It can be easily seen that the walls displace almost equally, in each of the two planar directions. This is a good indicator that the rigid diaphragm is effective and it behaves as expected.

3.5 Conclusions and personal contributions

Throughout this paper, a method of simulating the strengthening measures on a masonry structure has been proposed. The accurate simulation, when dealing with such complex materials and so many uncertainties, becomes a very difficult task.

The methodology proposed was the simulation of the improvement of diaphragm action of the floors by assessing two equivalent shell elements: one for simulating the initial floor and the second for simulating the strengthened floor.

The equivalent shell elements have been obtained by equivalating each of them with a detailed model of the floors (both in the initial and in the final state). The detailed floor models took into account most of the parameters which are relevant for the way the real floors behave. The assigning of an equivalent shell has been achieved by studying and fitting the modal response of the detailed model with the equivalent shell model.

After the equivalent shell element has been found, it has been inserted into a less detailed model of the whole structure and the results obtained have been accurate enough.

As a personal opinion, the accuracy of the models could be further improved by considering the nailed connection between the joists and the flooring. Another feat that could improve the effectiveness of the model would be the search for an interaction capable of accurately simulate the connection between the floors and the walls, especially for the strengthened model.

In terms of results and effectiveness of the applied rehabilitation measures, it has been observed that the effectiveness of the aforementioned interventions is clear, even in the analytical results. The decrease of compressive stresses in the masonry elements (about three times) has been a very good result. Also, the equal distribution, at the floor levels, of deformations has become evident. This helped to equally distribute the loads throughout the load bearing elements, avoiding concentrated stresses and improving the overall behavior of the building.

In terms of spectral response, the building had an increase of stiffness and, by the majority of the design codes, this would mean that for the design earthquake action a lower load will be employed (as the building is found in the first portion of the spectrum). This would not be a wrong assumption, as it has been observed that the amplification factor for the strengthened building is clearly lower than the initial amplification factor (see sections 3.3.3 and 3.4.3).

Overall, the efficiency of the rehabilitation measures has clearly been demonstrated in this paper and the proposed methodology for simulating them could serve as a starting point for developing future models for rehabilitation of historic masonry structures.

BIBLIOGRAPHY

- Vintzileou E.: "Three-leaf masonry in compression before and after grouting: A review of literature", International Journal of Architectural Heritage, Vol. 5 (4-5), pp. 513-538, 2011.
- Vintzileou and Miltiadou: "Mechanical properties of three-leaf stone masonry grouted with ternary or hydraulic lime based grouts", Engineering Structures, Volume 30, Issue 8, August 2008, Pages 2265-2276
- Tassios, Chronopoulos: "Aseismic dimensioning of interventions on low-strength masonry buildings", Middle East and Mediterranean Regional Conference on low-strength masonry in seismic areas, Middle East University, Ankara, 1986
- Valluzi M.-R.: "Consolidamento di murature in pietra. Iniezioni di calce idraulica natural", Collana Scientifica REFICERE, Gruppo Editoriale Faenza Editrice S.p.a., 2004, 128pp.
- Tassios, T. P.: "Rehabilitation of three-leaf stone masonry", in Evoluzione nella sperimentazione per le construzioni, Seminario Internazionale, 26 Sept. – 3 Oct. 2004, Centro Internazionale di Aggiornamento Sperimentale-Scientifico (CIAS)
- NIKER project presentation, www.niker.eu
- Glisovic, I., Stvanovic, P.: "Vibrational behavior of timber floors", World Conference on Timber Engineering (WCTE), 2010
- D. W. Green, J. E. Winandy, D. E. Kretschmann: "Mechanical Properties of Wood"
- T. N. Dao, J. W. van de Lindt: "New Nonlinear Roof Sheathing Fastener Model for Use in Finite-Element Wind Load Applications"
- ABAQUS User Manual v. 6.10-1. 2010. Dassault Systèmes, Simulia Corp., Providence, RI, USA.
- E. Vintzileou, H. Mouzakis, C.-E. Adami & L. Karapitta: "Strengthening of historical stone masonry buildings: Experimental testing and modeling of a 2-storey plain masonry building", accepted for publication in the Proceedings of the SAHC Conference, Wroclaw, October 2012**.**
- E. Vintzileou, H. Mouzakis, C.-E. Adami, L. Karapitta: "Assessement of dynamic behavior of three leaf stone masonry building models: seismic enhancement by grouting and improvement of box behavior", accepted for publication in the Proceedings of the SAHC Conference, Wroclaw, October 2012**.**